



## Review

## A state of review for graphene-based materials in preparation methods, characterization, and properties

Kang Yang <sup>a,b</sup>, Chao Wu <sup>a,b,c,\*</sup>, Guoqing Zhang <sup>d</sup><sup>a</sup> Key Laboratory of Functional Materials and Remanufacturing Technology of Aviation Equipments, Anyang Institute of Technology, Avenue West of Yellow River, Anyang 455000, China<sup>b</sup> Department of Mechanical Engineering, Anyang Institute of Technology, Avenue West of Yellow River, Anyang 455000, China<sup>c</sup> School of Mechanical Engineering, Sichuan University of Science & Engineering, 180 # Xueyuan Street, Huixing Road, Zigong 643000, China<sup>d</sup> Flight College, Anyang Institute of Technology, Avenue West of Yellow River, Anyang 455000, China

## ARTICLE INFO

## Keywords:

Graphene  
Preparation method  
Characterization technique  
Performance evaluation

## ABSTRACT

The advancement of the modern flexible and bendable technology has sparked increasing interest among researchers in graphene-based materials. When graphene and its derivatives are used as rubber reinforcement, the wear resistance and mechanical properties of the composite can be improved, suitable for smart wearable devices and protective materials. In this paper, preparation methods, characterization techniques and properties of graphene-based materials including graphene, graphene oxide (GO) and graphene/rubber nanocomposites are summarized. First of all, a comprehensive review of various methods for synthesizing graphene-based materials is presented, with an emphasis on their respective advantages and limitations. The subsequent discussion focuses on a range of characterization methods used to determine structure, morphology, and purity of graphene-based materials. It is final that the introduction of graphene-based materials in various properties encompassing their exceptional electrical and thermal conductivity, remarkable mechanical strength, as well as outstanding chemical stability, which make them widely used in electronics, catalysts, sensors and other related fields. The aim of this article is to provide reference for the preparation of graphene-based materials, further promoting their research and application in the diversified fields.

## 1. Introduction

Graphene, as common two-dimensional nanofiller, is a new functional reinforcement phase that plays a key role in improving the physical, mechanical, thermal and electrical properties of the elastomer matrix [1–3]. The term “graphene” is first proposed by Boehm in 1986 [4]. Graphene has a long history, dating back to the 1940 s when Schafhaeutl used sulfuric and nitric acids to embed and exfoliate graphite [5]. In 2004, Novoselov et al. [6] repeatedly peeled highly oriented pyrolytic graphite with the adhesive tape and successfully prepared graphene with a thickness of several atomic layers or even a single layer. In 2007, this group further introduced preparation methods of graphene in detail, including micromechanical stripping method, chemical vapor deposition (CVD) method, etc [7]. Meantime, it is revealed that graphene is hexagonal planar thin film with a honeycomb lattice composed of carbon atoms with  $sp^2$  hybrid orbitals, and it is a

two-dimensional material with only one atomic layer thickness. In recent years, the research and application of graphene has been continuously developed and expanded, and a present family of graphene-based materials have been generated, such as few-layer graphene, multi-layer graphene, graphene oxide, reduced graphene oxide (rGO) and functionalized graphene [8,9], widely used in material science, electricity and biology [10].

As two-dimensional basic unit of carbon, graphene can be folded into 3D-graphite [11], rolled into 1D-carbon nanotubes (CNTs) [12] and folded into 0D-Fullerene [13], as illustrated in Fig. 1. The unique two-dimensional structure endows graphene with many characteristics, including excellent Young's modulus ( $\sim 1.0$  TPa) [14], breaking strength [15,16], high thermal conductivity ( $\sim 5000$  W/mk at room temperature) and chemical stability, being an important reinforcing filler in polymer composites. These characteristics make graphene very potential material, which can be used in fields such as electronic devices, energy

\* Corresponding author at: Key Laboratory of Functional Materials and Remanufacturing Technology of Aviation Equipments, Anyang Institute of Technology, Avenue West of Yellow River, Anyang 455000, China.

E-mail address: [2304262838@qq.com](mailto:2304262838@qq.com) (C. Wu).

storage, sensors, biomedicine and so on. In comparison to graphene, GO exhibits enhanced dispersibility and is more straightforward to prepare composite materials. As material performance requirements continue to evolve, the application of elastomers in polymer matrices is poised to expand further [17]. It has been confirmed that the integration of graphene and its derivatives into elastomers has been shown to enhance the mechanical properties [18], mitigate resistivity, augment electrical and thermal conductivity, and reinforce gas barrier properties [19].

On the other hand, low friction coefficient of graphene shows excellent lubrication performance, which is beneficial to reduce the internal friction between nano-materials and the surrounding environment and minimize the generation of hot spots inside nano-materials [20,21]. Despite its great potential, graphene also faces challenges including high production cost [22], controlling quality problems [23], scalability problems, uncertainty of environmental and health impacts and difficulties in application integration, which limit its large-scale commercialization and wide application [24,25]. For instance, difficult to prepare graphene on a large scale and control its consistency often leads to structural defects of the material, such as lattice imperfections and edge defects, thus directly affecting its properties. Meantime, these properties of graphene are easily influenced by the external environment and chemical modification as well, especially in practical applications, it is difficult to maintain its unique conductivity and mechanical properties [26]. In addition, the dispersibility and interfacial compatibility of graphene in different elastomers are not ideal, which makes it difficult to give full play to the comprehensive properties of composites [3,27].

Based on above point of discuss on advantages and drawbacks for

graphene-based materials, this review integrates latest works on graphene, GO, and graphene/elastomer composites, focusing on the recent advancements in some preparation techniques, such as the application of novel functionalized graphene and methods to enhance its dispersibility in elastomer matrices. Meanwhile, the discuss on impact of these methods on composite properties is also conducted. Furthermore, the emphasis on multi-scale characterization contributes to gaining comprehensive analysis of relationship between microstructure and macro-properties, thus addressing the gaps in existing reviews. Finally, the targeted optimization strategies are proposed via comparing composite performances across different applications, which providing the solid foundation for developing specialized materials like conductive and wear-resistant rubber. This review aims to advance the practical applications of graphene/elastomer composites and inspire future research directions.

## 2. Graphene

### 2.1. Preparation methods

In recent years, the popularity of graphene has gradually increased owing to its many excellent properties, thus leading to the “gold rush” in the field of graphene [30,36–38]. However, due to the high cost of producing high-quality graphene, the development of its large-scale production is limited. In order to solve this problem, by summarizing the existing graphene production methods and exploring new methods and technologies, we could lay solid foundation for improving the production efficiency and quality of graphene and promote its application

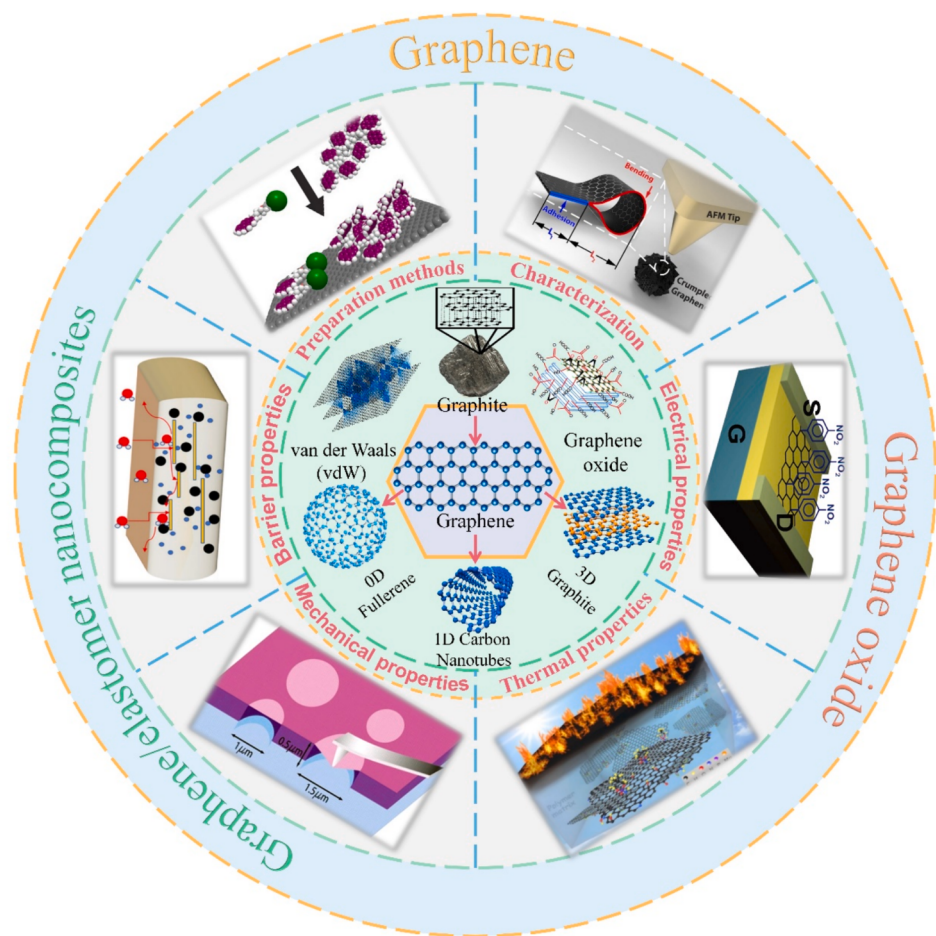


**Fig. 1.** Typical patterns showing the evolution process from graphite to multi-dimensional carbon-based materials, and their preparation method, characterization technology as well as related properties; Reprinted with permission from Refs.[8,28–35].

in various fields [39,40]. Therefore, we created the Table 1, in which the advantages and disadvantages of the main preparation methods, such as liquid phase stripping method [41,42], mechanical exfoliation [40,43], CVD [44], and chemical exfoliation [45,46], are compared and analyzed. So that readers could intuitively understand the characteristics and limitations of the various methods. In 2004, Novoselov et al. [6] pioneered preparation of graphene sheets with a thickness of only one atom by repetitive mechanical exfoliation of graphite, subsequently confirming existence of its unique structure. At present, this method had been proved that it could reliably produce few-layer graphene films with sizes up to 10  $\mu\text{m}$ . The large enough size made this method have great significance in practical application fields, such as electronic devices, sensors and so on. Furthermore, the geometric diameter of thicker film was increased from micron-scale (about 100um) to nearly millimeter scale, which made it clearly visible at a macroscopic level. However, this method has drawbacks such as large volume, high cost, extremely low yield, and limited scalability.

An extensible green method deserves attention, which is reported by Ding' s group using massive layered graphite materials to obtain thin graphene sheets in pure water [47]. Synthesis process of this stable aqueous graphene dispersion is very simple and efficient without any chemicals or surfactants, with the procreative graphene mainly consisting of less than 10 atomic layers, as illustrated in Fig. 2(a). Such water-soluble graphene showing excellent dispersibility, can be stored in the form of dispersion or filter cake for more than 6 months, which is of great significance for expanding production. In addition, some studies have confirmed that ultra-pure graphene with few layers can be

**Table 1**  
Comparative analysis of advantages and disadvantages of main methods for preparing graphene.

Preparation technology	Source materials	Advantages	Disadvantages	Ref.
Liquid phase stripping	graphite	Less energy intensive; Low-defective	Limit mass production; Small size	[50]
	graphite	High quality; High yield; High efficiency	NM	[41]
	graphite	Low-defective; nontoxic; Lower cost	NM	[42]
Ultrasound-aided liquid phase exfoliation	graphite	High quality; High yield; Low-defective; Lower cost; Scalable	Inhomogeneous flakes; Small size	[51]
	graphite	High quality; Low cost	Low yield; Uncontrollable defects; Random size	[40]
Mechanical exfoliation	graphite	High quality; Defect free; Larger size	Labour intensive	[43]
Chemical vapor deposition	Ni film; H <sub>2</sub> ; CH <sub>4</sub>	Low cost; Scalable	Size limitation	[62]
	H <sub>2</sub> ; CH <sub>4</sub>	High quality; Large size; Excellent conductivity; Choice of carbon precursors	Expensive; Complicated procedures	[44]
Chemical exfoliation	electro-polished; H <sub>2</sub> ; CH <sub>4</sub>	High quality	Time consuming	[71]
	H <sub>2</sub> ; CH <sub>4</sub>	High quality; Controllable number of layers; Simple operation; Functionalised	NM Large number of defects; Low quality	[73] [45]
	graphite	High purity; High yield; High quality	Slight oxidation	[46]

NM=Not mentioned.

generated by the ball milling using simulated microchemical stripping, in which grinding graphite compensates the  $\pi$ - $\pi$  interaction between graphene layers in bulk graphite, resulting in an effect similar to mechanical splitting [48,49]. When ball milling agent like oxalic acid is added to chemically functionalize graphite, efficiency of graphite stripping can be increased, which is fully meaningful for expanding production.

Compared with mechanical exfoliation method to prepare graphene, liquid phase stripping (LPE) utilizes solution infiltration and stripping for graphene preparation, which has been proven to be a scalable method [50]. This method utilizes inexpensive and abundant graphite flakes as precursors, and the resulting graphene products met the requirements of scalability, reproducibility, processability, and low production cost. Importantly, this method avoided the complex process of transferring the final graphene product onto a selected substrate [51]. Shear exfoliation, a commonly used LPE, could produce high-quality and large-area graphene sheets using very simple equipment, which was suitable for treating most samples as whole. However, the peeling efficiency was low, and the graphene obtained was usually more than two layers, with an average of about 3–7 layers, which limited production of single-layer graphene [52]. Meanwhile, production of single-layer and large-sized graphene also faced significant challenges, which were associated with solvent selection used in graphene LPE [53,54]. Normally, most solvents utilized for dispersing graphene were relatively expensive and toxic. In particular, polymers or surfactants as dispersing agents were difficult to remove, resulting in the poor performance of polymer or surfactant-assisted LPE-prepared graphene. In contrast, widely used layering technology was ultrasonic-assisted liquid phase stripping, which made the substance to be separated and the solvent move violently through the oscillation of ultrasonic waves, thus realizing the rapid separation of the substance to be separated, with the characteristics of high efficiency, rapidity and the absence of the need for additional chemical reagents. Qin et al. [55] employed ultrafast synchrotron X-ray phase contrast imaging technique to investigate the delamination kinetics of ultrasound-assisted liquid phase exfoliation in real time. Nevertheless, the process of the ultrasound-induced cavitation was the relatively harsh process, and the adverse conditions of cavitation may lead to damage to graphene. Thus, the graphene produced by ultrasound has more defects than expected. Moreover, if the position of the ultrasound vibration source was fixed, the cavitation field in the liquid was almost static. These disadvantages were unfavorable for effective exfoliation, and a large number of graphene flakes settling at the bottom remain unexfoliated. In addition, ultrasound exfoliation often leads to a decrease in the size of graphene nanoflakes. In the case of water only, graphene flakes were thinner (~3 layers) and larger (~1.5  $\mu\text{m}^2$ ), while in a mixture of water and surfactant, flakes with high yield and low defect could be obtained.

In term of scope of application of graphene, in comparison to mechanical stripping method and liquid phase stripping method for preparing small-area graphene samples, thermal exfoliation is suitable for preparing large-area graphene films, which is an effective and scalable method for producing graphene [56–58]. Kwon et al. [56] demonstrated a novel constraint-based approach to produce fairly large-sized fully oxidized graphene films with high conductivity and microporosity. Utilizing thermal shock program to induce the exfoliation of graphene, new macroscopic graphene-based materials were formed after reassembly or mixing, addressing challenge of mechanical delamination in producing large-sized graphene. Fig. 2(b) illustrated schematic diagram of thermal reduction/exfoliation of perforated graphene film. Wei et al. [57] obtained the honeycomb-like graphene sponge prepared by programmed thermal stripping of GO film, and investigated the influences of heating rate and external binding force on the stripping degree of graphene sponge. The results indicated that when the heating rate was  $10^\circ\text{C}\cdot\text{min}^{-1}$  and the temperature rose to 200°C, the rapidly decomposed functional groups generated a large amount of gas, which pushed the GO film to realize thermal peeling, and then graphene sponge with excellent

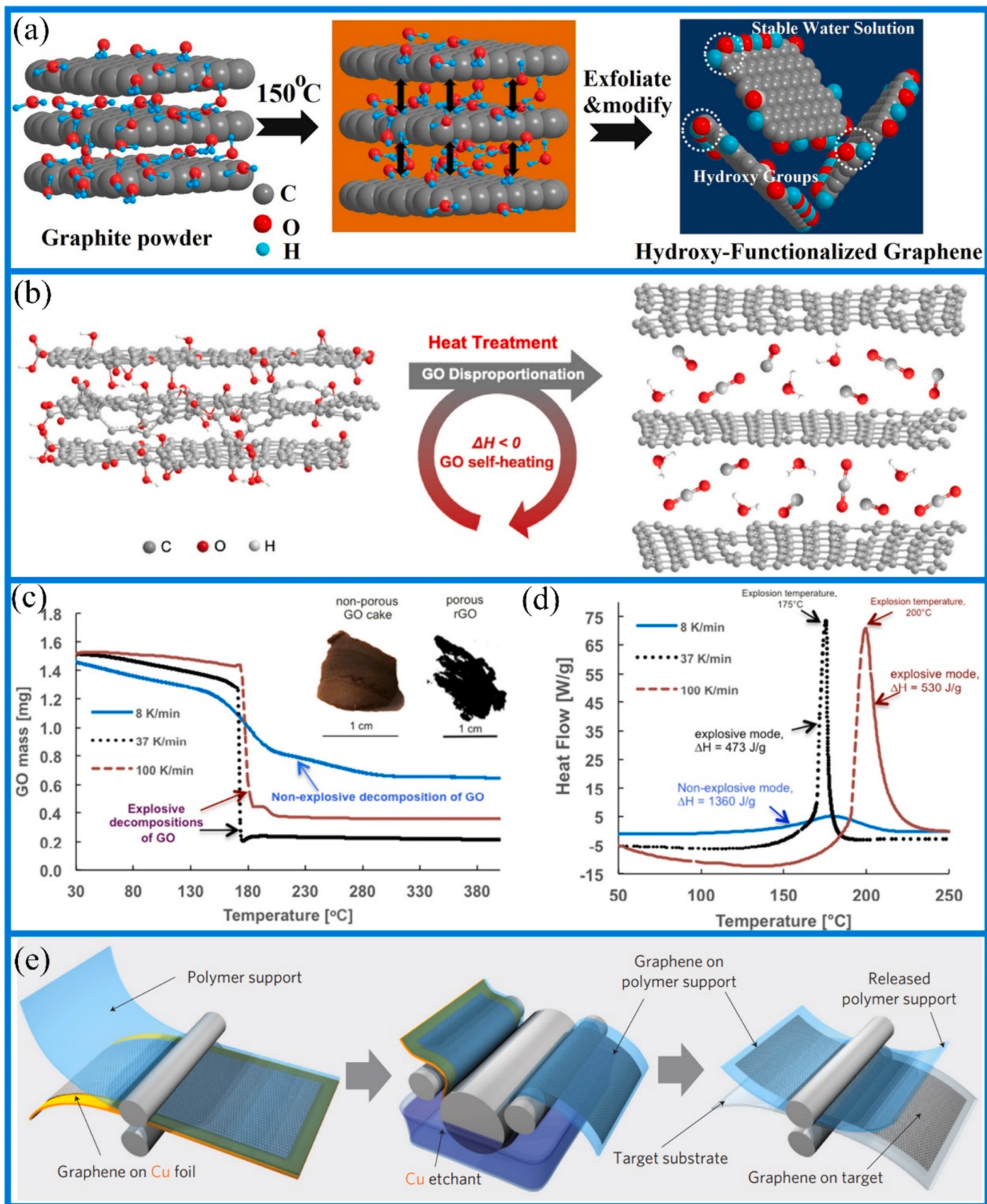


**Fig. 2.** (a) Schematic visual diagram of the exfoliation process from graphite to graphene; Reprinted with permission from Ref.[47]. (b) Schematic diagram of exothermic thermal reduction of few-layer and porous rGO films; Reprinted with permission from Ref.[56]. Thermal exfoliation of Hummers GO in standard TGA (c) mode or in DSC (d); Reprinted with permission from Ref.[58]. (e)The rolling production drawing of the graphene film growing on copper foil; Reprinted with permission from Ref.[67].

foldability was obtained. Meantime, the uniform thickness and peeling degree of the film were adjusted by external force to limit its free expansion. Thermal reduction parameters during the thermal oxidation exfoliation of graphene were further investigated by Qiu et al. [58]. By analyzing the thermogravimetric apparatus (TGA) (Fig. 2c) and differential scanning calorimeter (DSC) (Fig. 2d) curves of thermal spalling of GO under the heating rates applied by three external instruments, the GO did not explode at a lower external heating rate (<8 K/min). On the contrary, at higher external heating rate (>8 K/min), a sudden micro-explosion event would occur, accompanied by almost instantaneous mass loss. The micro-delamination behavior of different GO films within

target temperature and instrument heating rate ranges was systematically studied. These results were of highly significance for optimizing preparation conditions of GO. In general, localized thermal delamination of multilayered nano-flake films of GO could be used to control the pore structure and conductivity of planar and confined GO films. These films could be utilized in various applications such as solar cells, flexible electrodes, and sensors.

A significant phase in graphene synthesis was the insertion, thermal expansion, and ultrasonic delamination [59,60]. Gu et al. [59] reported a highly promising method for graphene production that involved inserting a mixture of hydrogen peroxide ( $H_2O_2$ ), sulfuric acid ( $H_2SO_4$ ),

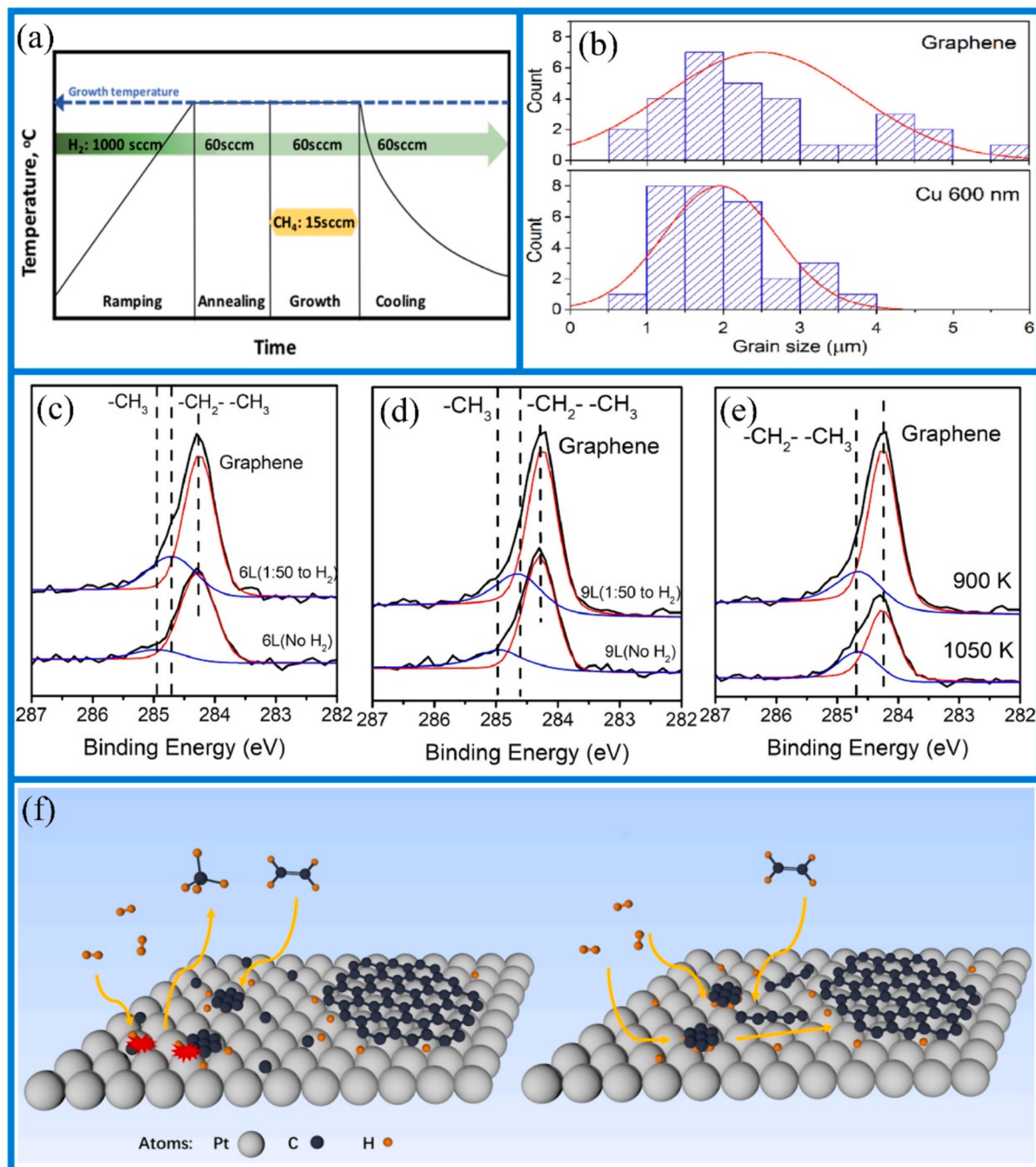


**Fig. 3.** (a) Several steps in growth of graphene through CVD; Reprinted with permission from Ref.[71]. (b) Grain size distribution for graphene and Cu film; Reprinted with permission from Ref.[88]. XPS C1s signals for graphene produced at different conditions: introducing (c) 6 L of  $C_2H_4$  at 900 K, (d) 9 L of  $C_2H_4$  at 900 K and (e) 9 L of  $C_2H_4$  at 900 K and 1050 K respectively; (f) Schematic diagram of H-etching hydrocarbons and intercalation of hydrogen; Reprinted with permission from Ref.[75].

and hydrogen gas ( $H_2$ ) into graphite layers. Subsequently, the graphite layers rapidly expanded to form worm-like peeled graphite. The obtained graphene was further processed in 1-methyl-2-pyrrolidinone suspension to form high-quality graphene flakes. While this method had potential for large-scale production of graphene, there was still significant room for improvement in terms of yield, consistent size, and overall quality of the final graphene flakes. For this purpose, Chia et al. [60] optimized the limiting parameters and identified the optimal approach. The results indicated that the optimum conditions for the highest yield of graphene sheets were as follows: an acid-oxidiser ratio of 5:1, thermal expansion time of 60 s at 900 °C and graphite flakes with an average flake size of 350 µm. It was worth noting that the initial size of graphite flake has a great influence on the efficiency of intercalation, expansion and peeling, and larger graphite flake usually produces wider graphite flake.

Since its initial reports in 2008 and 2009, chemical vapor deposition has also become an important method for the preparation and production of graphene [61–64]. This method allowed for the production of large-sized, high-quality graphene [65,66]. Fig. 2(e) illustrated the roll-to-roll growth of graphene film on copper foil [67]. Additionally, type of substrate also critically affected the synthesis temperature of graphene. At present, the metal substrates used included Cu, Ni, Co, Pt, or Ir, and they yield thick, controllable graphene sheets with reduced defects. Due to the high catalytic activity and low carbon solubility of Cu substrate, the growth temperature of graphene could be significantly reduced, resulting in high-quality monolayer graphene [68]. Oppositely, for monometallic catalysts such as Ni, Co, Fe, which had higher carbon solubility, the synthesis temperature of graphene could be lowered, but it became difficult to control the number of graphene layers. By adjusting the thickness of catalyst and the deposition conditions, more uniform and controllable high-quality graphene films could be obtained.

The CVD growth of graphene on Cu films represents another step towards the development of graphene transfer method compatible with large-area silicon wafers. Currently, the CVD growth graphene is typically grown on copper foil with a thickness of 25 µm or more, exhibiting acceptable crystal quality [69,70]. On the other hand, an alternative approach to growing graphene on evaporated Cu films on SiO<sub>2</sub>/Si wafers may offer a solution for developing more robust graphene transfer methods. Given that technical compatibility between Cu/SiO<sub>2</sub>/Si wafers and cold-wall CVD reactors, this approach held great promise. Cold-wall CVD reactors were gradually replacing traditional hot-wall CVD for graphene growth [71]. Fig. 3(a) illustrated the steps involved in synthesis and growth process of graphene in cold-wall CVD reactor. When treated at a high temperature of 1060°C, the density of multilayer graphene decreased by more than 50 %. Apart from multi-layer graphene, single-layer graphene without crystal defects could be grown on Cu films with cold-wall CVD reactor [59]. Fig. 3(b) presented a comparison of the grain sizes between monolayer graphene to the 600 nm thick Cu film substrate. The average grain size of single-layer graphene was ~ 2.5 mm, up to 6 mm, while for Cu was ~ 2 mm. Influenced by the grain size of catalytic metal substrate, typical growth on copper foil has great advantages in obtaining graphene with larger grain size, which provided a basis for further expanding the grain size of Cu and graphene. Analogously, Tao et al. [72] demonstrated the growth of monolayer graphene on evaporated Cu on SiO<sub>2</sub>/Si substrates using a cold-wall CVD reactor. They attempted to grow graphene at 875 °C and discovered that the grain size of graphene was related to the grain size of Cu. The average grain size of Cu with a film thickness of 1 µm ranged from 10 to 20 µm. In the recent study, Huet et al. [73] reported the growth of monolayer graphene on Cu by evaporating it on 3-inch SiO<sub>2</sub>/Si wafers using a hot-wall CVD furnace. At 1050 °C, the grain size grown on a 1 µm thick Cu film reached 1 mm, significantly larger than approximately 100 µm. Regarding film, a 1 µm thick Cu film could be considered thick and not suitable for graphene transfer involving Cu etching/removal. However, thinning Cu film gives rise another issue, which is Cu dehydration, especially at high temperatures (~1000 °C) [74].

Hydrogen plays an important role in the growth of graphene on metal substrates in metal-based CVD processes. However, the precise impact of hydrogen under different preparation conditions are difficult to determine [75–77]. Li et al. [75] prepared highly coverage graphene on Pt (1 1 1) substrate using gas-phase deposition method. These findings indicated that hydrogen can accelerate the growth of graphene and improve its quality at 900 K, without the necessity of particular hydrogen conditions. Fig. 3(c-e) depicted the XPS C1s spectra of graphene under different conditions. In-situ observations with low-energy electron microscopy revealed the penetration of hydrogen into graphene-platinum interface, suggesting that the interaction with the substrate promotes graphene growth. The mechanism was illustrated in Fig. 3(f). Graphene produced by CVD methods has advantages such as thin film thickness and minimal surface defects. Through controlled deposition processed, the graphene film could be uniform and clear. Furthermore, the reaction temperature was also the critical parameter in CVD for the synthesis of high-quality graphene. Different precursors have different pyrolysis temperature and pyrolysis ability, which will affect the required reaction temperature. The CVD process typically involved the decomposition of precursors at high temperatures, where gas atoms were in high-energy state, adsorb onto the substrate, and undergo surface chemical reactions to form continuous film [62]. The choice of precursor affected reaction temperature, as the adsorption deposition process could only occur at temperatures higher than the decomposition temperature of the precursor [78]. The most commonly used precursors for graphene are methane (CH<sub>4</sub>) and acetylene when using CVD [79–81]. These precursors require high reaction temperatures because breaking the chemical bonds requires high energy. When CH<sub>4</sub> was used as the precursor, reaction temperature needs to reach 900 °C. Below 600 °C, the required energy for bond cleavage cannot be achieved [82–84].

There are still many challenges for future applications. High-temperature synthesis of graphene leads to resource waste and increased costs, limiting its application in flexible electronic devices and military equipment [85,86]. In the optoelectronics field, the addition of graphene can significantly enhance the conductivity of devices. However, the incorporation of graphene in some optoelectronic devices required very low temperatures, typically below 600 °C. Therefore, it has become an inevitable trend for the future development of graphene to be prepared by CVD at low temperatures (<600 °C) [87]. To address the issue of high temperature, Soriadi et al. [88] employed a cold-wall CVD reactor to grow monolayer graphene on ultra-thin Cu films ranging from 100 to 600 nm at lower temperatures, just above the temperature where methane effectively decomposes to reduce dehydration. They successfully grew graphene on 8-inch Cu/SiO<sub>2</sub>/Si wafers using the cold-wall reactor, resulting in monolayer graphene with no crystalline defects. Although significant progress has been made in the preparation of graphene under low-temperature conditions, there are still significant challenges and issues. The deposition of graphene was often uneven and discontinuous, leading to lower-quality graphene. Additionally, the presence of impurities and polycrystalline substrates may pose further obstacles to producing high-quality graphene at low temperatures. In order to explore and study the production of graphene, researchers demand to delve deeper into achieving precise control over graphene production under low-temperature conditions [89]. In general, the liquid phase stripping method generally exhibits superior production efficiency and applicability compared to the mechanical stripping method. However, it requires more intricate procedural steps and raw material treatment.

## 2.2. Characterization

Graphene, despite being a nanomaterial, can be directly observed under an optical microscope because a single atomic layer absorbs approximately 2.3 % of visible light [90]. Compared with an optical microscope, scanning tunneling microscope (STM) has advantages in

observing high-resolution surface structure, which is closely related to the role of the tip of the probe enabling atomic resolution in STM. In comparison to conventional Pt-Ir STM probe, graphene probe had great potential [91]. When a low voltage was applied to the graphene probe in STM, it can generate a tunnel current of hundreds of picoampere, thereby enhancing the resolution of atomic regions. For instance, graphene probe and Pt-Ir probe were used to test molecules of arachidonic acid respectively. The results showed that, in Fig. 4(a), a clear image of arachidonic acid self-linkage molecules in air was obtained when graphene probes were used instead of Pt-Ir probes, indicating that graphene probes were particularly sensitive to carbon bonded structures [91]. Furthermore, high current graphene probe could also be used as scanning probe to measure molecular surface morphology in air instead of

ultra-high vacuum environment. It was worth noting that this technique relied on the size of the probe, and sharpness of the probe tip determines the lateral resolution of the STM. Similarly, in the field of surface observation, scanning electron microscopy (SEM) also has the ability of high resolution and supernal sensitivity, which is widely used in scientific research and industrial fields by analyzing samples and collecting quantitative data [92,93]. SEM images provided important indicators of material quality, such as the percentage of area covered by graphene, size and shape of particles, as well as nucleation density, which could be quantitatively analyzed. Different from the imaging principle and mode of electron microscope, atomic force microscope (AFM) senses the surface topology through the interaction between the probe and the sample surface [94,95]. Meanwhile, the functionalization of tip for AFM had

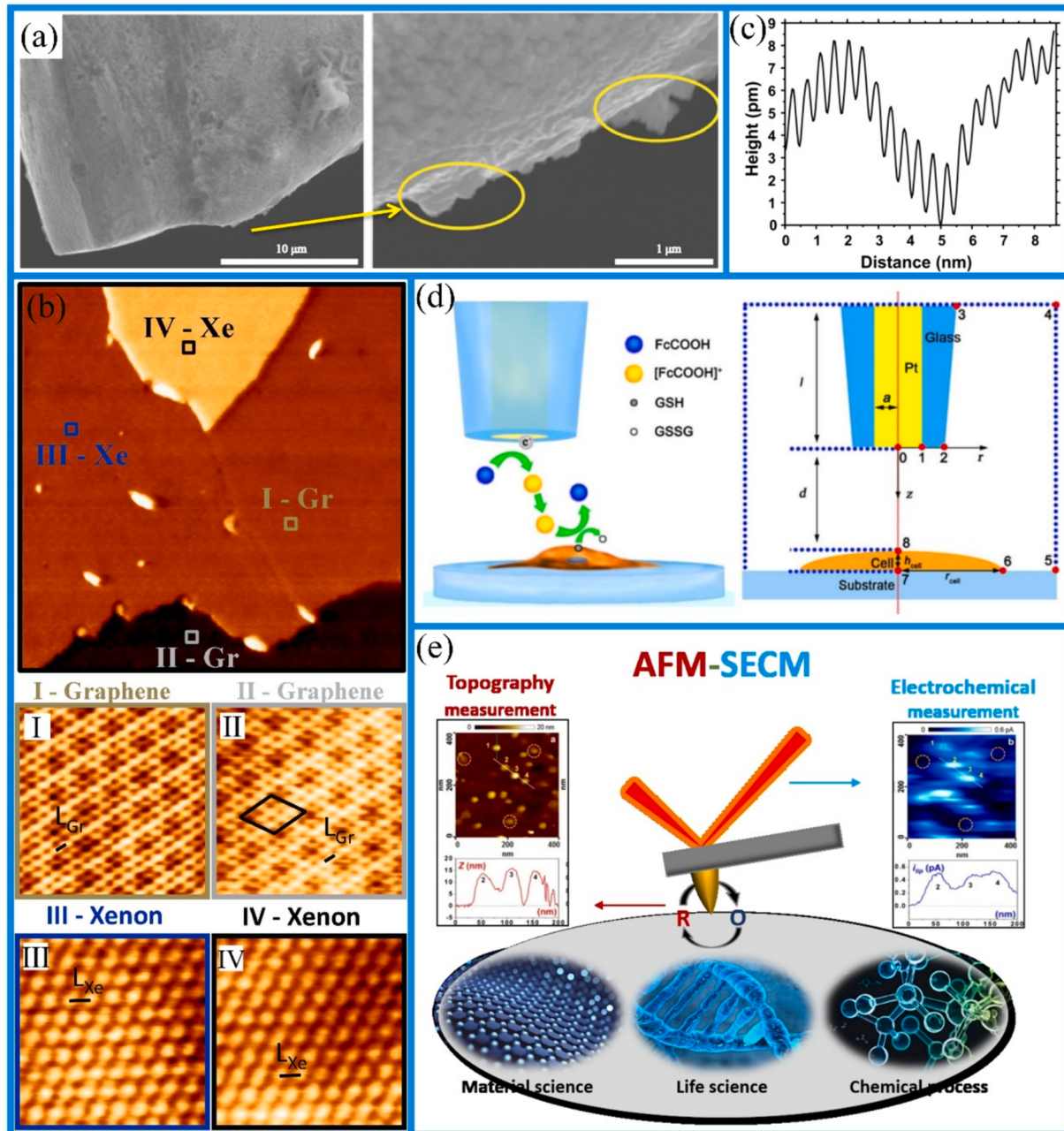


**Fig. 4.** (a) The observational SEM showing the graphene probe body and the tip for graphene protrusions; Reprinted with permission from Ref.[91]. (b) ncAFM images for Xe on Gr/Pt(111); (c) Height profile displaying the corrugation for Xe atoms and commensurate regions; Reprinted with permission from Ref.[95]. (d) Schematic drawing for SECM system and corresponding simulation model; Reprinted with permission from Ref.[99]. (e) The diagram of application direction for the AFM-SECM system; Reprinted with permission from Ref.[101].

been further revealed to be a powerful tool for achieving the higher resolution and allowing for the characterization of features within molecules. In the investigation of functionalization of non-contact atomic force microscope (ncAFM) tip, in-situ functionalization of it was achieved by the adsorption of Xe atoms on the surface of graphene [95]. Result demonstrated that Xe had lower reactivity compared to graphene, and the difference in reactivity was significantly enough to use force spectroscopy as an alternative method for identifying Xe. As shown in Fig. 4(b), ncAFM image of Xe on Gr/Pt(111) was presented. In order to further verify the realization of the functionalization of the tip, the extraction of Xe from the rare gas layer was explored by indentation method and scanning method. Fig. 4(c) showed indentation on the Xe layer and scanning this layer. With the folded two-dimensional sheet becoming the research focus as a new type of nano-materials, it was significantly important to explore the influence of crumpling on properties of two-dimensional materials, such as graphene and GO, by force indentation routines using AFM [28]. The force indentation and strain hardening of wrinkled graphene and GO exhibited significant nonlinearity. This detailed understanding of mechanical behavior at nanometer scale was contributed to the rational design of materials to enhance energy and material storage, energy absorption and friction modification [96].

In order to deep investigation on the structure and properties of graphene, scanning electrochemical microscopy (SECM) as high-resolution scanning probe technique, can be used to observe electrochemical reaction activity, electron transfer rate and electron transport performance of graphene surface in real time, thus providing important information about electrochemical behavior of graphene [97–99]. Fig. 4(d) presented schematic diagram of the classical SECM system [99]. While other techniques such as SEM and AFM can be combined to provide high spatial structural information, there are inevitably some mismatches when using these microscopes with SECM [100–102]. Fig. 4(e) represented schematic diagram of application direction for AFM-SECM system, such as material science, life science, and chemical process [101]. To address study of electrochemical activity and surface shape, another high-spatial mapping method called scanning electrochemical cell microscopy (SECCM) had been developed [103–105]. SECCM has become the powerful new technology in electrochemistry and interface science, demonstrating its ability to quantitatively map interfacial charge transfer at the nanoscale. This technique builds on principles of well-established electrochemistry and general scanning probe microscopy and emphasized reliable mass transport and electric field calculation model.

The SECCM approach is particularly appealing because nano-materials require minimal processing and encapsulation and can be studied almost in their pristine state [106]. By simultaneously recording the position of nano-droplet and the electric current in the droplet, the electrochemical activity and appearance of the nano-droplet's surface can be obtained. However, during SECCM scanning process, particularly on three-dimensional surfaces with different curvatures, it is challenging to maintain droplet size consistently, which affected accurate characterization of electrochemical activity [105]. A development of more robust electrochemical imaging methods also required the investigation of the electrochemical properties of three-dimensional surfaces, such as wrinkled graphene.

It is anticipated that in the future, SECCM will be expected to become a highly effective method for the nanomanufacturing and visualization under electrochemical control, especially since reaction imaging studies have demonstrated that this technique can be applied to substrate materials ranging from conductors to insulators. As for the SECCM technology itself, it is possible to further reduce the probe size, although doing so may require further development of SECCM models to accommodate potential substrate and liquid transfer bilayer effects. There are also many options to enhance the probe, such as constructing additional channels for delivery, detection, and monitoring of interface processes. In the study of Jin et al. [107], solid polyacrylamide (PAM),

was used as substitute for the traditional liquid electrolyte to establish a solid-state SECCM. Solid PAM nanospheres were formed at the tip of a nanocapillary in contact with graphene, providing information about the morphology and initial electrochemical measurements. In comparison to droplets, solid nanospheres are stable and provide consistent contact area at various positions on the graphene. Additionally, unlike the liquid SECCM mode, there is no residual droplet left on the material surface after each use of the solid nanosphere, avoiding the inevitable droplet spacing. Ultimately, the new solid-state SECCM achieves high spatial resolution for continuous surface mapping. A complete scan of wrinkles on graphene recorded low currents on the walls of the wrinkles and relatively high currents at the center of the wrinkles. The heterogeneity of wrinkled electrochemical activity demonstrates different electron transfer characteristics on surfaces with different curvatures, which were difficult to observe with current electrochemical or optical methods. The successful establishment of this high-spatial-resolution electrochemical microscopy overcame the challenges in studying electrochemical activity of materials at the nanoscale, which was important for a better understanding of electron transfer in materials. Through SECM technology, the electrochemical properties of graphene are quantitatively analyzed, which provides an important reference for the application of graphene in the fields of electrochemical sensing, catalysis and energy storage. But there are some limitations in sample applicability and operation ability. The choice of microscope depended on the specific observation requirements and the nature of the sample.

With respect of tracking the insertion and exfoliation of graphite and the formation of graphene, X-ray diffraction (XRD) detection technology has played the crucial role, extremely in help of researchers on understanding the crystal structure, insertion and exfoliation effects of materials and the quality characteristics of graphene [91]. X-ray is type of high-energy electromagnetic radiation [108]. Crystalline materials with atomic networks could cause scattering of incident X-rays and produce an interference pattern. Example diffraction pattern had been shown in Fig. 5(a). The resulting pattern could be analyzed to obtain information about the atomic or molecular structure. Meanwhile, scherrer equation was inevitably used in the analysis of diffraction pattern, and then the size and shape of graphene fragments sample can be obtained effectively. Lim et al. [109] modified scherrer equation by introducing an empirical additive constant. The specific derivation process was as follows:

$$L_a = \sqrt{\text{area}} \quad (1)$$

$$I(Q) = f(Q)^2 \sum_{i=1}^N \sum_{j=1}^N \frac{\sin Qr_{ij}}{Qr_{ij}} \quad (2)$$

$$Q = \|\mathbf{Q}\| = \frac{4\pi \sin \theta}{\lambda} \quad (3)$$

$$I(Q) \approx \frac{1}{N} f(Q)^2 \left( N + 2 \sum_{k=1}^{N_{\text{bins}}} n_k \frac{\sin Qr_k}{Qr_k} \right) \quad (4)$$

$$L_a = K' \frac{\lambda}{B \cos \theta} + c \quad (5)$$

Herein,  $L_a$ : the side length for a square fragment,  $I$ : the scattered intensity,  $f$ : the atomic form factor,  $N$ : the number of atoms,  $r_{ij}$ : the scalar distance between the  $i^{\text{th}}$  and  $j^{\text{th}}$  atoms,  $\mathbf{Q}$ : the scattering vector,  $\lambda$ : the incident X-ray wavelength,  $\theta$ : the diffraction angle,  $r_k$ : the interatomic length represented by the bin,  $N_{\text{bins}}$ : the number of bins,  $K' = 2$  and  $c$ : the constant to be determined.

By defining  $L_a$  as the square root of the fragment area, a general expression was generated, and then a modified equation containing a small additional constant was introduced, thus solving the well-known size dependence problem in the shape factor. This new form eliminated almost all size dependence, was independent of diffraction peaks,

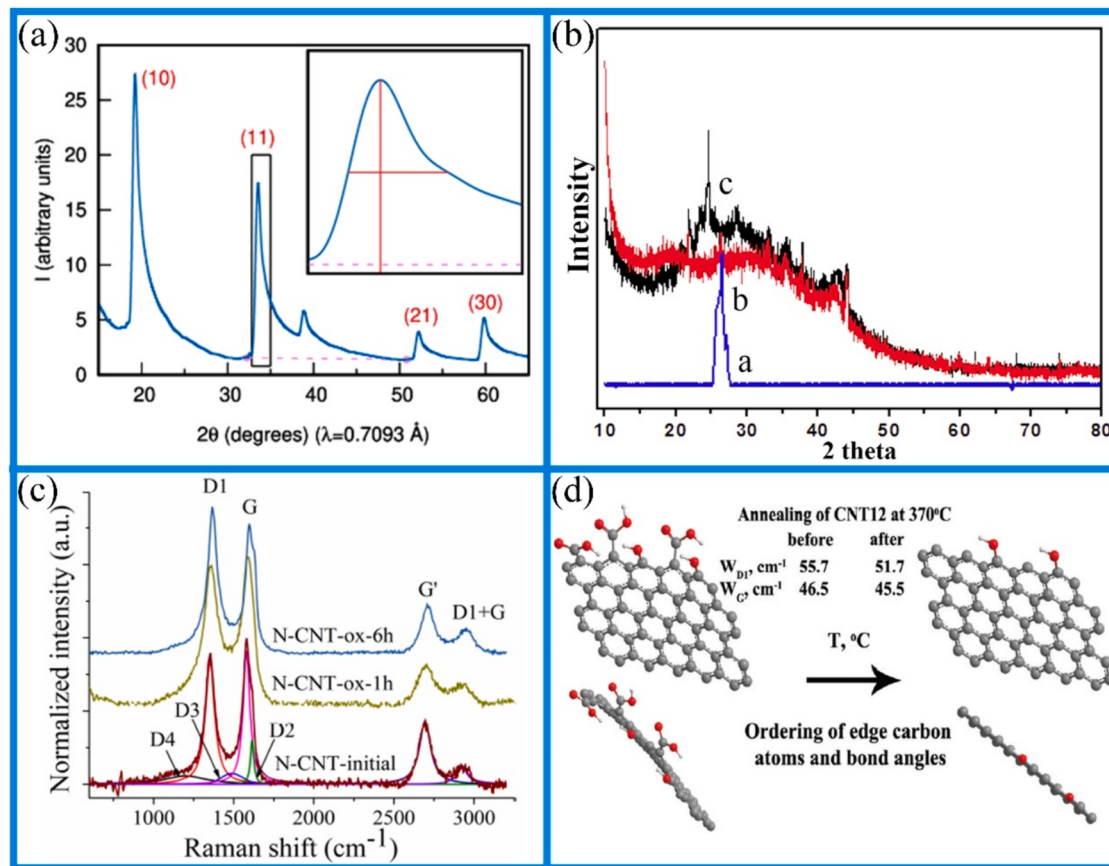


**Fig. 5.** (a) Example of diffraction pattern; Reprinted with permission from Ref.[109]. (b) XRD peaks of carbon-based materials: graphene, GO and rGO; Reprinted with permission from Ref.[110]. (c) The relationship between the Raman spectra and the normalized intensity of pristine and oxidized N-CNTs; Reprinted with permission from Ref.[117]. (d) Schematic diagram for changes in the CNT12 edge after annealing; Reprinted with permission from Ref.[119].

and was also suitable for all kinds of regular polygons. XRD analysis of the obtained diffraction patterns using the scherrer equation allows for a relative estimation of the average number of layers in graphene. Besides, in observing the oxidation degree of graphite, it required minimal sample preparation, and the interpretation of the resulting data was often straightforward [110]. Fig. 5(b) showed the XRD patterns of graphite, GO and rGO. The results indicated a clear interlayer spacing between graphite powder (0.34 nm of layer distance) and graphene oxide (0.88 nm of layer distance) was ascribed to the introduction for oxygen containing functional groups at the layers. Such fast and powerful technique for material identification and characterization, widely used in various fields of earth sciences and physical sciences, as well as extensively applied in industry.

Raman spectroscopy could provide relative information about the structure, number of layers, defects, stress and phonon spectrum of graphene, widely used in the research and application of graphene-based materials [111,112]. Raman spectroscopy has been used to investigate the structure and physical properties of graphene materials. It is employed to determine the number and orientation of layers and provides valuable information on edge atomic structure, disorder, defects, charge, and strain. In turn, this offers insights into all  $\text{sp}^2$ -bonded carbon allotropes since graphene serves as their fundamental building block. Typical Raman spectroscopy measurement setups feature back-scattering geometry, which can reveal structure, graphitization defects, and the presence of impurities such as amorphous carbon [113,114]. In 1970, Tuinstra and Koenig published a study on the raman spectrum of graphite and proposed that a single raman band was generated only around  $\sim 1575 \text{ cm}^{-1}$  due to the stretching of the graphite lattice in an infinite crystal [115,116]. This band fail to originate from disordered

carbon but rather from boundaries between small or large crystals. Later studies showed that the D band originated from the dual resonance process can explain the dual resonance process, which could be seen well that when the energy was increased, the resonance caused by the defects appeared to raman line and moved to a higher frequency. When the graphite single crystal was destroyed by the edge atom or miscellaneous atom, the D band appeared in the Raman spectrum with the structure of nano-carbon. Fig. 5(c) presented changes of raman spectra of nitrogen-doped carbon nanotubes (N-CNT) structure [117]. The presence of D1 ( $\sim 1370 \text{ cm}^{-1}$ ) band was related to the asymmetry of graphene mode, which was caused by the appearance of bound nitrogen atoms and marginal carbon atoms. Besides, the raman spectroscopic parameters of materials were related to their defects, which depended on synthesis conditions and subsequent treatments such as oxidation, functionalization, and annealing [118]. Fig. 5(d) illustrated variations of the edge for CNT12 after annealing at  $370^\circ\text{C}$  [119]. The appearance of the moderate bond-angle disorder was attributed to the steric repulsion of groups. At the same time, in the process of defunctionalization, the ordering of marginal carbon atoms led to the D1 band narrowing. The way of using mathematical analysis to explain the structural changes of carbon nanomaterials under different conditions has played an enhanced role in raman data [120,121].

### 2.3. Properties

Graphene, consisting of carbon atoms arranged in a hexagonal lattice with  $\text{sp}^2$  hybridization, has many excellent properties, including excellent mechanical properties, high thermal conductivity and high electrical conductivity [122]. Its strength exceeds that of many traditional

materials, and it has extremely high tensile strength and elasticity, which makes graphene have broad potential in nano-mechanical applications. Meantime, its high thermal conductivity makes it an ideal choice for efficient heat dissipation materials and thermal management devices, while its high thermal conductivity makes it have a wide application prospect in electronic devices, flexible electronics and optoelectronics. These excellent properties will have a far-reaching impact on many practical applications, from improving the performance of electronic equipment to enhancing the performance of engineering materials, as well as innovative applications in the fields of energy, medical care and environmental protection, which will be significantly promoted and improved [123]. Thus, on the basis of summarizing the existing research results, we sort out the key performance indexes of graphene and its specific applications in the different fields, and summarize them in Table 2, which covers the data of mechanical properties, electrical properties, thermal properties and chemical stability of graphene, thus making graphene show great potential in many high-tech fields.

From mechanical perspective, stable two-dimensional lattice structure and powerful covalent bonds of graphene endow it with high tensile strength and hardness, and can withstand external stress without being easily broken or fracture [124]. Typical carbon atom structure distribution diagram was shown in the Fig. 6(a) [125]. Graphene is a two-dimensional array of carbon atoms, where the atoms were connected to form a hexagonal structure. To date, some key mechanical parameters of graphene had been determined through various testing methods. Concretely, Lee et al. [30] developed nanoscale pressure marking technique to measure the intrinsic fracture strength of single-layer graphene, with the magnitude of Young's modulus being  $\sim 130$  GPa and  $\sim 1$  TPa. A specific nanoindentation on graphene film was shown in Fig. 6(b). Concurrently, they observed typical brittle crack behavior in graphene, with maximum tensile strain reaching  $\sim 5\%$ . For single-layer graphene, the approximate calculated value of in-plane Young's modulus using the planar isotropic model was usually around 1000 GPa, making them ideal reinforcement materials in composite materials

**Table 2**  
A summary on literature studies for graphene in properties and applications.

No	References	Property	Parameter size	Primary applications
1	Panagiotis Gavallas et al. [29]	stiffness tensor; Coefficient of variation	1080 GPa, 450 GPa, 54 GPa, 1GPa; 9.5%, 2.8%	Automobile industry
2	C. Bessaguet et al. [145]	Percolation thresholds; permittivity	4.2, 3.19 vol %; 2.7, 83, 210	aeronautical and space industries
3	M. Tahani et al. [147]	The $E_g$ value for monolayer PG; the elastic modulus of monolayer PG	2.4 Ev; 257.40 N/m	metal-free catalyst for CO oxidation
4	Mohamad Amin Bin Hamid et al. [148]	The charge accumulation	$5.645 \times 10^{-4}$ e	High-frequency electronic device
5	C. Justin Raj et al. [149]	ID/IG; EG-SA electrode	$1.182; \sim 21 \mu\text{Fcm}^{-2}$	supercapacitor
6	Alexander A. Balandin et al. [135]	Thermal conductivity	$(4.84 \pm 0.44) \times 10^3$ to $(5.30 \pm 0.48) \times 10^3$ W/mK	photoelectric detector
7	Changgu Lee et al. [30]	Average modulus of elasticity ; Breaking strength	$1.0 \pm 0.1$ TPa; $42\text{Nm}^{-1}$	aerospace
8	Jinglei Xiang et al. [150]	in-plane thermal conductivity through-plane conductivity	$178 \pm 12$ W/mK $1.28 \pm 0.12$ W/mK	2D heat conduction material

[126]. Graphene nanoplates (GNPs), composed of a few graphene layers (typically up to 10 layers) connected by weak van der Waals (vdW) interaction, are the potential substitutes for single-layer graphene, and usually obtained in the final stage of graphene production [29]. GNPs exhibited significant variations in their mechanical behavior both in-plane and out-of-plane. The calculated values of their stiffness modulus may vary depending on the method employed and the thickness of the multilayer graphene [127].

In comparison to single-layer graphene, double-layer graphene sheets have higher stiffness and strength, and the calculated values of mechanical properties of them will change significantly with the increase in layers [128, 129]. In order to accurately calculate the mechanical properties of double-layer carbon graphene sheets, molecular structural mechanics, as one of the most commonly used calculation methods, often simulated and predicted mechanical properties of materials by numerically simulating interaction between atoms [128]. The results of stiffness and strain curves of graphene sheets demonstrated that, as shown in Fig. 6(c), Young's modulus depended heavily on the change of strain, and there was an obvious inverse proportional function relationship between them. Inversely, the number of layers of graphene sheets has no significant effect on Young's modulus. Furthermore, the stiffness varying with thickness was calculated by using representative surface elements. As could be seen from Fig. 6(d), when the interlayer distance decreased, its value increased significantly. With regard to in-plane stiffness, the out-of-plane behavior of GNPs is controlled by vdW interactions and is much lower than the in-plane stiffness. The number of layers affects the volume of the plane. When number of layers was large, the modulus should approach that of graphite. In addition, it was discovered that the mechanical properties of double-layer graphene could be effectively adjusted by changing the rotation angle [129]. Fig. 6(e) indicated the effect of representative rotation angles ( $0^\circ, 10^\circ, 15^\circ, 20^\circ$  and  $30^\circ$ ) on the mechanical properties of double-layer graphene. From the tensile stress  $\sigma$ -strain  $\epsilon$  curve, it was observed that the double-layer graphene was characteristic by linear elasticity. When  $\theta_{\text{upper}} = 0$ , its tensile strength and tensile properties reached to the maximum. Instead, a progressive fracture could be detected. Meanwhile, fracture strength ( $\sigma_f$ ) and Young's modulus ( $E$ ) of double-layer graphene was also investigated under different rotation angles. In range of  $0^\circ$  to  $30^\circ$ ,  $\theta_{\text{upper}}$  was inversely proportional to  $\sigma_f$ , but had nothing to do with  $E$ . Based on this series of results, it was easy to indicate that the stress-strain curve included linear and nonlinear stages, and presented a gradual brittle fracture behavior, which was attributed to the different mechanical properties of each layer of graphene.

Analogously, the special structure of graphene and the arrangement of carbon atoms also provide the basis for its high thermal conductivity and electrical conductivity [130]. With regard to thermal conductivity, the close arrangement of carbon atoms in graphene facilitates transfer heat energy in an efficient manner, which is achieved through the vibration between atoms and the conduction of electrons [131, 132]. This endowed graphene with excellent thermal properties and thermal stability, thus being widely used in fields of thermal conductivity materials, electronic devices and energy storage [133]. Especially, when used to improve the thermal conductivity and electromagnetic interference shielding effect of polymer composites, graphene is usually selected as the preferred filler [134]. Graphene possessed high thermal conductivity, especially single-layer graphene, which could reach up to  $\sim 5000$  W/mK [135]. The thermal stability of graphene was related to its layers. Furthermore, it had also been reported that the thermal stability of graphene was closely related to the interactions between its layers in atmosphere. Nan et al. [136] investigated the thermal stability of graphene in argon using raman mapping and AFM, and result demonstrated that multilayer graphene exhibited better stability. It was worth noting that thermal stability of graphene was also affected by factors such as time, atmosphere, and fabrication methods. Graphene nanofluids could further improve thermal conductivity of graphene by forming a thermal conduction channel, making it a candidate for the

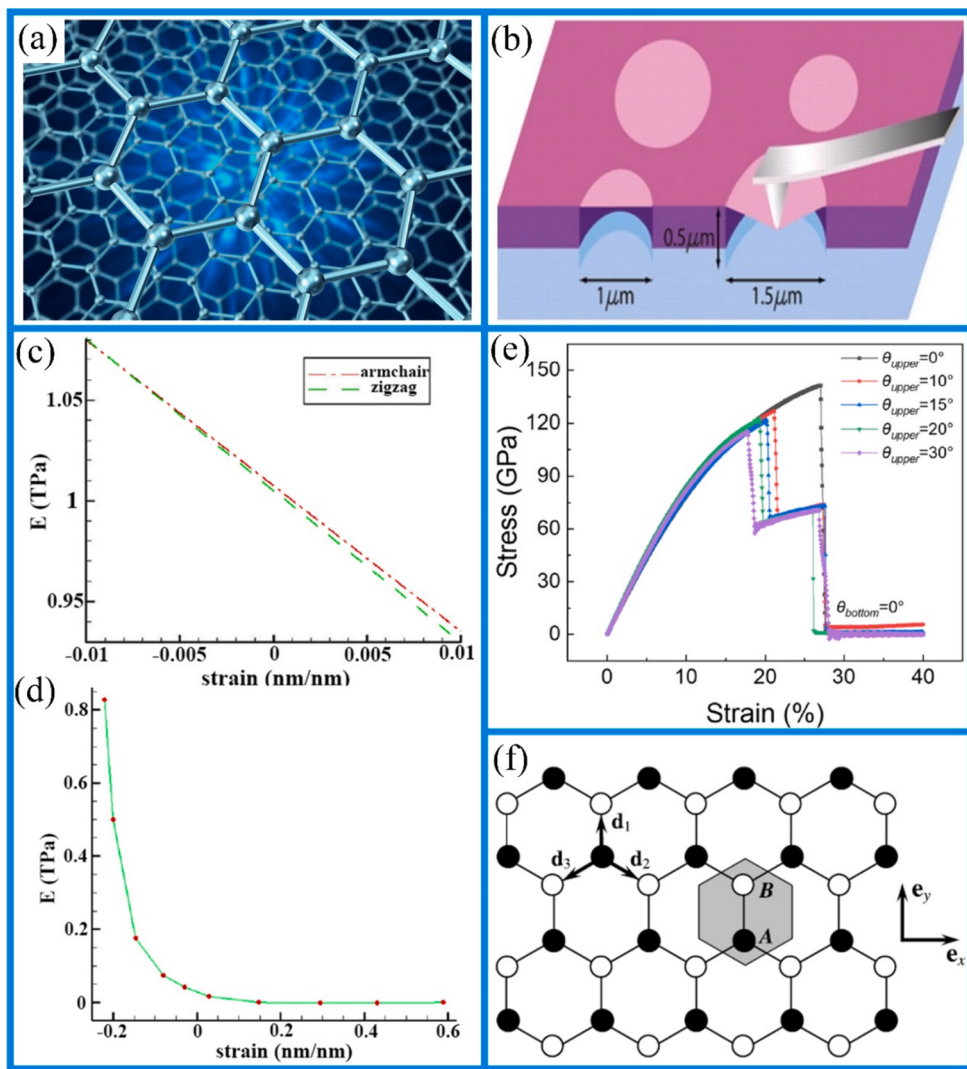


**Fig. 6.** (a) Schematic diagram of carbon atoms in graphene associated nanostructures; Reprinted with permission from Ref.[125]. (b) Illustration of the nano-indentation in a suspended monolayer graphene membrane; Reprinted with permission from Ref.[30]. The stiffness–strain curves in plane (c) or thickness-wise (d); Reprinted with permission from Ref.[128]. (e) The stress–strain curves for bilayer graphene samples with rotation angles from 0° to 30°; Reprinted with permission from Ref.[129]. (f) The vertical view for 2D hexagonal lattice structure; Reprinted with permission from Ref.[140].

next generation of heat transfer media. They were usually combination of nanoparticles with low volume fractions and good liquid dispersion, holding great potential for achieving high efficiency, energy saving, and cost reduction in thermal management devices [137]. In addition, research in recent years have confirmed that the usage of modifying graphene fluoride was considered as feasible strategy for effective enhancement in the thermal stability of polymer materials. After fluorination treatment, original properties of graphene have been adjusted and expanded, including an improvement of the chemical stability and an enhancement for thermal stability, as well as changed electronic structure of graphene affecting its electrical conductivity. This inspires us focusing on the developing new synthesis methods and application technologies to make full use of the potential of fluorinated graphene [138].

In addition to being an excellent heat dissipation material and preparation material for thermal management devices, graphene has a wide application prospect in the fields of electronic devices and flexible electronics due to its excellent characteristics such as high conductivity, high mobility and low resistivity [139]. In graphene, each carbon atom can contribute  $\pi$  electrons, and due to its long-range conjugated network structure, electrons can move freely in the lattice without hindrance.

This endowed graphene with an extremely high theoretical electron mobility of up to 250,000 cm<sup>2</sup>V<sup>-1</sup>s<sup>-1</sup>. Particularly, the sp<sup>2</sup> structure of graphene with 2p<sub>z</sub> orbitals perpendicular to the plane (Fig. 6(f)) enabled high carrier mobility (electrons and holes), with a theoretical conductivity of single-layer graphene at around 1,000,000 S/cm [140]. Graphene exhibited intrinsic semiconductor-like arrangements with fermi level and Dirac-like linear spectra. Bilayer graphene would have a parabolic spectrum with a gap of approximately 1.6 meV. When considering the band structure of graphene with three or more layers, they were formed by multiple charge carriers that exhibit overlapping conduction and valence bands. The percolation threshold depended only on the aspect ratio of conductive particles [141,142], and the larger the particle diameter ratio, the lower the percolation threshold. For example, the percolation threshold of carbon black was around 8–10 vol % [143], while that of CNTs was less than 0.4 vol% [144]. Additionally, the logical shape of graphene makes it easier to modify electrocatalytic processes in a beneficial way, and it possessed remarkable electrochemical reaction mechanisms, whether as an auxiliary catalytic material or non-metallic active electrocatalyst [145,146].

### 3. Graphene oxide

#### 3.1. Preparation methods

Graphene oxide is carbon material with similar chemical, optical, and electrical properties to graphene based on framework of graphene [151]. However, from typical structures of graphene (a) and GO (b) as shown in Fig. 7 [152], the difference between them is the existence of oxygen atoms in GO, thus resulting in the formation of a series of active oxygen-containing groups for GO, including epoxy and hydroxyl groups on the plane, as well as carbonyl and carboxyl groups at edges [153,154]. These functional groups contribute to endowing it with high negative charge density and hydrophilicity, which has garnered

significant attention [155]. For example, in process of graphene-modified CuO nanoparticle synthesis, the surface functional groups between GO interacted with CuO nanoparticles, thus realizing interface connection of composites and improving the mechanical properties and electrical conductivity of materials [64]. In addition, GO synthesized via electrochemical oxidation method was simple and efficient, which made it high conductivity (as illustrated in Fig. 7(c)), which was of great significance for reducing cost, mass production and expanding its application fields [156]. Clearly visible, besides enhanced performance for nanoparticle, simplicity of production process is of great significance for reducing cost, improving efficiency, ensuring quality, thus facilitating large-scale production as well as promoting technical application. More detailed information about merits and demerits for preparation

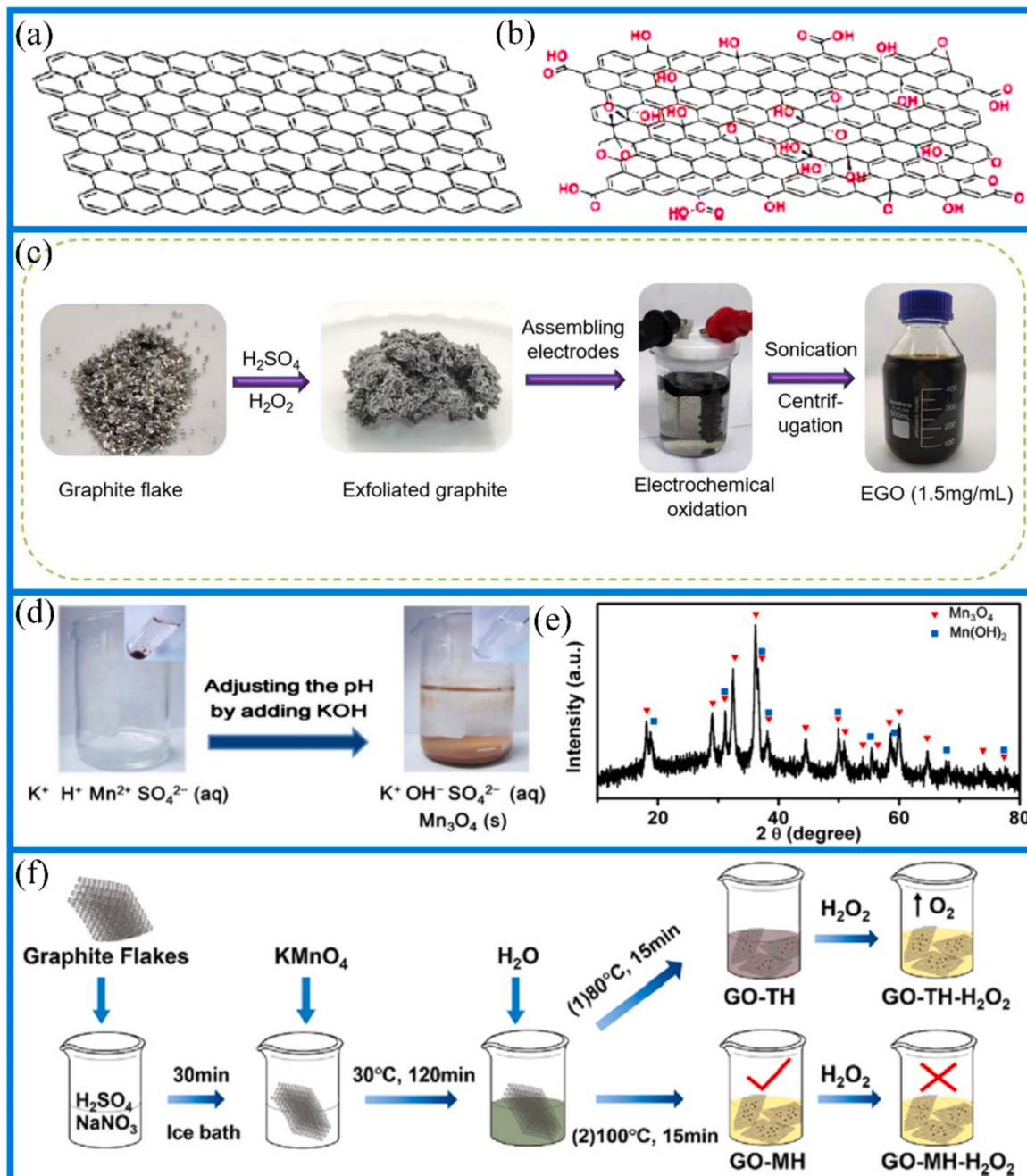


Fig. 7. Typical structures of graphene (a) and GO (b); Reprinted with permission from Ref.[152]. (c) Representative graph of each step of fabrication process for GO; Reprinted with permission from Ref.[156]. (d) Schematic drawing of wastewater post-treatment; (e) XRD spectrum for the precipitation containing Mn; Reprinted with permission from Ref.[160]. (f) The schematic drawing of synthesis process for GO; Reprinted with permission from Ref.[163].

methods including Brodie's method, Staudenmaier's method [157], Tour's method [158], Hummers method, and improved Hummers method are summarized in Table 3.

The earliest method to preparing graphene oxide was reported by Brodie in 1859 [152]. Nevertheless, this approach has several inherent constraints, including intricate operational procedures, elevated environmental contamination risks and low product purity, which collectively restrict its extensive deployment in the synthesis of GO. In order to make up for these shortcomings, in 1958, Hummers method was developed for synthesizing GO [159]. Subsequent researchers have continuously improved and refined the methods for producing GO based on the Hummers method. Utilizing an enhanced Hummers method, the graphite flakes of 3  $\mu\text{m}$  to 20  $\mu\text{m}$  can be completely converted into single-layer GO [69]. Importantly, the synthesis process of GO can be integrated with the purification step into a continuous process, making it possible to produce GO in large quantities at a relatively low cost [160]. The low cost was reflected in the effective treatment of wastewater collected during the synthesis and purification of GO. As shown in Fig. 7(d), with the Mn<sup>2+</sup> ions within the waste water converting into the precipitate upon addition of KOH, they could be readily removed.

**Table 3**  
Summary on outline of advantages and disadvantages of methods for preparing GO.

Preparation technology	Source materials	Advantages	Drawbacks	Ref.
Brodie's method	Slurry graphite HNO <sub>3</sub> ; KClO <sub>3</sub>	First synthesis	Complicated operation; Risk of explosion; low-purity	[152]
Staudenmaier's method	Slurry graphite; H <sub>2</sub> SO <sub>4</sub> / HNO <sub>3</sub> ; KClO <sub>3</sub>	Improved reaction efficiency	Complicated operation; Risk of explosion	[157]
Hummers	graphite; K <sub>2</sub> MnO <sub>4</sub> ; NaNO <sub>3</sub> ; H <sub>2</sub> SO <sub>4</sub> ; H <sub>2</sub> O <sub>2</sub>	Short experiment time; Can be mass-produced	Have security risks.; Will release toxic gases; Chemicals are difficult to remove	[159]
Tour's method	Graphite; KMnO <sub>4</sub> ; H <sub>3</sub> PO <sub>4</sub> ; H <sub>2</sub> SO <sub>4</sub>	High oxidation rate and product quality; Temperature control and no harmful gases	There are security risks, environmental pollution and unstable yield	[158]
Improved Hummers method using small graphite flakes	graphite powder (1.0 g); concentrated H <sub>2</sub> SO <sub>4</sub> (23 mL); KMnO <sub>4</sub> (3.0 g)	High yield; high-quality; low cost; Can be produced on a large scale.	There are requirements for the size of raw materials	[69]
Improved Hummers method using coconut shell waste	graphite-based coconut charcoal (1 g); NaNO <sub>3</sub> (0.5 g); H <sub>2</sub> SO <sub>4</sub> (25 mL); KMnO <sub>4</sub> (3 g)	Simple operation; Low cost	Difficult to remove impurities	[161]
Improved Hummers method without NaNO <sub>3</sub>	graphite powder; H <sub>2</sub> SO <sub>4</sub> (27 mL); H <sub>3</sub> PO <sub>4</sub> (3 mL); KMnO <sub>4</sub> (1.32 g)	Reduce cost and no toxic gas emission	Incomplete oxidation for graphite	[162]
Improved Hummers method without H <sub>2</sub> O <sub>2</sub>	flake graphite (1.0 g); K <sub>2</sub> MnO <sub>4</sub> (4.0 g); NaNO <sub>3</sub> (0.5 g); H <sub>2</sub> SO <sub>4</sub> (30 mL)	Safety, environmental protection, simplicity and low cost	High requirements for parameter adjustment	[163]

Subsequently, the sediment was characterized by XRD, as showed in Fig. 7(e). The presence of Mn<sub>3</sub>O<sub>4</sub> containing small amount of Mn(OH)<sub>2</sub> further indicated conspicuous efficiency of removing Mn<sup>2+</sup> ions from the waste water. Moreover, with the usage of the graphite produced from the coconut shell waste to synthesize GO, Hummer method has been improved to be also used to the low cost manufacturing [161]. Properly, safety also performed an indispensable role in the production process of GO. NaNO<sub>3</sub> was not used when GO was synthesized this method adopted by Zaaba et al. [162], which could reduce the cost and release toxic gases, thereby enhancing the overall safety factor of producing GO. Simply adjusting the experimental parameters is also helpful to achieve this effect. Zhou et al. [163] prepared high quality GO without H<sub>2</sub>O<sub>2</sub> through adjusting the reaction temperature/time and the dosage of concentrated H<sub>2</sub>SO<sub>4</sub>, which avoided dramatically exothermic reduction reaction. The detailed process of utilising the modified H<sub>2</sub>O<sub>2</sub>-free Hummers' method was illustrated in Fig. 7(f). In comparison to the traditional method, improved method could ensure a higher degree of oxidation and abundant oxygen-containing functional groups. Besides, advantages of this method including simple, low-cost, and safe, made it have great potential in industrial production and green energy carbon materials [164]. Unfortunately, both these methods and the original Hummers method fail to achieve complete conversion from graphite to GO [165,166]. To sum up, a method of completely converting graphite into GO has not been found yet, but by improving reaction conditions and employing diverse preparation methods, the conversion rate and purity can be improved, and higher quality GO can be obtained.

### 3.2. Characterization

Due to the wide application of GO in various processes and applications, its structure has been investigated through a series of characteristic techniques [167,168]. The characteristic of GO lies in the presence of epoxy groups on its surface, such as epoxy, hydroxyl, and carboxyl oxygen [169]. The accuracy of identifying functional groups using X-ray photoelectron spectroscopy (XPS) becomes increasingly important. An oxygen containing functional group as a more reactive substance was observed, which contributed to obtain more reaction information on O 1 s spectra. Kwan et al. [81] identified the functional groups present in GO produced by the Hummer's process by in-situ thermal annealing and XPS. As showed in Fig. 8(a), the result of comparison of C 1 s and O 1 s spectra in functional groups showed when using the O 1 s spectra, changes in the composition of the functional groups were more clearly discerned which further emphasized significance of utilizing O 1 s spectrum in the analysis process. Additionally, the binding energies of the O 1 s spectra also showed the existence of four types of oxygen functional groups, namely hydroxyls, epoxides, carbonyls and carboxyls. Among of them, formation temperatures of carboxyl were between 543 and 561 K, as showed in Fig. 8(b). Although we hope to determine the canonical model of GO in order to reliably identify oxygen functional groups on GO and develop more efficacious chemical techniques to remove oxygen groups from GO, complications arise in the process of achieving this goal.

High-resolution images also play an important role in detection and characterization of GO, which can clearly show the morphological characteristics, microstructure, defects and nano-scale characteristics of samples, thus deeply understanding structure and properties of GO. SEM, as important complementary techniques for material characterization, which can fully reveal the morphology, structure and properties of materials. Yuan et al. [170] synthesized GO-MnPO<sub>4</sub> H<sub>2</sub>O composites using modified Hummers method, and investigated the formation mechanism of it through the way of combination computer simulations with experimental explorations. The result showed that uniform petal MnPO<sub>4</sub> H<sub>2</sub>O particles in size of  $\sim$ 1.2  $\mu\text{m}$  were formed on GO nanosheets. Subsequently, Mn<sup>2+</sup> ions generated by oxidation reaction were distributed around oxygen atoms of GO sheet through electrostatic adsorption and further reacted with oxygen-containing functional groups of GO.

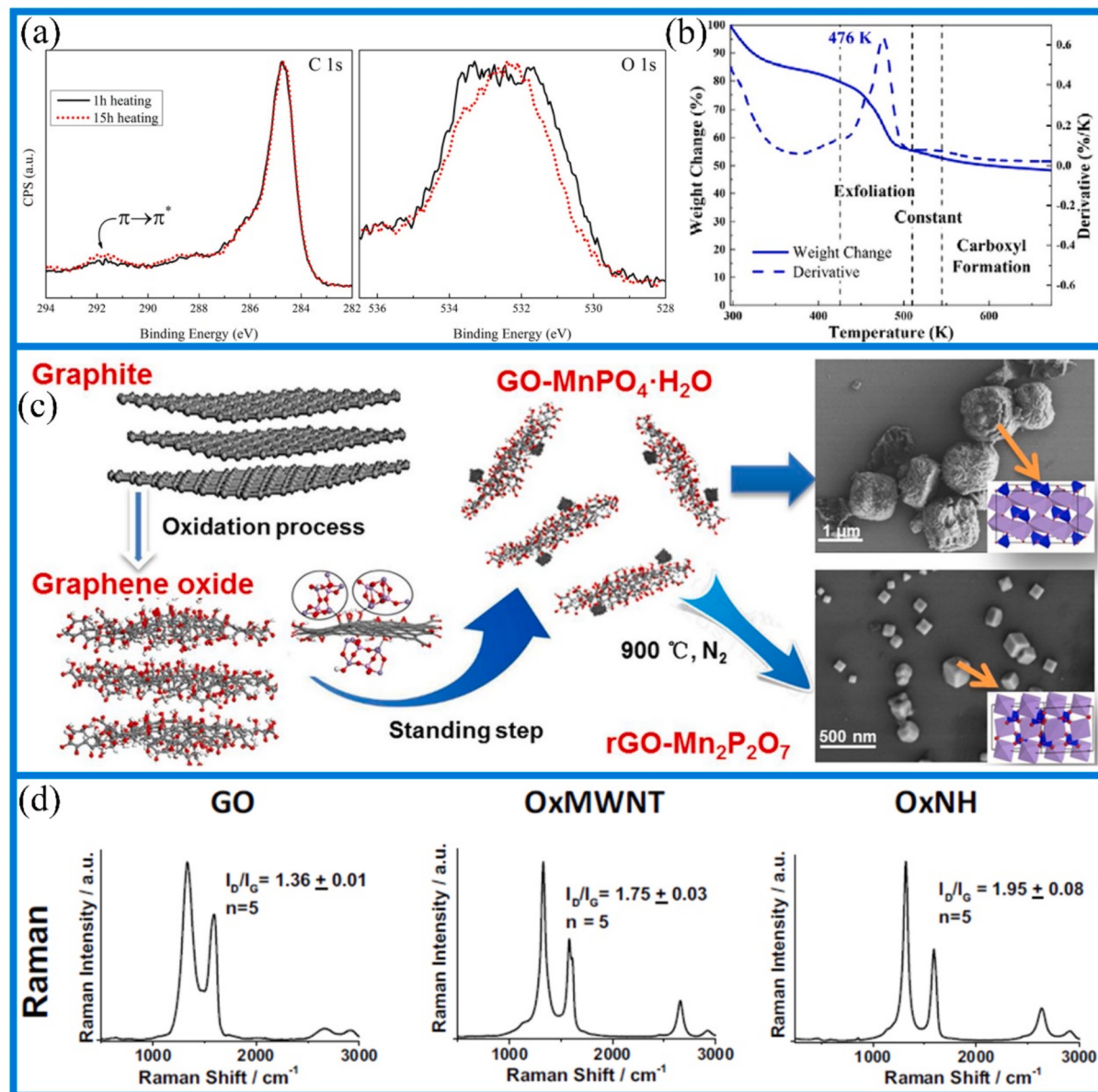


**Fig. 8.** (a) C 1 s and O 1 s spectra of NaOH mixed with GO; (b) Diagram of thermogravimetric analysis results for GO; Reprinted with permission from Ref.[81]. (c) Synthesis process for GO-MnPO<sub>4</sub>·H<sub>2</sub>O composite material; Reprinted with permission from Ref.[170]. (d) Raman intensity of starting oxidised carbon nanomaterials: GO, OxMWNT and OxNH; Reprinted with permission from Ref. [180].

Ultimately, formed GO-Mn<sup>2+</sup> served as the anchor site for the growth of MnPO<sub>4</sub> H<sub>2</sub>O, thus generating the GO-MnPO<sub>4</sub> H<sub>2</sub>O composite. The specific information of the synthesis procedure of GO-MnPO<sub>4</sub> H<sub>2</sub>O composite material was depicted in Fig. 8(c). The composite material synthesized by this method showed better performance than single component, and could be further used to produce conductive materials, supercapacitors and other functional materials as precursors. Besides analyzing the morphology, it was also very important to accurately detect and quantify the existence and concentration of GO [171,172]. Ultraviolet-visible spectroscopy (UV-Vis) could indirectly determine existence and concentration of GO by measuring its absorption peak in solution, which could reveal chromophores, and are molecular components that contain easily excited non-bonding electron pairs. This includes functional groups containing oxygen. Measurement can be performed on liquid or gas samples. Thus, graphene and GO must be dissolved in suitable solvents. UV-visible spectra of graphene and GO typically show peaks related to aromatic C-C bonds. The peak values for

GO and graphene are close to 230 nm and 270 nm respectively, and for GO samples, a peak related to the C=O bond is also observed around 300 nm. UV-Vis has been used to determine the optical absorption properties of GO films [173]. It is well known that the UV-Vis absorption spectrum of GO exhibits two features [174]: the maximum at 231 nm corresponds to the  $\pi \rightarrow \pi^*$  transition of aromatic C=C bonds, while the shoulder peak at ~ 300 nm corresponds to the  $n \rightarrow \pi^*$  transition of C=O bonds [175,176]. Additionally, during the thermal treatment of GO, carbon fragments such as CO and CO<sub>2</sub> were released along with H<sub>2</sub>O. In contrast, graphite did not show any mass loss, explaining the absence of oxygen-containing functionalities [177].

Similar to UV-Vis, raman spectroscopy, as another commonly used spectroscopy method, is often used to study the lattice structure, impurities and defects of graphene oxide, which is more suitable for non-destructive analysis [178,179]. Raman spectroscopy could provide strong support for its biological and medical exploration, when evaluating the biodegradability of GO [180]. In a study of Newman et al, the

physical and chemical changes of carbon oxide nanomaterials during degradation were closely monitored by using a series of techniques such as raman spectroscopy, transmission electron microscopy (TEM) and AFM. The characterization result of the Raman spectra for GO, oxidised multiwall carbon nanotubes (OxMWNT) and carbon nanohorns (OxNH) were illustrated in Fig. 8(d). Compared with G-band, the scattering intensity of D-band was enhanced, which indicated that there were defects and the material was expected to be oxidized. Furthermore, due to its unique physicochemical features, GO would degrade faster than the other nanomaterials such as OxNH and OxMWNT. Analogical to the oxygen-containing functional groups of GO, electronic structure of graphene could also be uniquely captured in its raman spectrum [181]. Observing the variation of the 2D band with number of layers under excitation at 514.5 nm and 633 nm, obviously, in the comparison to monolayer graphene, bilayer graphene exhibited broader and upshifted 2D energy band. Besides, a further increase in layers resulted in a significant reduction of the relative intensity of the lower frequency 2D peaks, which could contribute to distinguish a single layer, bilayer and few (less than 5) layers of graphene [182,183]. In general, different detection methods cooperate with each other in the characterization and analysis of graphene oxide, and through multi-directional analysis of the sample from different angles and levels, the properties and characteristics of the material can be comprehensively understood, providing the basis and support for the application and research of the material [184,185].

### 3.3. Properties

GO has in recent years attracted widely extensive attention of researchers due to it showing excellent thermal conductivity and stability when it is introduced into polymer materials [186,187]. More summaries about corresponding performance indexes and their application area are listed in Table 4, where containing its electrical conductivity, thermal conductivity, mechanical strength and soon on. GO is one of the

functionalized types of graphene, and it has been widely used in composite materials due to the easy reactivity of oxygen functional groups (OH, COH, and COOH) in graphene sheets with monomers [188]. However, the main drawback of using GO is the generation of structural defects and gaps, which impede the  $sp^2$  lattice characteristics of graphene and significantly deteriorate its electronic performance and conductivity. This results in low dielectric loss and poor electrical performance [189,190]. Due to a presence of surface functional groups on GO, it possesses some distinct properties that are different from pristine graphene. Extensive studies on the mechanical properties of GO have been conducted through experimental and theoretical methods [191,192]. In a work of Guo et al. [193], significant improvement in toughness and crack resistance of materials via addition of GO had been confirmed. Prepared multifunctional polyimide composite film showed high in-plane thermal conductivity, excellent electromagnetic interference shielding effect as well as favorable tensile strength. Among them, GO/expanded graphite (GO/EG) as the top material, played a great role in heat conduction and electromagnetic interference shielding, which was ascribed to the reason that brittleness of EG film was solved by optimizing the ratio of GO to EG, thus achieving balance of mechanical properties, thermal conductivity and electromagnetic interference shielding performance.

As a derivative of graphene material, GO with excellent barrier properties can effectively shield electrons, heat and gas, and has excellent thermal conductivity, so it has great application potential [194–196]. Particularly, with the emergence of 5th generation mobile communication technology (5G), improved inherent data transmission bandwidth of 5G, ameliorative terminal link equipment and elevated real-time data exchange, led to huge heat accumulation, which promoted and required development of high thermal conductivity and electrical insulation materials [194,196]. To ensure the working stability and reliability of 5G equipment as well as the security of transmitted information and data, designing and preparing new high-performance electromagnetic interference shielding materials played a decisive role in meeting the shielding requirements of new electronic products in the 5G era, even accelerating the universal applicability of 5G communication technology [195].

Moreover, the excellent wear and corrosion resistance of GO can not be ignored. Researchers had confirmed that GO coatings prepared by electrodeposition in NaCl electrolyte have a corrosion rate six times lower than pure copper, fully showing the protective ability of GO coatings. Therefore, GO is considered as a strong candidate for protective coatings with excellent anti-friction and anti-corrosion properties [197]. However, many oxidized functional groups on the surface of GO could form strong interaction with the water molecules, showing strong hydrophilicity, which resulted in forming large agglomerates. Specifically, the hydrophilicity of GO varied depending on the presence of oxygen functional groups in the oxidized and non-oxidized regions, thereby resulting in hybridization between  $sp^3$  and  $sp^2$  orbitals [10]. Functionalized GO (amidation, esterification, sulfonation, etc.) was helpful to improve the dispersibility of graphene in various solvents (water solvents and organic solvents). For instance, amino acids were chosen to the fabrication of bio-functionalized graphene [198]. As shown in Fig. 9a, firstly carboxylic acid, hydroxyl and epoxy functional groups was introduced to carbon layers of graphene by using chemical oxidation technology to fabricate GO. Subsequently, nucleophilic reactions and condensation reactions occurred between amino groups of amino acids and epoxy groups and carboxyl groups on surface of GO. The obtained amino acid functionalized graphene displayed stable dispersibility in water and common organic solvents, which made it have a wide application prospect in the fields such as electronic devices, catalysts, energy storage, sensors, medical applications and sewage treatment.

Due to its high conductivity and mobility, GO can also be employed in the fabrication of high-speed electronic devices, including scalable flexible electronics devices and high-speed transistors. Thus, it is very

**Table 4**  
A summary on literature studies for GO in properties and applications.

No	References	Property	Parameter size	Primary applications
1	Songdi Zhang et al. [201]	Specific surface area of monolayer GO	2418 m <sup>2</sup> /g ; ~2391 ( $\pm 1292$ ) m <sup>2</sup> /g	Catalyst support
2	Seungyoung Park et al. [202]	Electric conductivity of VrGO; Out-of-plane thermal conductivity	4000 S/m; 6.202 W m <sup>-1</sup> K <sup>-1</sup>	Supercapacitor
3	Junjie Chen et al. [203]	Thermal conductivity	72 W/(mK), 670 W/(mK)	Heat dissipation coating
4	Ana Paula Martins Leandro et al. [204]	Electrical conductivity	4800 Sm <sup>-1</sup>	Electrochemical energy storage
5	Ji Won Suk et al. [192]	effective Young's modulus; prestress	207.6 $\pm$ 23.4 GPa; 76.8 $\pm$ 19.9 MPa	Aerospace
6	Wei Gao et al. [205]	Electrical conductivity	$\sim 0.5$ S m <sup>-1</sup> , 2.02 $\times$ 10 <sup>4</sup> S m <sup>-1</sup>	Organic light emitting diodes
7	Khira Zlaoui Riahi et al. [206]	Dielectric constant	10 <sup>10</sup> F m <sup>-1</sup>	Supercapacitors
8	D. Torres et al. [207]	Capacitive value	49.2F g <sup>-1</sup> , 12.0F g <sup>-1</sup> , 7.2F g <sup>-1</sup>	Supercapacitor

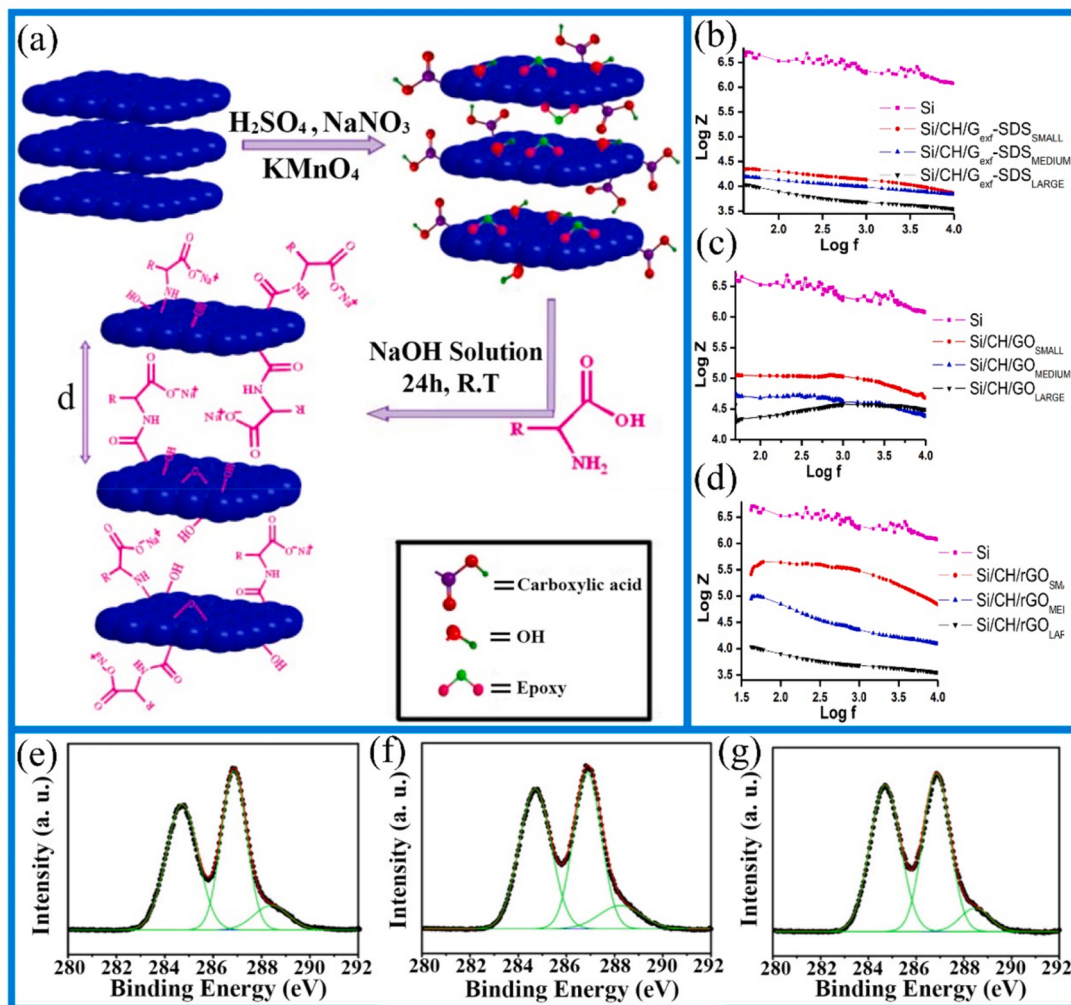


**Fig. 9.** (a) Synthesis for GO and graphene functionalized with different amino acid types; Reprinted with permission from Ref.[198]. Functional relationship between Log Z and Log f for  $\text{G}_{\text{ext}}\text{-SDS}$  (b), GO (c) and rGO (d); Reprinted with permission from Ref.[199]. XPS spectra of C 1 s for GO supernatants collected after different conditions: S1 (e), S2 (f) and S3 (g); Reprinted with permission from Ref.[200].

significant to further explore the influencing factors of the a.c conductivity of GO. In the work of Deka et al, it was demonstrated that the transverse dimension of GO sheet is in positive proportion to its a.c conductivity [199]. Specifically, as showed in Fig. 9, with increase of lateral dimensions, impedance of the sodium dodecyl sulphate (SDS) mediated exfoliated graphene  $\text{G}_{\text{ext}}\text{-SDS}$  (b), GO (c) and rGO (d) decreased significantly, thus showing higher conductivity. It was explained that compared with the smaller sheet, the sheet with larger transverse dimension has more surface area, which can reduce the discontinuity in the system and provide more conductive channels for electron movement, thus increasing the conductivity. Moreover, the a.c conductivity of GO was also affected by factors such as oxidation degree and impurities. During oxidation process, a large number of defects and impurities would be introduced, which would affect the transmission of electrons. Therefore, it was necessary to control the degree of oxidation when preparing GO sheets in order to obtain higher conductivity. Chen et al. obtained GO nanosheets with controllable size distribution and C/O ratio via the centrifugation technique, and investigated optical property of the products of GO nanosheets with different size distributions by XPS [200]. The result showed that the C/O atomic ratios of three supernatant sample collected under different speeds increase from 1.88 (e), 2.28 (f), to 2.31 (g), as showed in Fig. 9, which indicated the C/O ratio increases with the size of GO nanosheets increasing. The phenomenon could be explained by that GO nanosheets with small size

having a high degree of oxidation, meaning a high oxygen content. Ulteriorly, based on a density functional theory, it can also be explained that the presence of a high oxygen content in graphene sheet implied the existence of an increased number of  $\text{sp}^3$  bonds between O and C atoms, thereby facilitating the formation of numerous relatively small  $\text{sp}^2$  carbon clusters with a comparatively large band gap.

#### 4. Graphene/elastomer nanocomposites

##### 4.1. Preparation methods

Nanocomposites composed of at least one or more fillers of nanoscale dimensions, can prevent premature failure in initial applications, thereby improving their toughness and elongation [208]. Nanoscale fillers can provide additional advantages to the base polymer matrix, including enhanced mechanical strength, thermal stability, chemical stability, antibacterial and anticancer properties [209–212]. Elastomers, as a fascinating class of materials capable of elastic deformation at strains, can be added to nanocomposites to enhance performance including mechanical characteristics, thermal properties, and higher conductivity [213]. In particular, process for preparing graphene/elastomer nanocomposites have been reported in related literature, as illustrated in Fig. 10(a). The existence of elastomer was helpful to regulate the dielectric properties of composites, such as dielectric

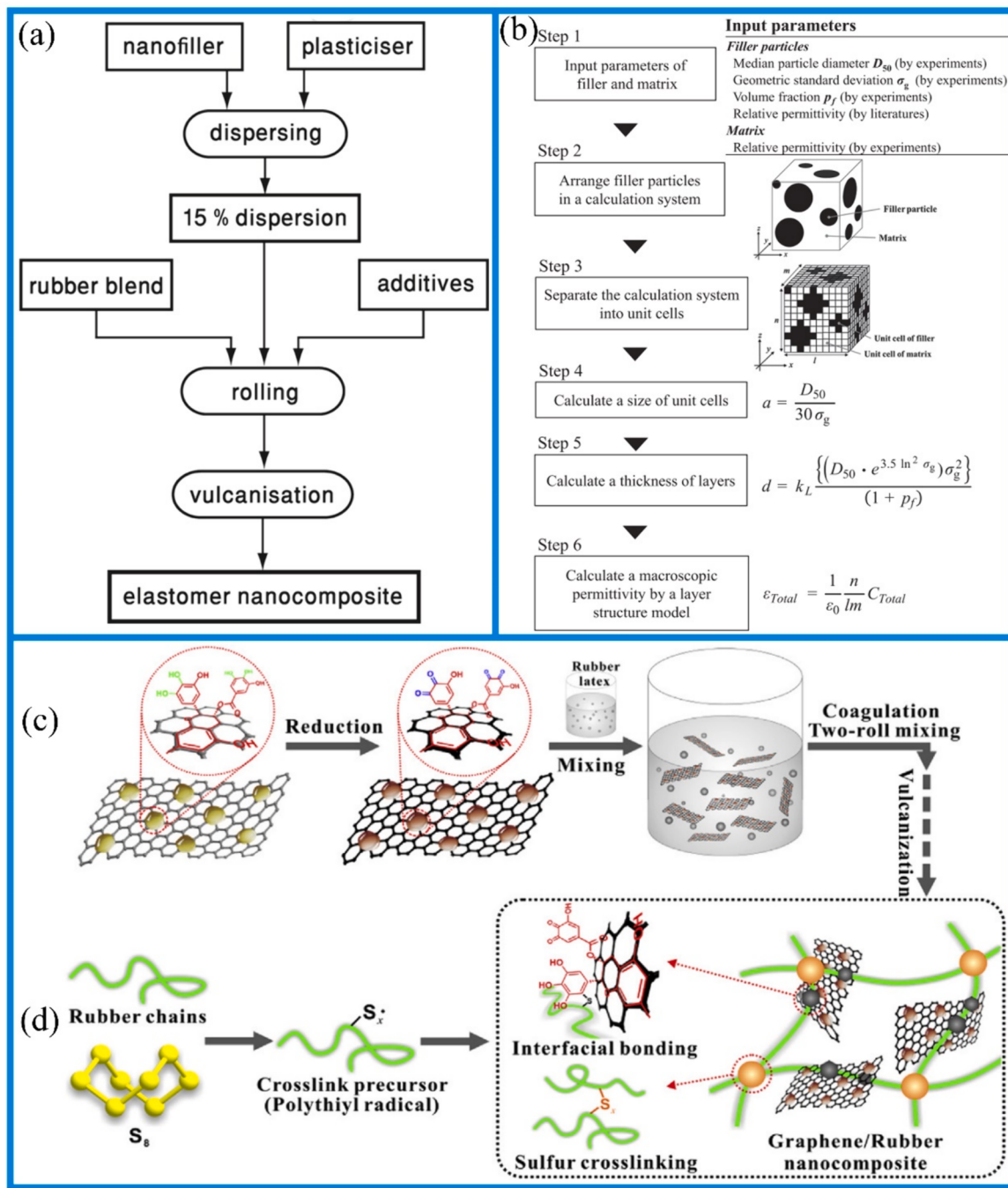


**Fig. 10.** (a) Manufacturing process flow chart of elastomer nanocomposites; Reprinted with permission from Ref.[213]. (b) Flow chart of estimating macro dielectric constant via the proposed model; Reprinted with permission from Ref.[214]. Schematic drawing about preparing for graphene/rubber nanocomposites (c) and formation mechanism of their covalent interface (d); Reprinted with permission from Ref.[216].

constant and dielectric loss, and made them have better insulation performance and electric energy storage capacity. To quickly and effectively evaluate the effects of different elastomer components and structures on electrical conductivity and dielectric constant, as shown in Fig. 10(b), the new model for estimating macroscopic dielectric constant was proposed to predict the dispersion state of filler particles in particle composites, thus contributing to guiding materials in synthesis and preparation procedures [214]. Furthermore, graphene shows unparalleled physical properties, such as excellent mechanical performance, and has been proposed as an efficient reinforcing material for elastomers [7,215]. In a study of strong covalent interface between graphene and styrene-butadiene rubber (SBR) nanocomposites as shown in Fig. 10(c),

dynamically energy loss of prepared graphene/rubber composites was significantly lower compared to the carbon black-filled rubber [216]. Fig. 10(d) illustrated the formation mechanism of the covalent interface between graphene and rubber matrix. During this process, the interfacial crosslinking between *ortho*-quinones modified graphene and rubber chains constrained the restacking of the nanosheets very effectively, thus resulting in excellent dispersibility of graphene. It should be noted that different dispersion states of inorganic fillers could attribute distinct characteristics to the resulting nanocomposites. Choosing appropriate preparation methods could achieve this goal. The most important four kinds of preparation techniques described in the literature would be discussed next, such as melt mixing, solution blending, latex blending,

and in-situ polymerization, with emphasis on discussion about advantages and drawbacks of these technologies displaying in [Table 5](#).

Melt mixing commonly used process for preparing graphene-based nanocomposites is to disperse the fillers in a molten state in an elastomeric matrix by application of shear forces [217]. Fillers such as CNTs and carbon fibers are usually compounded with plastics including polypropylene, polystyrene, polycarbonate as well as polyamide. For example, the single dispersion of CNTs composed of rolling into a cylindrical shape for graphene sheets in the matrix was challenging, which was highly dependent on their atomic arrangement [218]. On this basis, CNTs could be divided into three types of structures: zigzag, armchair and chiral structures ([Fig. 11\(a\)](#)). Sui et al. [219] prepared the thermoplastic polyurethane (TPU) composites with unmodified MWCNTs via melt mixing, and systematically investigated the dispersion of fillers in TPU matrix and macroscopic properties of composites. The results showed that when the content of MWCNT was more than 2.5 wt %, the melt mixing under high shear force could achieve uniform dispersion. It could be observed that the shear force regulated by rotating speed played a leading role in the dispersion of MWCNTs in polymer melt. In detail, as the increase of rotating speed, the shear force became strong enough to overcome the van der Waals interaction and electrostatic force between filler particles, thus unwinding the entangled MWCNT aggregates. This discovery was of great significance for the preparation of polymer/CNT composites with excellent dispersion. For the operating conditions of melt mixing, high temperature and strong shear force are essential. Using this method may destroy the capacity of nanoparticles and make polymer chains diffuse into the gaps of nanoparticles. Nevertheless, a reduction in the size and structural deformation caused by strong shear stress would reduce the reinforcement efficiency of graphene on polymers, which may make the formed composites unsuitable for some applications with high temperature environment, high strength requirements, special chemical environment and high precision requirements [220].

In order to meet the material requirements of electronic devices, automobile parts, aerospace and other fields, rubber products, coatings, fibers, plastics and composite materials are prepared by solution blending method, which possesses the advantages of simple operation, wide applicability and cost-effectiveness [221,222]. Mao et al. [221] incorporated GO into the natural rubber (NR) composites through latex co-coagulation technology and characterized the composites by a series of techniques. The results showed that the tensile strength, tear strength and modulus of the composites had been significantly improved. Specific enhancement mechanism of GO on NR was attributed to the high surface area of GO sheet and the microstructure of GO sheet which was highly exfoliated in NR. The formation process of GO incorporated into NR was shown in [Fig. 11\(b\)](#). Due to the easy detachment of GO in water and the fact that most rubbers have a latex-like nature that is easily

compatible with GO suspensions, latex blending technology is more effective method for preparing GO/rubber composite materials. But there were still some drawbacks about this method [219]. Firstly, the solvation process could induce the reaggregation of GO flakes. Secondly, the removal of solvents could cause environmental pollution, which has been persistent issue in practical implementation. The latex blending process is similar to the solution blending process, with the only difference being that the elastomer is presented as form of latex [222,223]. Compared to the solution blending method, the latex blending method allowed graphene to be distributed along specific pathways, forming an isolated structure. With this technique, the nano-fillers are encapsulated by polymer latex particles, forming an isolated network. Latex technology has been employed in preparing polymer/graphene composites with an array of polymers, including polyethylene, polypropylene, and polyphenylene-co-acrylonitrile. However, its application scope was narrow, limited to conductive materials. When compared to polymer/graphene composites prepared by solution blending, composites through latex technology have better dispersion and enhanced performance. The disadvantage is that physical adsorption between polymer latex and nano-fillers is not strong enough to prevent some nano-fillers from depositing in the polymer latex solution, resulting in poor distribution of nano-fillers in the polymer matrix. Enhancing chemical interaction between polymer chains and graphene is a feasible method to improve dispersion [223].

In comparison to the mechanical mixing or the solution mixing methods, in-situ polymerization can control dispersion and uniformity of nanoparticles more effectively, thus improving performance stability of composites [224,225]. The mechanism of in-situ polymerization involves blending modified graphene with monomers or pre-polymers to form stable chemical bonds, followed by the addition of suitable initiators to trigger polymerization under heating or radiation conditions, ensuring uniform dispersion of fillers within the polymer matrix. This enhances the interaction between fillers and polymers in the resulting composite materials, facilitating stress transfer. In this method, the filler (graphene or its derivatives) is dispersed within a monomer (or multiple monomers), and then agglomerated in the presence of the filler through certain means. Compared to the aforementioned preparation methods, in-situ polymerization has such following advantages: (1) more uniform filler dispersion and stronger interaction with the polymer interface; (2) applicable for preparing highly filled and ultra-high molecular weight nanocomposites, where highly filled composites can also serve as masterbatches for further melt blending with other polymers to prepare corresponding composite materials; (3) compared to solution intercalation methods, it does not require a large amount of organic solvents, making it more environmentally friendly [225]. However, this method also has some limitations. In the majority of instances, monomers can only polymerize in solvents or at least in the presence of GO solution. At

**Table 5**

Summary on outline of advantages and disadvantages of methods for preparing graphene/elastomer nanocomposites.

Preparation technology	Source materials	Advantages	Disadvantages	Ref.
Melt mixing	Polypropylene; GO; Thermoplastic elastomer	Improved mechanical properties; Environment-friendly	Complex preparation; High cost	[227]
Solution blending	Graphite; Thermoplastic polyurethane GO; dimethyl formamide; hydrogenated carboxylated nitrile-butadiene rubber/tetrahydrofuran;	Economic and environmental protection Simple operation; High controllability	Uneven distribution Requirement to specific solvent; Pollution for environment	[228] [229]
Latex blending	Butyl rubber; Modified graphene GO; Natural rubber GO; Styrene-butadiene rubber; Carboxylated acrylonitrile butadiene rubber	Evenly dispersed; Controllable preparation process Evenly dispersed; Strong interface interaction Evenly dispersed; Strong binding force	Complicated process Need of precise control Complicated process	[230] [221] [231]
In-situ polymerization	GO; polyimide; epoxy; polyurethane; polystyrene; polyaniline; polyvinyl alcohol; dopamine Multi-layered graphene; Styrene-Butadiene rubber	Evenly dispersed; Strong binding force; Suited to high-filling composite materials; Environment friendly Evenly dispersed	Complicated process; Need precise control; High cost; Hardly prepared in batches High parameter control requirements	[225] [232]

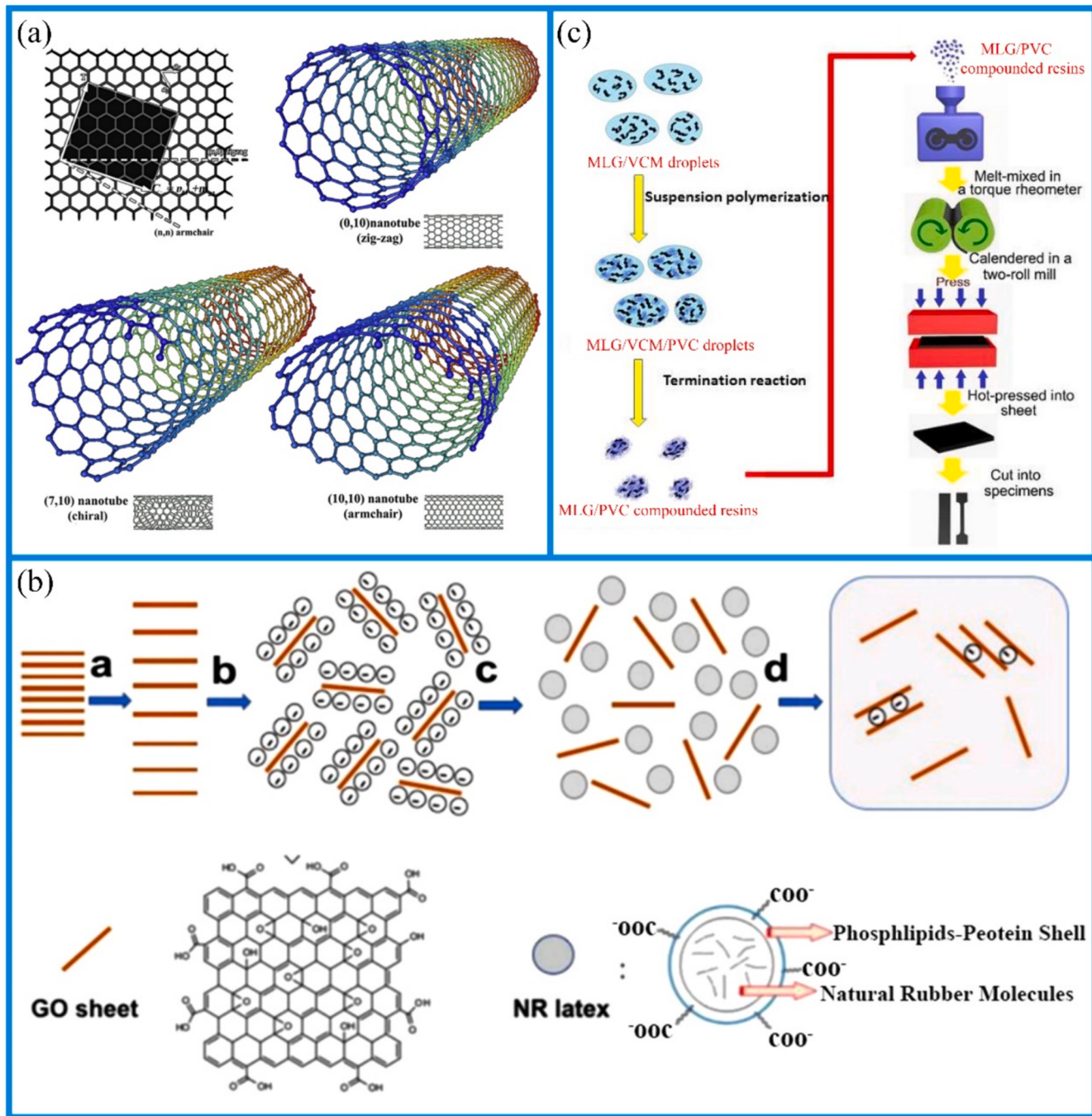


**Fig. 11.** (a) Molecular model for single-walled carbon nanotubes based on chirality; Reprinted with permission from Ref. [218]. (b) Schematic drawing for mixing and blending process; Reprinted with permission from Ref. [221]. (c) Schematic drawing of preparing MLG/PVC composites; Reprinted with permission from Ref. [226].

this point, the high viscosity of uniformly diluted graphene nanosheets becomes a major issue in the bulk-phase polymerization process. Additionally, a loss in the polymerization rate at later stages is another drawback. The combination of various preparation methods can effectively obtain composite materials with uniform filler dispersion and significantly enhanced properties. Specifically, Fig. 11(c) showed the production scheme of polyvinyl chloride mixed with multilayer graphene composites, which has two fabrication processes: in-situ suspension condensation and melt blending process [226]. Such preparation method effectively improved mechanical properties for composites, and the uniform dispersion of graphene in composites was found. It can be seen that the combination of different preparation methods can give full

play to their respective advantages, improve the performance and preparation efficiency of materials, which provides reference for meeting diverse application requirements.

#### 4.2. Characterization

Interaction between graphene and elastomeric materials affects the physicochemical properties of the final composite material. Accordingly, in many literatures, the surface chemistry is applied to different components of the system to ensure their chemical compatibility [233,234]. In addition, the interaction between elements can also lead to the formation of chemical bonds. The focus is that it can improve the

performance and filler of the initial material, thereby obtaining satisfactory dispersal state. These methods included surface functionalization, in-situ microemulsion polymerization, and the use of surfactants, etc. However, these methods still have many shortcomings, and the specific processes have not been perfected yet, since degree of functionalization is uncontrollable, and expensive solvents and chemicals are used in this process. Different spectroscopic techniques such as FTIR, XPS, etc., can be used to evaluate interactions between fillers and confirm the functionalization of fillers. In addition, electron microscopy methods such as TEM, SEM, and even AFM are preferred for studying the dispersion of fillers.

As common surface analysis techniques, fourier transform infrared spectroscopy (FTIR) and XPS perform a significant role in understanding

the surface composition, structure and chemical characteristics of graphene/elastic nanocomposite, which provides the important information and guidance for material design, performance optimization and application development [235–237]. Hexachlorocyclotriphosphazene and glycerol were used to modify surface of oxidized graphene oxide in order to achieve uniform dispersion and strong filler-matrix interface in epoxy (EP) resin [235]. The functionalized graphene oxide (FGO)/EP nanocomposite was obtained via in-situ thermal polymerization, and the thermal decomposition process of EP and FGO/EP nanocomposites was studied using real-time FTIR. The results indicated that EP/2%FGO nanocomposites showed a relatively small strength at 350°C, which may be attributed to the catalytic effect of FGO on the degradation of epoxy resin. In addition, the strong interaction between FGO and EP matrix

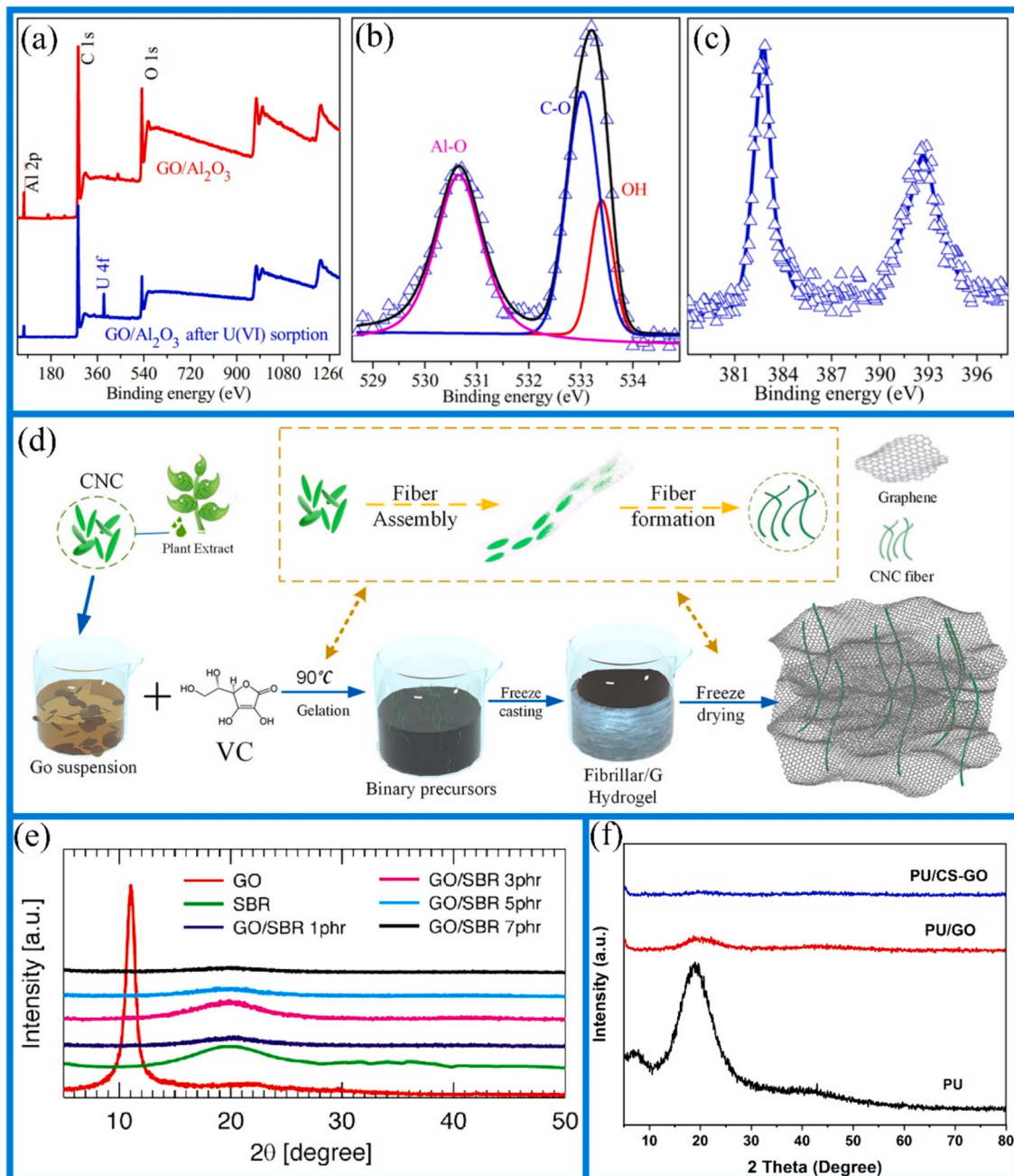


**Fig. 12.** (a-c) XPS analysis for U(VI)-bearing GO/Al<sub>2</sub>O<sub>3</sub> composites; Reprinted with permission from Ref.[237]. (d) Schematic drawing of preparation for cellulose-derived graphene aerogel; Reprinted with permission from Ref.[239]. (e) XRD spectra for GO/SBR composites with different amounts of GO; Reprinted with permission from Ref.[19]. (f) XRD diffractograms for the PU/CS-GO nanocomposite films; Reprinted with permission from Ref.[242].

was also one of the reasons why FGO enhanced the thermal stability of nanocomposites. Improving the dispersion and interfacial interaction of graphene in polymer matrix could effectively improve properties of composites, and then promote their further application in research and industrial fields. In the work of Jeon et al. [236], the wear resistance and tensile strength of graphene/TPEE (thermoplastic polyether elastomer) composites with graphene content of only 1 wt% increased by 11 times and 43 % respectively, which was attributed to the high dispersibility and lubrication of two-dimensional graphene filler. XPS analysis of the chemical elements on the surface of carbon fillers also suggested that these hydrophilic functional groups are expected to enhance the dispersion of carbon fillers in the polymer matrix. A variety of oxygen-containing functional groups were one of important reasons for the efficient adsorption of nanocomposites [237]. Taking the prepared GO/Al<sub>2</sub>O<sub>3</sub> composites as an example, they have various oxygen-containing functional groups, large surface area, and abundant reticular structure. Infrared spectroscopy analysis indicated that hydroxyl and carboxyl groups in GO/Al<sub>2</sub>O<sub>3</sub> composite materials played a major role in the adsorption of U(VI) as a regular nuclear raw material, and nano-Al<sub>2</sub>O<sub>3</sub> transformed into amorphous secondary minerals such as boehmite after adsorbing U(VI). Meanwhile, the XPS analysis results further suggested that the efficient adsorption of U(VI) by GO/Al<sub>2</sub>O<sub>3</sub> composites were related to various oxygen-containing functional groups, as shown in Fig. 12(a-c).

Electron microscope has the characteristics of high resolution, which can observe the details of microstructure in materials, provides a powerful analytical tool for materials science and engineering, and plays the significant role in the detection of composite materials [238–240]. Liu et al. [238] introduced GNPs into fluororubber (FKM) matrix and evaluated their tear fracture energy through pure shear tests. The tear energy increased linearly with volume fraction of GNPs. SEM confirmed that the formation of voids at the ends of sheets during deformation was the reason for the significant enhancement ( $\sim 1 \text{ kJ/m}^2$ ) in interfacial debonding energy. Processing elastomers with fillers of different morphologies and surface characteristics was challenging task. Luo et al. [239] reported simple and sustainable method for fabricating lightweight and elastic graphene/cellulose nanocrystal (CNC) aerogel (GCA) monoliths. Fig. 12(d) illustrated schematic of preparing cellulose derivative graphene aerogel. SEM images confirmed the anisotropic three-dimensional structure and well-arranged pores that appeared after the addition of mixed CNC. It can be observed that GCA has a layered porous structure similar to pure graphene aerogel, mimicking the structure of cork at the micron scale. In addition, high-resolution TEM analysis showed orientation arrangement of translucent wrinkled GO sheets with a thickness of about 5–10 nm and rod-shaped cellulose clusters, confirming the assembly of nanocrystals and nanofibers. It is well known that tear resistance is key mechanical property for various elastomer applications. Das et al. [240] investigated heterogeneity of ionic supramolecular interactions and demonstrated the self-healing properties of strong carboxylic nitrile rubber through the introduction of low-cost and commercially available materials. By incorporating an ionic liquid (IL) and zinc oxide compound-modified IL into GO for the synthesis of XNBR rubber, GO and branched oxide ILs were successfully synthesized. The morphological analysis of rubber composite materials was observed through SEM. The results indicated that the GO sheets were well dispersed in the matrix, after the addition of GO to XNBR rubber. After adding grafted graphene oxide (GO-IL) to XNBR rubber, the ions dispersed evenly through GO, which solved the problem of ion aggregation in IL particles. This uniform dispersion is helpful to improve the mechanical properties and self-healing ability of materials. TEM was used to investigate the dispersion of modified GO into XNBR rubber, and it was found that the IL salt was uniformly dispersed in the rubber matrix through the GO. SEM results and TEM analysis strongly demonstrated the preparation of GO and ion salt-grafted GO, and well dispersion of modified GO in the rubber matrix. Mathias et al. [241] prepared 3-phase nanocomposite material by combining hydrophilic Ti<sub>3</sub>C<sub>2</sub>T<sub>x</sub> MXene and

hydrophobic CNTs with elastomer latex, resulting in significant improvements in both mechanical and functional properties. Microscopic photographs showed enhanced dispersion compared to nanocomposites containing non-assembled fillers. The morphology of the composite material was characterized by scanning electron microscopy and transmission electron microscopy, with SEM micrograph of a clean elastomer which had a smooth surface without any prominent particles. When 2.1 vol% MXene was added to elastomer, it appeared as individual or agglomerated particles dispersed in the matrix.

Composite materials containing graphene or GO particles can also be analyzed using XRD. XRD revealed significant differences between samples of graphite, graphene, and GO. Meantime, composite materials containing graphene or GO particles can also be analyzed using XRD. The characteristic peaks of graphite could effectively indicate the interlayer distance of graphene. However, the characteristic peaks of the matrix could completely alter the spectrum. Therefore, it is necessary to compare the XRD spectra of the pure matrix with those of the composite material to draw correct conclusions. Fig. 12(e) showed the XRD spectra of GO/SBR composite materials with different GO contents. In the case of pure GO, a characteristic peak indicating the interlayer spacing could be observed. Due to the interlayer functional groups, its angle was smaller than that of graphite. This peak was not present in the spectrum of the composite material, indicating complete exfoliation during the mixing process [19]. The XRD diffraction patterns of MXene, MWCNTs, mMWCNTs, pure nitrile rubber, and nitrile rubber/hybrid filler nano composites was showed, which also demonstrated good exfoliation and dispersion of hybrid fillers within the matrix [241]. Mohammadi et al. [242] incorporated chitosan-modified graphene oxide nanosheets (CS-GO) into a polyurethane (PU) matrix and synthesized polyurethane nanocomposite films (PU/CS-GO). The XRD spectra of GO and CS-GO were shown in Fig. 12(f). Compared with blank PU, the crystallinity of PU/GO and PU/CS-GO was lower. After chitosan modification, the CS-GO nanosheets exhibited additional peaks that are characteristic of chitosan as a crystalline biopolymer. It is evident that GO nanosheets and CS-GO nanosheets have a negative impact on the crystallinity of the prepared nanocomposite material. Furthermore, the amorphous structure of the PU/CS-GO sample may be attributed to the good dispersion of CS-GO nanosheets in the PU matrix, resulting in a lower degree of phase separation.

In conclusion, characterization technology is of great significance to graphene and graphene-based materials. For example, structure, purity, composition, or crystallinity of graphene, graphene oxide and graphene/elastomer nanocomposites can be observed and analyzed by using the position or shape of specific diffraction peaks in XRD patterns. Besides XRD, SEM can also be used to observe and analyze the surface morphology, microstructure and the composition of graphene, graphene oxide and graphene/elastomer nanocomposites. Raman spectroscopy can observe the structure of graphene and GO. Moreover, AFM, TEM and UV-Vis are also suitable techniques to characterize graphene and graphene oxide. The suitable characterization techniques for graphene oxide and graphene/elastomer nanocomposites are FTIR and TGA. More detail information about different techniques and corresponding detected target for such three kinds of materials are listed in Table 6.

#### 4.3. Properties

The introduction of inorganic nano-level filler has proven to be a successful method for improving the performance of substrate, which is due to that the filler can “combine” their own high rigidity and strength to the overall material, and inhibit the spread of cracks, thereby ultimately delaying the rupture of material. Common types of fillers, such as Ag nanoparticles [252,253], CNTs [254,255], GO [256], and graphene [257,258], have been incorporated into the polymer matrix to improve their performance. Among them, a series of data of graphene reinforced elastic matrix in applications have been presented in Table 7. For instance, researchers utilized in-situ polymerization techniques to

**Table 6**

Different characterization techniques and corresponding detected target used for three kinds of materials such as graphene, GO, and graphene/elastomer nanocomposites.

NO	Designation of techniques	Detected target		
		graphene	GO	nanocomposites
1	XRD	Determine structure and purity [243]	Determine Structure [245]	Determine Structure and crystallinity [242]
		Determine Structure and composition [244]	Determine Structure and composition [246]	Determine Dispersion state of ODA-GO [247]
2	SEM	Determine Surface morphology and structure [91,248]	Determine Morphology [245]	Determine Microstructure [238]
				Determine Morphology [242]
3	Raman Spectroscopy	Determine structure [91,249]	Determine structure [250]	NM
4	AFM	Determine structure [249]	Determine structure [176]	NM
5	TEM	Determine Morphology and structure [243,249]	Determine structure [176]	NM
6	UV-Vis	Analyze optical transmittance and absorbance [248,251]	Determine oxidation degree [110]	NM
			Analyze optical absorption characteristics [173]	
7	FTIR	NM	Analyze functional groups [245]	Analyze chemical interaction [240]
			Determine the functional groups [173]	
8	TGA	NM	Determine thermal stability [173]	Analyze thermal stability and degradation behavior [242]

NM=Not mentioned.

prepare GO-filled composite materials and founded that the presence of GO particles could effectively enhance the Young's modulus and yield stress of TPEE [259,260]. Thermoplastic elastomers (TPEs) utilize

physical crosslinking to achieve elastomeric properties, making them easier to process compared to traditional rubber. However, their mechanical performance is limited relative to thermoplastic plastics. Therefore, TPEs are often reinforced with inorganic fillers. With the addition of GNPs, the crystallinity remains unchanged. The preliminary evaluation of the mechanical properties for prepared nanocomposites was conducted through the tensile testing. The relationship between the mechanical properties including Young's Modulus (a) and Yield strength (b) of the nanocomposites and the volume fraction of GNPs was shown in Fig. 13. The mechanical performance from the tensile test indicated a significant improvement in stiffness and yield strength of the material. At lower filler contents, the modulus of the composite material showed linear growth, while it exhibited superlinear increase after reaching the percolation threshold volume fraction. However, the most significant feature of controlling nanocomposite materials performance is the dispersion of the filler in the matrix.

The use of most elastomers can contribute to achieve this goal, that is, to significantly improve its original low positive modulus, thus improving properties and application potential of elastomer/graphene nanocomposites [238,261]. TPEE is a relatively new member of the TPEs family that has gained development in recent years. In order to expand the application range of TPEE, it is necessary to improve its mechanical strength and thermal stability, and hybridization with inorganic particles is a commonly used strategy. Jeon et al. [105] used TPEE and electrochemically exfoliated graphene to prepare thermoplastic elastomer nanocomposites with improved wear performance through various extrusion processes. The tensile strength of graphene/TPEE composites with a graphene content of only 1 wt% increased by 43 %. FKM systems are widely used elastomers in the aerospace and automotive industries due to their excellent barrier properties against corrosive non-polar chemicals. However, most FKM materials used for sealing components operate at high temperatures and often endure static and extreme working environments, which can lead to material failure. Therefore, it is important to improve the tear resistance of FKM components by introducing high-performance inorganic fillers such as graphene-related materials. Li et al. [238] fabricated FKM/GNPs nanocomposites using solid-state blending method on a two-roll mill, followed by pure shear tests on the FKM/GNPs nanocomposites to obtain the effective tear energy of the samples. The results indicated that at the maximum GNP content, the tear resistance is improved by three times, indicating the effective toughening of GNPs. Overall, the addition of GNPs improves tear resistance. Polyurea is fast-reacting elastomer that exhibits excellent mechanical properties and unique viscoelasticity. However, conventional polyurea elastomers were often limited by insufficient strength and lack of functionality. Meng et al. [261]

**Table 7**

Summary of preparation strategies and various applications for elastomer-based nanocomposites.

Elastic matrix	Enhancement	Fabrication method	Characterization technique	Applications	Ref.
Styrene Butadiene Rubber	Graphene	NM	FTIR; XPS	Auto tires	[216]
Natural Rubber	Graphene oxide	Latex Cocoagulation	TEM; XRD; FTIR	Vehicle	[221]
Fluoroelastomer	Graphene nanoplatelets	Mixing-curing	SEM	Aerospace and Automotive industries	[238]
Thermoplastic Polyester Elastomer	Graphene nanosheets	Melting mixing	TEM; XPS	Automotive and Electronic	[259]
Pristine polyurea elastomers	Functionalized graphene nanoplatelets	NM	SEM; AFM	Temperature sensor	[261]
Thermoplastic olefins	Graphene nanoplatelets	Melt compounding	SEM	Wheel lips and Rear bumper fascia	[266]
Natural Rubber	Graphene-based nanomaterials	Latex mixing method	TEM and SEM	Conductive rubber composites	[316]
Natural rubber	Graphene	Latex mixing method	TEM; XPS	Vulcanization kinetics	[257]
Natural rubber	Graphene	Self-assembly integrating latex compounding technology	TEM; XPS; AFM	Electrostatic paints; flexible displays; implantable devices	[258]
Styrene-butadiene rubber	Graphene platelets	Solution-mixing	XRD; TEM; SEM	NM	[317]

NM = Not mentioned.

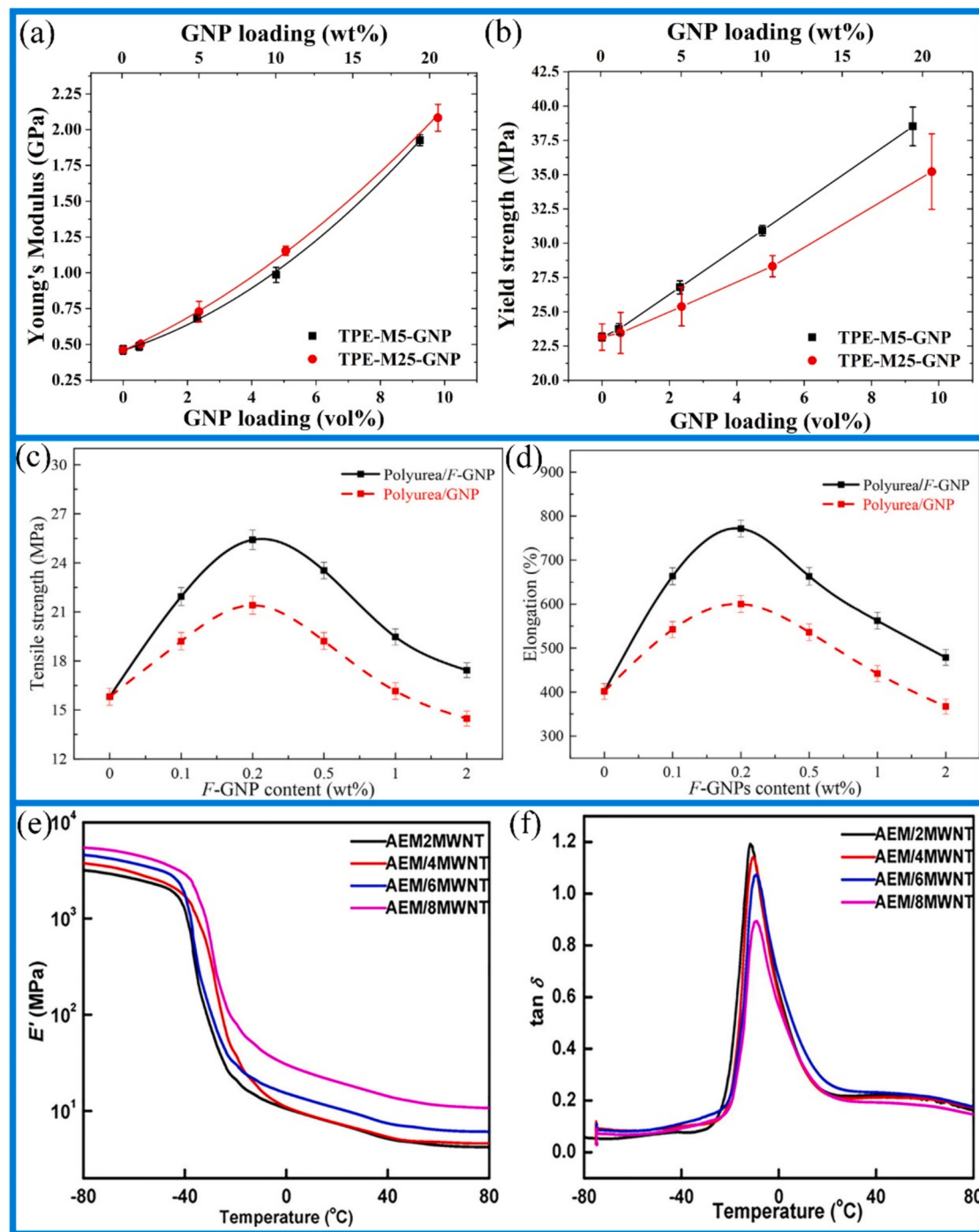


**Fig. 13.** The variation of Young's modulus (a) and yield strength (b) with the volume fraction of filler; Reprinted with permission from Ref.[260]. Tensile Strength (c) and elongation (d) of polyurea/F-GNP and GNP nanocomposites; Reprinted with permission from Ref.[261]. Storage modulus (e); Reprinted with permission from Ref.[265].

prepared intelligent, multifunctional, and mechanically elastic nanocomposites by in-situ polymerization of functionalized graphene nanoplatelets (F-GNPs) with polyurea. Subsequently, the nano-composite was tested by tensile experiment. Fig. 13 showed the tensile strength (c) and elongation (d) at the break of two sets of polyurea nanocomposites, one containing F-GNPs and the other containing non-functionalized GNPs. The tensile strength and elongation at break of the polyurea/F-GNPs nanocomposites are significantly higher than those of the non-functionalized system. When the mass fraction of F-GNPs is 0.2 wt%, the tensile strength (60.7 %) and elongation at break (92.1 %) of the

nanocomposite materials both showed significant improvement, and the impact resistance was also noticeably enhanced.

The high-temperature resistant fluid acrylic elastomer (AEM) is a highly flexible elastomer that is ideal for developing functional nanocomposites with various potential applications [262,263]. Researchers successfully prepared conductive nanocomposites using ethylene AEM and multi-walled carbon nanotubes (MWNTs) as the base materials and carried out dynamic mechanical analysis [264]. Result showed that the addition of MWNTs increased the storage modulus and glass transition temperature of AEM matrix. In a case of the work of Sahoo [265] et al,

electron beam (EB) crosslinked AEM/MWCNTs nanocomposite materials were successfully prepared by varying the dosage of EB and the MWCNT loading level. The storage modulus ( $E'$ ) (e) and loss tangent (f) of MWCNTs-reinforced AEM nanocomposite materials under a radiation dose of 200 kGy were shown in Fig. 13. The results of dynamic mechanical analysis indicated that  $E'$  increases with increasing EB dosage and MWCNTs, suggesting that the applied load was absorbed due to a decrease in the free volume of the system. Currently, the focus is on the development of green and sustainable elastomeric polymers that are environmentally friendly. To achieve this goal, Kiziltas et al. [266] selected thermoplastic olefin, which was made entirely from sustainable materials, and melt-compounded it with recycled polypropylene (RPP) obtained from discarded carpets, along with silver chrysanthemum rubber, and reinforced it with GNPs. The mechanical properties of the composite material were determined through tensile, flexural, and impact tests. When 10 % GNPs was added, the tensile modulus increased by 76 %. However, the inclusion of natural rubber in RPP initially led to the decrease in both flexural strength and tensile strength, which was due to the presence of soft segments. Overall, graphene can provide a large interfacial area when mixed with nanocomposite materials, which disrupted the migration of macromolecular chains at high temperatures and imposes a nanoscale confinement effect on the chains. This greatly enhanced storage modulus of graphene-based elastomeric nanocomposite matrices. Excellent tensile properties could make graphene/elastic nanocomposite materials easier to deform and shape during processing, reduce processing difficulty and improve production efficiency.

By investigating the impact of inorganic fillers on polymer nanocomposites, the thermal stability of composites can be effectively enhanced, thereby expanding their application fields in high-temperature environments and improving their operational temperature range and performance [267]. Polydimethylsiloxane (PDMS) is frequently employed as the matrix of thermal conductive polymer composites due to its flexibility, processability and exceptional chemical stability. Nevertheless, low intrinsic thermal conductivity of PDMS is inadequate for the immediate requirements of high thermal conductivity polymer composites in the field of high-tech electronics. In order to solve this problem, some studies have prepared thermal conductivity PDMS-based composites by adding graphene-based materials and other materials as high thermal conductivity fillers to PDMS matrix, which has obviously improved its thermal conductivity [186,187,268]. The obvious thermal conductivity is  $4.00 \text{ W m}^{-1}\text{K}^{-1}$  of GO/f-CNTs/PDMS composites fabricated by Wang et al. [186], which is  $\sim 20$  times than that of pure PDMS composite ( $0.20 \text{ W m}^{-1}\text{K}^{-1}$ ) with same amount of randomly dispersed fillers. And its thermal conductivity is higher than that of the other two groups experiments ( $2.10 \text{ W m}^{-1}\text{K}^{-1}$  [187] and  $0.65 \text{ W m}^{-1}\text{K}^{-1}$  [268]) as well. Concurrently, GO/f-CNTs/PDMS composite exhibited remarkable thermal stability, with a thermal conductivity deviation of merely 3 % after 500 thermal cycles ( $20 \sim 200^\circ\text{C}$ ). According to the above report, the two-dimensional structure and high specific surface area of graphene-based materials with excellent thermal conductivity contribute to the establishment of three-dimensional thermal conduction network in polymer matrix, which is particularly important for improving the thermal management ability of composites. Moreover, the thermal conductivity of graphene-based composites depends on the effective thermal conductivity of graphene and the thermal conductivity of graphene/matrix interface. By improving the dispersion of graphene in polymer matrix and constructing a three-dimensional graphene thermal conductivity network, the thermal conductivity of composites can be effectively improved.

Recently, there have been numerous studies on the impact of adding graphene-based materials to the elastic matrix on thermal stability, as reported in many literature sources [267,269,270]. These results indicate that performance of polymer nanocomposites depends on several factors, such as the elastic matrix, the preparation method, the dispersion of graphene, and presence of other additives (such as surfactants).

Specifically, Cruz et al. [271] prepared the new polyamide-11 (PA11) nanocomposite and characterized its thermal stability. Through thermogravimetric analysis, it was found that the addition of GNP increased the thermal stability of PA11, especially when GNP content was 1.0 wt %. Polylactic acid (PLA) was the commonly used elastomer, which was based on plants, biodegradable, biocompatible and met the requirements of green development [272]. Wang et al. [270] used fully exfoliated functionalized GO nanosheets (f-GO) as effective nanofillers to prepare PLA-starch-f-GO nanocomposites. Thermal analysis results indicated that addition of f-GO significantly enhanced the thermal stability of PLA-starch-f-GO, synchronously, with increase of f-GO concentration, the thermal stability gradually improved. Polyvinylidene fluoride (PVDF) is the semi-crystalline polymer with excellent thermal stability and typical processing properties of engineering thermoplastic materials. Lapinska et al. [273] proposed the simple and low-cost method for the preparation of PVDF/GNPs nanocomposites. They conducted thermal analysis by differential scanning calorimetry and thermogravimetric analysis. The shape of the DSC curve (Fig. 14(a)) was typical for partially crystalline polymers. Their experimental results showed that preparation process parameters, material composition, and compatibility between the filler and matrix all had an impact on the properties of nanocomposites. From this, it can be concluded that the thermal stability is improved in the presence of GNP.

Furthermore, formation of aggregates, and the thermal contact resistance caused by the extremely thin aspect ratio of graphene fillers, all affect the thermal conductivity of composite materials [274–276]. Cruz et al. [271] prepared novel PA11 nanocomposite material reinforced with commercial GNPs at 1.0, 2.5, and 5.0 wt%. The PA11-graphene nanocomposites were prepared using in-situ polymerization method with GNPs dispersed in a water suspension as raw materials. This enhanced the thermal stability and confirmed the good dispersion of the fillers in the matrix. Adding graphene to the polymer matrix can improve the polymer's thermal conductivity [277]. Thermal analysis showed a significant improvement in thermal stability of the nanocomposites. Furthermore, well-dispersed GNP flakes resulted in a larger interface area between GNP and matrix, leading to a tighter bonding of the polymer compared to loosely bound polymers. This minimizes the thermal contact resistance caused by close contact between graphene flakes, thereby maximizing the improvement in the thermal conductivity of the composite materials [278–280]. The above literature reports on the thermal conductivity of graphene/elastomer composites have demonstrated that the unique thermodynamic properties of graphene improve the heating rate of the composite materials. Significance of electrical properties in rubber-based composites can't be disregarded in field of materials science and engineering. Conductive multifunctional polymer nanocomposites prepared through introducing conductive fillers into non-conductive polymer matrix have excellent conductivity and versatility, and can be used in electronic devices, sensors, electrostatic elimination materials, antistatic coatings and electromagnetic shielding materials. This kind of composite material can not only keep the characteristics of the original polymer matrix, but also have electrical conductivity, which provides new possibilities for wide application.

Understanding and optimizing the electrical performance parameters of rubber-based composites, such as electrical conductivity and dielectric properties, is helpful to improve the electrical performance and reliability of materials and expand their application prospects in the fields, such as electronics, automobiles, medical care and so on. The solid fillers and structural uniformity of conductive polymers mainly determine their performance. The preparation methods of conductive polymers also affect their performance, and introducing conductive fillers into non-conductive polymer matrices is the simple and effective method for producing conductive multifunctional polymer nanocomposites [281]. To further improve the conductivity of polymers, secondary conductive fillers such as carbon, graphene [282], and silver are usually added. This method can be used to manufacture conductive

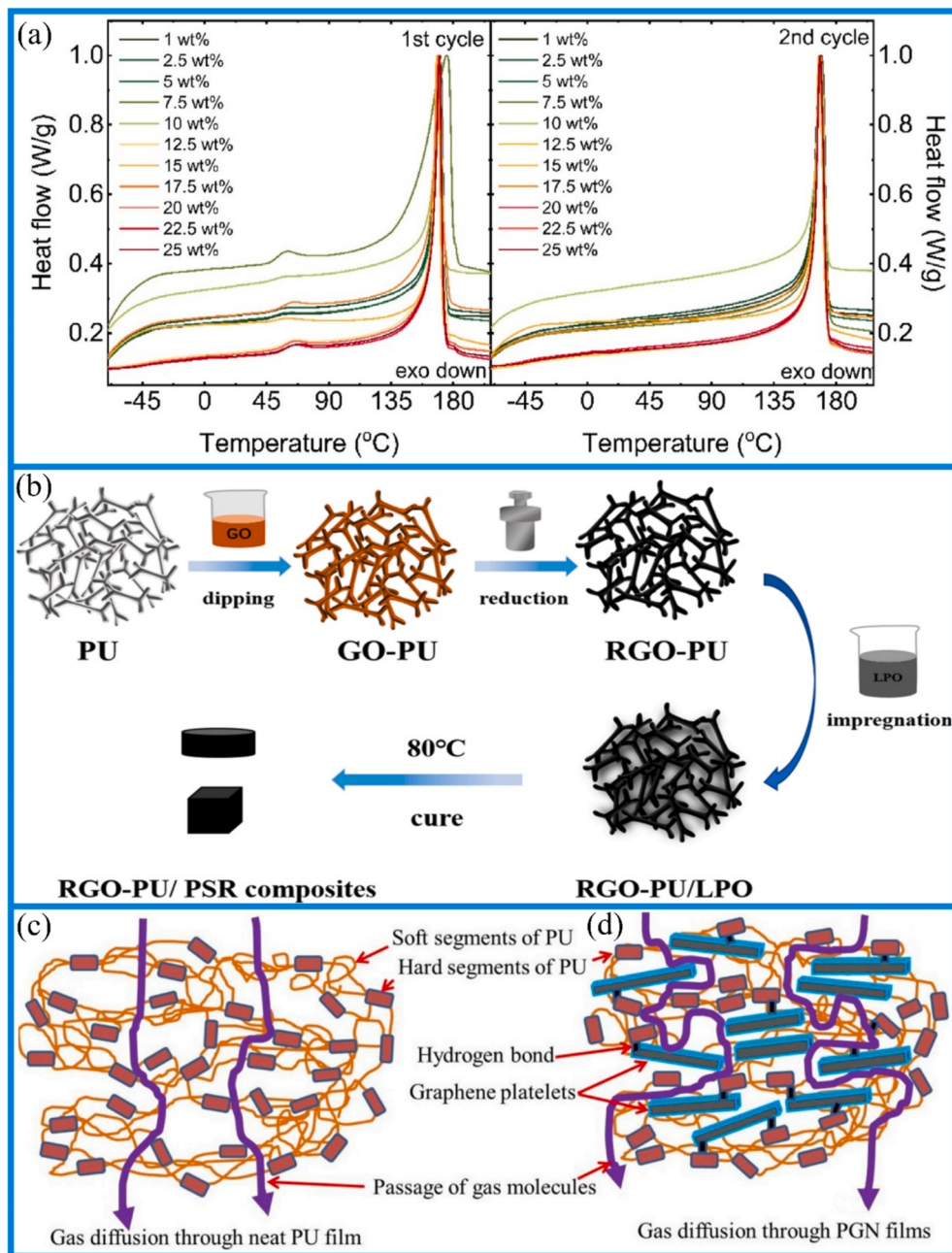


**Fig. 14.** (a) Scanning calorimetry graph of melting temperature region for PVDF/GNP nanocomposites of different filler loading with after first and second cycle; Reprinted permission from Ref.[273]. Preparation process (b) for RGO-PU/PSR composites; Reprinted with permission from Ref.[293]. Schematic drawing of gas passing through pure PU (c) and PGN films (d); Reprinted with permission from Ref.[308].

polymer composites using special polymers with customized chemical and physical properties [283]. Due to its high intrinsic conductivity and extremely large surface area, graphene has once again become the “ideal” filler for the preparation of conductive nanocomposites. GNPs were composed of several layers of graphene and have mechanical properties, electrical conductivity, and thermal conductivity that are close to those of single-layer graphene. More importantly, GNPs contain a low proportion of oxygen-containing functional groups, such as epoxy groups, which can be used to form strong interfaces with polymer matrices. From the previous discussion, it has been concluded that the higher the purity of the filler, the better the conductivity of the nanocomposite at a given loading. Therefore, quality of graphene in nanocomposites affects conductivity, and appropriate synthesis methods and suitable filler quality must be used to enhance the conductivity of

conductive polymers. Besides, the electrical properties of polymer-graphene nanocomposites are greatly influenced by various crucial factors, including the filler and matrix types, geometry of graphene, interphase region characteristics, quantum tunneling effect, and filler volume fraction within the matrix [284–288].

The dispersion state and other properties of graphene, which were influenced by different processing conditions, are undoubtedly important in determining the electrical performance of graphene/polymer nanocomposites [142,289]. As an example of taking in-situ polymerization, from low viscosity oligomers, allowing effective dispersion of fillers into the low viscosity matrix and stabilizing them as the polymerization progresses. Specifically, Cho et al. [290] proposed the synthesis of polyamide 6 by in-situ ring-opening polymerization of e-caprolactam and edge-selectively functionalized graphene nanosheets.

The basal plane of graphene nanosheets is defect-free, synthesized through a ball milling process with dry ice. Therefore, the final graphene nanocomposite material has highly dispersed fillers and enhanced conductivity due to its undistorted  $sp^2$  hybridization. This method is a promising approach to effectively achieve highly conductive graphene in polymer composites without aggregation and compromising its inherent properties after functionalization. Guan et al. [291] employed hydroiodic acid as a reducing agent to chemically reduce GO water suspension using poly(p-phenylene terephthalamide) organic fibers, and prepared graphene-based composite hydrogels. To enhance the conductivity of the hybrid aerogel, the organic fibers were subjected to high-temperature annealing, transforming them into carbon fibers with higher conductivity. The resulting graphene/carbon fiber aerogels (GCFAs) exhibited excellent conductivity ( $>10^2$  S/m), surpassing chemically reduced graphene aerogels reported previously by four orders of magnitude. The in-situ formed carbon fibers enhanced the porous structure and provided further interconnections between graphene flakes, resulting in high conductivity and significantly improved electrical performance of the obtained GCFAs. Liang et al. [292] developed template method to fabricate three-dimensional GNPs/rGO/EP nanocomposites with excellent conductivity, where the electrical conductivity was enhanced from  $2.8 \times 10^{-3}$  to 179.2 S/m. Tao et al. [293] utilized a PU sponge as a template and combined GO with PU through hydrothermal reduction to construct a three-dimensional rGO-PU foam. Under vacuum assistance, the three-dimensional rGO-PU skeleton was impregnated with liquid polythioether oligomer and subjected to heat treatment to fabricate the rGO-PU/polythioether rubber (PSR) composite material (as shown in Fig. 14(b)). The electrical conductivity of the rGO-PU/PSR composite material was superior to that of pure PSR. This is attributed to the introduction of the three-dimensional rGO-PU foam, which provides pathways for electron transfer and phonon transport. Additionally, the dielectric properties indicated that the rGO-PU/PSR composite material has a higher dielectric constant than pure PSR.

Currently, many preparation methods for polymer/GNP nanocomposites require the use of environmentally unfriendly organic solvents. In order to achieve the green production, in the work of Meng et al. [261], GNPs were mechanically delaminated and then modified to fabricating polyurea nanocomposites. The modification enabled the formation of a stable and strong interface between GNPs and polyurea. At the same filling fraction, polyaspartic acid-modified polyurea/GNP nanocomposites showed higher conductivity compared to unmodified nanocomposites, which was attributed to the interface modification leading to better exfoliation and uniform dispersion of GNPs within the matrix.

Polymer composites with high dielectric constant and good flexibility can meet the requirements of different application scenarios, such as electronics, sensing, flexible electronics equipment and electromagnetic shielding. What people typically need is polymer composite materials with high dielectric constant and good flexibility. Polymers possess excellent flexibility, ease of processing, and low dielectric loss, but their dielectric constants are generally low [294]. Therefore, the incorporation of high dielectric constant (high-k) fillers is an effective approach to enhance the dielectric constant of polymer composites and expand their application range. Graphene, with its wide electron mobility and large specific surface area that promotes interface polarization, has been reported for driving applications. Moreover, significant dielectric enhancement can be achieved in dielectric polymers at relatively low concentrations while maintaining the flexibility of composite materials. Compared to pure graphene, oxidized graphene is considered a better dispersant candidate in liquid solutions because it possesses enhanced functionality, resulting in extremely high dielectric stability. Similarly, RGO is utilized as a critical nanofiller for enabling smooth charge transfer, which was related to high strength of electrical breakdown in dielectric media [295]. Chen et al. [296] incorporated colossal dielectric-constant  $\text{CaCu}_3\text{Ti}_4\text{O}_{12}$  (CCTO) particles and rGO into a

polyvinylidene fluoride (PVDF) matrix through solution processing to fabricate flexible composite materials with high-k and low dielectric loss. RGO was used as the secondary phase, aiming to maintain the flexibility of composite material by reducing the overall filler content. However, high dielectric enhancement could only be achieved near the percolation threshold. Specifically, a higher dielectric constant (~40.4) and relatively low dielectric loss tangent (0.08) were obtained when the volume fractions of RGO and functionalized CCTO were 0.61 vol% and 12.5 % vol%, respectively. Additionally, composite material could not withstand high electric fields close to the percolation threshold. Therefore, it is necessary to strike a balance between increasing the dielectric constant and maintaining low dielectric loss and flexibility of the composite material. Zhang et al. [297] successfully fabricated fully perfluoroctanoic acid-doped reduced polyaniline/rGO/poly (vinylidene fluoride) (PFOA-rPANI/rGO/PVDF) nanosheets. The doping of PFOA reduced the aggregation of rPANI/rGO, enhanced the interface interaction with the PVDF matrix, thereby significantly improving the dielectric constant of the polymer nanocomposite at very low graphene content. The prepared PFOA-rPANI/rGO/PVDF nanocomposites possessed excellent flexibility, high dielectric constant, and high dielectric loss. When the filler volume fraction was 0.5 %, the nanocomposite achieved a maximum dielectric constant of 1754. In addition, reasonable preparation method could ensure the uniform dispersion of rGO nanosheets that could enhance charge transport properties, resulting in a high dielectric constant and exceptional charge polarization [298].

In the study by Zhang et al. [299], a relationship between dielectric constant and mechanical strength was discovered. The concrete experimental results showed that while the dielectric constant of nanocomposites was significantly strengthened, the mechanical strength and electromechanical properties failed to improve significantly. This difference may be due to moderate adhesion between the polymer and graphene nanosheets, but it may also depend on the competition between an increase in dielectric constant perceived by the polymer as well as a decrease in electric field caused by interface polarization. A similar competitive relationship was also reflected in the study of Yassin et al. [300], where they used solution mixing technology to add different proportions of GO to poly (ethylene-co-vinyl alcohol) (EVOH) copolymer to prepare novel nanocomposite material. SEM results showed that the coverage of GO with EVOH forms a sandwich-like structure, preventing contact and network formation of GO sheets, thereby significantly improving the dielectric performance. The increase in the proportion of GO in the nanocomposites improved the interface polarization between GO and EVOH, thereby enhancing the local electric field. This enhancement, in turn, strengthens the migration of charge carriers, and the accumulation of charge carriers has significant impact on the dielectric constant of the medium, especially in the low-frequency region.

In addition, graphene, with its anisotropic sheet-like properties, can form a liquid crystal phase. The liquid crystal (LC) phase with the parallel alignment of its layers, is difficult to create a conductive pathway, thus offering the method for achieving high dielectric performance composite [301]. However, graphene fails to spontaneously form the LC phase, whereas GO can self-assemble into the nematic LC phase in polar solvents and maintain the LC state in polymers. Thus, Zhang et al. [302] used high-temperature reduction and curing reactions to fabricate graphene/PDMS nanocomposites. Experimental results revealed that at a filler content of 4 wt%, the nanocomposites exhibited an 800 % increase in dielectric constant compared to pure PDMS, with a loss tangent not exceeding 0.5. Consequently, graphene liquid crystals can significantly enhance the dielectric performance of nanocomposites and offer a novel approach for fabricating high dielectric performance composite materials. In summary, the parameters that ultimately affect the dielectric properties of graphene-based elastomers are similar to most properties, such as the chemical structure of the polymer, the uniformity and reinforcing ability of the filler, as well as its shape and quantity in the

composite material.

As we all know, pure rubber usually exhibits inadequate gas barrier properties, thus limiting its application under certain special conditions, such as current aerospace, tire inner layers, and vacuum insulation applications. The demand for material protection in different fields is satisfied with the excellent barrier properties of rubber-based composites [303,304]. Therefore, green and simple method for preparing graphene oxide/nitrile rubber nanocomposite membranes was proposed [305]. Experimental results confirmed that addition of GO improved the barrier performance of composite material, which was attributed to the strong interfacial interaction between graphene oxide and nitrile rubber. Similarly, Zhu. et al. [306] prepared GO/polyaniline composite material by in-situ polymerization method. Under strong interaction between GO and polyaniline, the prepared composite material exhibited the excellent water dispersibility and good barrier performance, suitable as a corrosion inhibitor for water-based anti-corrosion coatings. Furthermore, GO contained various hydrophilic functional groups, including epoxides, hydroxyls, and carboxyl, which allowed for good interfacial interactions between GO and polar polymers, facilitating the load transfer between GO and the polymer matrix. By contrast, graphene, owing to its two-dimensional structure and complete arrangement of carbon atoms, was relatively superior to GO in gas barrier properties. Specifically, the sheet-like structure and extremely small geometric pore size (0.064 nm) of graphene could improve the gas barrier performance of polymers by increasing the tortuous path of gas diffusion. Based on this, Nielsen et al. [307] proposed a simple model to determine the gas transport behavior of polymer nanocomposites filled with inorganic nanosheets. According to the solution-diffusion model, the gas permeability in polymer membrane could be expressed as the product of diffusivity and solubility, and the expression was as follows:

$$P = DS \quad (6)$$

$$S = S_0(1 - \phi) \quad (7)$$

$$D = \frac{D_0}{\tau} \quad (8)$$

$$\tau \equiv \frac{l}{l} \quad (9)$$

$$\frac{P}{P_0} = \frac{1 - \phi}{\tau} \quad (10)$$

$$l' = l + N \cdot \frac{L}{2} \quad (11)$$

$$\tau = 1 + \frac{L}{2W} \cdot \phi \quad (12)$$

$$\frac{P}{P_0} = \frac{1 - \phi}{1 + \frac{\alpha}{2} \phi} \quad (13)$$

Herein,  $P$ : the gas permeability of the polymeric membrane,  $D$ : the diffusivity of a gas molecules,  $S$ : the solubility of a gas molecules,  $S_0$ : the solubility of the pure polymer matrix,  $\phi$ : volume fraction of the filler,  $D_0$ : the diffusivity of the pure polymer matrix,  $l$ : the distance between pathways through the membrane,  $l'$ : the membrane thickness,  $P_0$ : gas permeability of pure polymer matrix,  $N$ : the average number of inorganic platelets,  $\alpha$ : the aspect ratio of the platelets.

Compared with other inorganic fillers, one of the advantages of graphene is its high aspect ratio, which prolongs the curvature of the diffusion path of gas molecules in nanocomposites. For example, in the experiments conducted by Adak et al. [308] on thermoplastic PU/functionalized-graphene nanocomposite films, the reduction in permeability or improvement in gas barrier performance of PGN films was conducted, which was ascribed to an increase in tortuosity of gas molecules in the nanocomposite material, as shown in Fig. 14(c-d).

Additionally, the presence of graphene restricted the chain motion of PU and slightly enhanced the crystallinity, which also contributed to the improvement in helium gas barrier performance. With an increase in graphene concentration, the helium gas barrier of the nanocomposite film gradually improves, with a reduction in permeability of approximately 30 % observed at a graphene loading of 3 wt%. Besides, the stacking structure of layered graphene is also a key factor affecting its gas barrier performance. Nevertheless, low resistance to water vapor or gas permeability after film formation is drawback, which may attribute to the lack of graphene in functionality [309]. To sum to, when evaluating the liquid and gas barrier performance of graphene/elastomer nanocomposites, some factors need to be considered, such as the interaction between solvents and graphene, properties of polymers, interfacial regions, and dispersion of solvent molecules.

Vulcanization is the process of converting predominantly thermoplastic rubber or raw rubber into an elastic or rigid rubber state. The main process of rubber vulcanization is that the vulcanizing agent reacts with the double bonds in rubber to form a cross-linked structure, thus making rubber exhibit various excellent properties [310–313]. Hernández et al. [220] prepared nanocomposites of NR and functionalized graphene using conventional two-roll mixing method. The excellent mechanical properties of them were ascribed to the strong interaction between rubber and fillers accelerated the crosslinking reaction. Besides, the study on vulcanization of GO in acrylonitrile-butadiene rubber (NBR) was conducted [314]. It was observed that compared to pure nitrile rubber, NBR/GO nanocomposites exhibited improved physical and mechanical properties owing to the additional crosslinking between the polymer chains of NBR facilitated by presence of sulfurization additives and GO reinforcements. In addition to the usage of vulcanization additives, material modification technology that leads to vulcanization through radiation also plays an important role in the rubber industry and the processing of other polymer materials. Natural rubber can undergo significant improvement in its physical and mechanical properties through radiation-induced crosslinking [315]. Phetarporn et al. [316] used electron beam irradiation technology for green vulcanization of graphene-based nanomaterials/natural rubber nanocomposites. They conducted vulcanization on both latex and film forms of the composites using gamma rays and EB. As the intensity of EB irradiation increased, the tensile and electrical properties of NR composites were enhanced. Moreover, conventional vulcanization methods lack environmental friendliness, particularly in large-scale production, while this straightforward approach is eco-friendly and easily applicable to other elastomeric materials.

## 5. Conclusions and perspectives

In this paper, the preparation techniques, characterization methods and properties of graphene, graphene oxide and graphene/elastomer nanocomposites are systematically reviewed. Graphene, with its excellent mechanical strength, thermal conductivity and electrical conductivity, has shown great application potential in many high-tech fields such as heat conducting materials, electronic equipment and energy storage. Graphene oxide has a wide application prospect in the fields of composite materials and energy because of its high specific surface area, the excellent mechanical properties and thermoelectric properties. The research further reveals that embedding graphene into elastomer can significantly improve comprehensive properties of composites, including mechanical strength, electrical conductivity and thermal conductivity, which makes graphene/elastomer nanocomposites a new material with great application value and is expected to play a crucial role in many industrial fields such as automobiles, aerospace, electronic appliances and so on. In addition, a series of advanced characterization techniques, such as SEM, TEM, XRD and XPS, are introduced in detail, which are very important for an understanding on the structure and properties of the above materials. Through these characterization methods, researchers can evaluate the application properties of

materials more accurately and provide scientific basis for the design and development of high-performance composites in the future.

Although the great potential of graphene-based materials has been proved in many applications, there are still several key problems to be solved to further deepen our understanding of graphene-based materials and expand their application prospects.

- (i) The preparation method of graphene has a decisive influence on its structure, number of layers and specific surface area. Therefore, it is very important to select the appropriate preparation technology based on the specific application requirements of graphene. At present, the mainstream preparation technologies include liquid phase stripping, ultrasonic stripping, mechanical stripping and chemical vapor deposition. Although these methods have their own advantages, the technology to realize large-scale, low-cost, high-quality and large-size graphene production still faces challenges. At present, the research focus is on developing new preparation technologies to improve the performance of graphene, reduce the cost and promote its wide application in the fields of electronics, energy and composite materials.
- (ii) The traditional preparation methods of graphene oxide, such as Brodie method, Staudenmaier method, Hummer method and Tour method, exist in problems including complicated operation, high cost, poor product quality and dispersion stability, and potential environmental risks. Future research will give priority to the development of green, environmentally friendly and efficient preparation technologies to solve these environmental and safety problems. This requires precise modification of the structure, oxidation degree and functional groups of graphene oxide to improve its performance and expand its application range.
- (iii) The preparation methods of graphene/elastomer nanocomposites are mainly divided into four categories: melt mixing, solution mixing, latex mixing and in-situ polymerization. When fabricating these composites, it is very important to choose a method that matches the expected application and characteristics. At present, the main challenges in the development of graphene/elastomer nanocomposites are the uniform dispersion of graphene in elastomer, the enhancement of interfacial adhesion and the realization of cost-effectiveness and mass production. Thus, it is of great significance to explore more effective and simple preparation methods to improve the functionality of graphene in composite materials, which is helpful to manufacture composite materials with enhanced characteristics and various properties, thus promoting its application in automobiles, electronic equipment, aerospace and biomedicine.

To sum up, if graphene-based materials can be applied to commercial and industrial applications on a large scale, it will make great contributions to the progress of human science and technology. It is hoped that many achievements and future challenges will stimulate more research interests in the field of graphene-based materials and further promote the broad engineering or commercial application prospects of graphene-based materials.

#### CRediT authorship contribution statement

**Kang Yang:** Writing – original draft. **Chao Wu:** Writing – review & editing. **Guoqing Zhang:** Supervision.

#### Declaration of competing interest

The authors declare that they have no known competing financial interests or personal relationships that could have appeared to influence the work reported in this paper.

#### Data availability

No data was used for the research described in the article.

#### Acknowledgments

This investigation is supported by the Anyang Institute of Technology Key Laboratory of Functional Materials and Remanufacturing Technology of Aviation Equipments (SYS202406); Project for Science and Technology Plan of Henan Province (242102220054); Key Training Project of Young Teacher of Henan province (2021GGJS149); Scientific cultivation Foundation of Anyang Institute of Technology (YPY2024003); Innovation Center for Chengguang High Performance Fluorine Material, Sichuan University of Science and Engineering (SCFY2208).

#### Appendix A. Supplementary material

Supplementary data to this article can be found online at <https://doi.org/10.1016/j.mseb.2024.117698>.

#### References

- [1] S. Zhang, M. Sharifuzzaman, S.M.S. Rana, M. Abu Zahed, S. Sharma, Y. Shin, H. Song, J.Y. Park, Highly conductive, stretchable, durable, skin-conformal dry electrodes based on thermoplastic elastomer-embedded 3D porous graphene for multifunctional wearable bioelectronics, *Nano Res.* 16 (5) (2023) 7627–7637, <https://doi.org/10.1007/s12274-023-5429-5>.
- [2] M.V. Timoshenko, S.V. Balabanov, M.M. Sychov, Influence of the Method of Graphene Introduction on Physical and Mechanical Properties of Thermoplastic Elastomers, *GLASS PHYSICS AND CHEMISTRY* 49 (5) (2023) 520–525, <https://doi.org/10.1134/S1087659623600515>.
- [3] Q. Chen, Y. Zhang, X. Li, Q. Wang, Y. Zhao, J. Wang, J. Wang, M. Kang, Q. Li, J. Wang, Boosting of polyurethane elastomer nanocomposites by low doped graphene, *FlatChem* 42 (2023) 100582, <https://doi.org/10.1016/j.flatc.2023.100582>.
- [4] H.P. Boehm, R. Setton, E. Stumpf, Nomenclature and terminology of graphite intercalation compounds, *Carbon* 24 (2) (1986) 241–245, [https://doi.org/10.1016/0008-6223\(86\)90126-0](https://doi.org/10.1016/0008-6223(86)90126-0).
- [5] H.-P. Boehm, E. Stumpf, Citation errors concerning the first report on exfoliated graphite, *Carbon* 45 (7) (2007) 1381–1383, <https://doi.org/10.1016/j.carbon.2006.12.016>.
- [6] K.S. Novoselov, A.K. Geim, S.V. Morozov, D. Jiang, Y. Zhang, S.V. Dubonos, I. V. Grigorieva, A.A. Firsov, Electric Field Effect in Atomically Thin Carbon Films, *Science* 306 (5696) (2004) 666–669, <https://doi.org/10.1126/science.1102896>.
- [7] A.K. Geim, K.S. Novoselov, The rise of graphene, *Nat. Mater.* 6 (3) (2007) 183–191, <https://doi.org/10.1038/nmat1849>.
- [8] A. Olatomiwa, T. Adam, C. Edet, A. Adewale, A. Chik, M. Mohammed, S. C. Gopinath, U. Hashim, Recent advances in density functional theory approach for optoelectronics properties of graphene, *Heliyon* 9 (3) (2023) E14279, <https://doi.org/10.1016/j.heliyon.2023.e14279>.
- [9] I.E.G.L. Souza, L.V. Cambraia, V.S. Gomide, E.H. Nunes, Short review on the use of graphene as a biomaterial –PROSPECTS, and CHALLENGES in Brazil, *J. Mater. Res. Technol.* 19 (2022) 2410–2430, <https://doi.org/10.1016/j.jmrt.2022.05.170>.
- [10] C. Shivananda, S. Madhu, G. Poojitha, A. Sudarshan, S. Jeethendra, K.N. Reddy, Structural, chemical and morphological properties of graphite powder, graphene oxide and reduced graphene oxide, *Mater. Today.: Proc.* 89 (1) (2023) 49–53, <https://doi.org/10.1016/j.mtpr.2023.04.608>.
- [11] Y. Zhang, J.P. Small, W.V. Pontius, P. Kim, Fabrication and electric-field-dependent transport measurements of mesoscopic graphite devices, *Appl. Phys. Lett.* 86 (7) (2005) 073104, <https://doi.org/10.1063/1.1862334>.
- [12] Z.Q. Yao, K.N. Zhang, A.Q. Xia, D.Z. Wang, C.G. Wang, H.F. Li, Y.L. Chen, One-step in-situ growth of CNTs on oxidized carbon fiber: Effects of catalyst concentration and growth time on mechanical properties of carbon fiber, *Polym. Compos.* 45 (7) (2024) 5827–5838, <https://doi.org/10.1002/pc.28163>.
- [13] A. Kausar, I. Ahmad, Nanocomposites of thermoplastic matrices with non-covalent fullerene reinforcement-Structural diversity, physical impact and potential, *J. Thermoplast. Compos. Mater.* 08927057241233568 (2024), <https://doi.org/10.1177/08927057241233568>.
- [14] S. Singh, M.R. Hasan, P. Sharma, J. Narang, Graphene nanomaterials: The wondering material from synthesis to applications, *Sensors International* 3 (2022) 100190, <https://doi.org/10.1016/j.sinti.2022.100190>.
- [15] X. Fu, J. Lin, Z. Liang, R. Yao, W. Wu, Z. Fang, W. Zou, Z. Wu, H. Ning, J. Peng, Graphene oxide as a promising nanofiller for polymer composite, *Surf. Interfaces* 37 (2023) 102747, <https://doi.org/10.1016/j.surfin.2023.102747>.
- [16] M.Y. Khalid, A. Kamal, A. Otabil, O. Mamoun, K. Liao, Graphene/epoxy nanocomposites for improved fracture toughness: A focused review on

- toughening mechanism, *Chemical Engineering Journal Advances* 16 (15) (2023) 100537, <https://doi.org/10.1016/j.cejadv.2023.100537>.
- [17] S. Utrera-Barrios, R. Verdejo, M.A. López-Manchado, M.H. Santana, Self-healing elastomers: A sustainable solution for automotive applications, *Eur. Polym. J.* 190 (2023) 112023, <https://doi.org/10.1016/j.eurpolymj.2023.112023>.
- [18] J.N. Sevening, S. Dottin, V.M. Torres, R.J. Hickey, Soft hybrid elastomers containing polymer grafted nanoparticles, *Giant* 12 (2022) 100133, <https://doi.org/10.1016/j.giant.2022.100133>.
- [19] P. Sayfo, D.Z. Pirityi, K. Pölöskei, Characterization of graphene-rubber nanocomposites: a review, *Mater. Today Chem.* 29 (2023) 101397, <https://doi.org/10.1016/j.mtchem.2023.101397>.
- [20] J. Gao, M. Zhou, G. Cheng, M. Tang, L. Sun, Y. Chen, C. Luo, Multilayer coatings of periodically co-deposited graphene and ag substrate: Improving the electrified friction interface by modifying the strength-ductility combination, *Surf. Coat. Technol.* 482 (2024) 130667, <https://doi.org/10.1016/j.surfcoat.2024.130667>.
- [21] A. Vasava, D. Singh, Development of hybrid surface composite of AA7075-T651 using TiO<sub>2</sub> and graphene through friction stir processing, *Mater. Today: Proc.* (2023), <https://doi.org/10.1016/j.matpr.2023.04.668>.
- [22] X. Zhang, Y. Ding, Z. Su, Y. Hu, M. Dai, H. Yang, S. Wang, Y. Tian, P. Hu, Growth of centimeter-scale single-crystal graphene on polycrystalline copper foil for ultrahigh sensitive sweat sensors, *Chem. Eng. J.* 497 (2024) 154716, <https://doi.org/10.1016/j.cej.2024.154716>.
- [23] J. Jin, Y. Su, J. Guo, Z. Zhang, B. Peng, M. Chen, L. Wu, Flexible Composite Films with Ultrahigh Through-plane Thermal Conductivity yet Low Graphene Content, *Compos. B Eng.* 111780 (2024), <https://doi.org/10.1016/j.compositesb.2024.111780>.
- [24] D.S. Sacanamboy, L. Quispe-Corimayhua, E.A. Tilvez, O. Yañez, Adsorption of aminomethylphosphonic acid on pristine graphene and graphene doped with transition metals: A theoretical study, *Chem. Phys. Lett.* 850 (2024) 141481, <https://doi.org/10.1016/j.cplett.2024.141481>.
- [25] H. Zhang, X. Liu, J. Han, W. Niu, B. Wang, Z. Wu, Z. Wei, Y. Zhu, Q. Guo, X. Wang, Acid-resistant chitosan/graphene oxide adsorbent for Cu<sup>2+</sup> removal: The role of mixed cross-linking and amino-functionalized, *Int. J. Biol. Macromol.* 273 (2024) 133096, <https://doi.org/10.1016/j.ijbiomac.2024.133096>.
- [26] R. Okuda, K. Kokubu, K. Hatada, E. Hashimoto, Y. Shinada, T. Watanabe, S. Koh, Conductive three-layer-stacked polycrystalline graphene intercalated with FeCl<sub>3</sub>, *Diam. Relat. Mater.* 148 (2024) 111469, <https://doi.org/10.1016/j.diamond.2024.111469>.
- [27] Y. Ting, K. Daqiang, H. Weiyi, Y. Yunjie, W. Chaoxia, Room-temperature self-healing graphene/rubber-based supramolecular elastomers utilized by dynamic boroxines and hydrogen bonds for human motion detection, *Colloids Surf A Physicochem Eng Asp* 657 (2023) 130411, <https://doi.org/10.1016/j.colsurfa.2022.130411>.
- [28] S. Raghuraman, S.A. Shah, M.J. Green, J.R. Felts, Mechanics of nanoscale crumpled graphene measured by Atomic Force Microscopy, *Extreme Mech. Lett.* 40 (2020) 100873, <https://doi.org/10.1016/j.eml.2020.100873>.
- [29] P. Gavallas, D. Savvas, G. Stefanou, Mechanical properties of graphene nanoplatelets containing random structural defects, *Mech. Mater.* 180 (2023) 104611, <https://doi.org/10.1016/j.mechmat.2023.104611>.
- [30] C. Lee, X. Wei, J.W. Kysar, J. Hone, Measurement of the elastic properties and intrinsic strength of monolayer graphene, *Science* 321 (5887) (2008) 385–388, <https://doi.org/10.1126/science.1157996>.
- [31] G. Huang, W. Chen, T. Wu, H. Guo, C. Fu, Y. Xue, K. Wang, P. Song, Multifunctional graphene-based nano-additives toward high-performance polymer nanocomposites with enhanced mechanical, thermal, flame retardancy and smoke suppressive properties, *Chem. Eng. J.* 410 (2021) 127590, <https://doi.org/10.1016/j.cej.2020.127590>.
- [32] Z. Huang, J. Zhang, Z. Wang, X. Peng, J. Fang, C. He, P. Fang, Study on NO<sub>2</sub> barrier properties of RTV silicone rubber by incorporation of functional graphene oxide, *Materials*, 2023, p. 1982.
- [33] J.A. Mann, W.R. Dichtel, Noncovalent functionalization of graphene by molecular and polymeric adsorbates, *J. Phys. Chem. Lett.* 4 (16) (2013) 2649–2657, <https://doi.org/10.1021/jz4010448>.
- [34] A. Sinitskii, A. Dimiev, D.A. Corley, A.A. Fursina, D.V. Kosynkin, J.M. Tour, Kinetics of diazonium functionalization of chemically converted graphene nanoribbons, *ACS Nano* 4 (4) (2010) 1949–1954, <https://doi.org/10.1021/nm901899j>.
- [35] E. Umar, M. Ikram, J. Haider, W. Nabgan, M. Imran, G. Nazir, 3D graphene-based material: Overview, perspective, advancement, energy storage, biomedical engineering and environmental applications a bibliometric analysis, *J. Environ. Chem. Eng.* 11 (5) (2023) 110339, <https://doi.org/10.1016/j.jece.2023.110339>.
- [36] Y. Xu, H. Cao, Y. Xue, B. Li, W. Cai, Liquid-Phase Exfoliation of Graphene: An Overview on Exfoliation Media, Techniques, and Challenges, *Nanomaterials* 8 (11) (2018) 942, <https://doi.org/10.3390/nano8110942>.
- [37] Xu, Chao, Yichang, Jin, Longzhi, Yang, Jianyi, Xiaoqing, Jiang, Characteristics of electro-refractive modulating based on Graphene-Oxide-Silicon waveguide, *Opt. Express* 20 (20) (2012) 22398–22405, <https://doi.org/10.1364/OE.20.022398>.
- [38] S.V. Morozov, K.S. Novoselov, M.I. Katnelson, F. Schedin, D.C. Elias, J. A. Jaszczak, A.K. Geim, Giant Intrinsic Carrier Mobilities in Graphene and Its Bilayer, *Phys. Rev. Lett.* 100 (1) (2008) 016602, <https://doi.org/10.1103/PhysRevLett.100.016602>.
- [39] L. Syam Sundar, M. Amin Mir, M. Waqar Ashraf, F. Djavanroodi, Synthesis and characterization of graphene and its composites for Lithium-Ion battery applications: A comprehensive review, *Alex. Eng. J.* 78 (2023) 224–245, <https://doi.org/10.1016/j.aej.2023.07.044>.
- [40] M. Yi, Z.-G. Shen, A review on mechanical exfoliation for the scalable production of graphene, *J. Mater. Chem. 3* (22) (2015) 11700–11715, <https://doi.org/10.1039/C5TA00252D>.
- [41] M. Yi, Z. Shen, J. Zhu, A fluid dynamics route for producing graphene and its analogues, *Chin. Sci. Bull.* 59 (16) (2014) 1794–1799, <https://doi.org/10.1007/s11434-014-0303-9>.
- [42] N. Song, J. Jia, W. Wang, Y. Gao, Y. Zhao, Y. Chen, Green production of pristine graphene using fluid dynamic force in supercritical CO<sub>2</sub>, *Chem. Eng. J.* 298 (2016) 198–205, <https://doi.org/10.1016/j.cej.2016.04.022>.
- [43] M.S.A. Bhuyan, M.N. Uddin, M.M. Islam, F.A. Bipasha, S.S. Hossain, Synthesis of graphene, *Int. Nano Lett.* 6 (2) (2016) 65–83, <https://doi.org/10.1007/s40089-015-0176-1>.
- [44] N. Kumar, R. Salehiyan, V. Chauke, O. Joseph Botlhoko, K. Setschedi, M. Scriba, M. Masukume, S. Sinha Ray, Top-down synthesis of graphene: A comprehensive review, *FlatChem* 27 (2021) 100224, <https://doi.org/10.1016/j.flatc.2021.100224>.
- [45] L. Zhang, X. Li, Y. Huang, Y. Ma, X. Wan, Y. Chen, Controlled synthesis of few-layered graphene sheets on a large scale using chemical exfoliation, *Carbon* 48 (8) (2010) 2367–2371, <https://doi.org/10.1016/j.carbon.2010.02.035>.
- [46] A.M. Abdellkader, A.J. Cooper, R.A.W. Dryfe, I.A. Kinloch, How to get between the sheets: a review of recent works on the electrochemical exfoliation of graphene materials from bulk graphite, *Nanoscale* 7 (16) (2015) 6944–6956, <https://doi.org/10.1039/C4NR06942K>.
- [47] J.-H. Ding, H.-R. Zhao, H.-B. Yu, A water-based green approach to large-scale production of aqueous compatible graphene nanoplatelets, *Sci. Rep.* 8 (1) (2018) 5567, <https://doi.org/10.1038/s41598-018-23859-5>.
- [48] S. Velmurugan, J. Anupriya, S.H.A. Chen, P. Traiwatcharanon, S.-H. Cheng, C. Wongchoosuk, Synergies of WO<sub>3</sub> and Co<sub>3</sub>O<sub>4</sub> intercalated ball milling exfoliated graphene 3D helix electrocatalyst: A highly sensitive electrochemical detection of mesotriione herbicide in vegetable samples, *Food Chem.* 432 (2023) 137221, <https://doi.org/10.1016/j.foodchem.2023.137221>.
- [49] Z. Li, Z.-Y. Gao, J. Hu, C. Mattioli, P. Ding, W. Xu, Y. Sun, J. Li, D. Zhong, Y. Huang, G. Li, F. Song, A. Gourdon, L.N. Kantorovich, F. Besenbacher, M. Yu, Large-distance quantum confinement passing through a single-layer graphene, *Cell Reports Physical Science* 4 (7) (2023) 101492, <https://doi.org/10.1016/j.xcrp.2023.101492>.
- [50] M. Yi, Z. Shen, Fluid dynamics: an emerging route for the scalable production of graphene in the last five years, *RSC Adv.* 6 (76) (2016) 72525–72536, <https://doi.org/10.1039/c6ra15269d>.
- [51] A.V. Tyurnina, J.A. Morton, A. Kaur, J. Mi, N. Grobert, K. Porfyrikis, I. Tzanakis, D.G. Eskin, Effects of green solvents and surfactants on the characteristics of few-layer graphene produced by dual-frequency ultrasonic liquid phase exfoliation technique, *Carbon* 206 (2023) 7–15, <https://doi.org/10.1016/j.carbon.2023.01.062>.
- [52] T.R. Lee, Quantitative correlation between interlayer distance and shear rate in liquid-based exfoliation of graphene layers, *Carbon* 129 (2018) 661–666, <https://doi.org/10.1016/j.carbon.2017.12.068>.
- [53] L. Cai, G. Tan, X. Jing, Y. Wu, Z. Liu, How to obtain high monolayer content in liquid phase exfoliation of graphene: A molecular dynamic simulation, *J. Mol. Liq.* 382 (15) (2023) 121873, <https://doi.org/10.1016/j.molliq.2023.121873>.
- [54] A. Amiri, M.H. Naraghi, G. Ahmadi, M. Soleymaniha, M. Shanbedi, A review on liquid-phase exfoliation for scalable production of pure graphene, wrinkled, crumpled and functionalized graphene and challenges, *FlatChem* 8 (2018) 40–71, <https://doi.org/10.1016/j.flatc.2018.03.004>.
- [55] L. Qin, B.M. Maciejewska, T. Subroto, J.A. Morton, K. Porfyrikis, I. Tzanakis, D.G. Eskin, N. Grobert, K. Fezzaa, J. Mi, Ultrafast synchrotron X-ray imaging and multiphysics modelling of liquid phase fatigue exfoliation of graphite under ultrasound, *Carbon* 186 (2022) 227–237, <https://doi.org/10.1016/j.carbon.2021.10.014>.
- [56] Y. Kwon, M. Liu, C. Castilho, Z. Saleeba, R. Hurt, I. Külaots, Controlling pore structure and conductivity in graphene nanosheet films through partial thermal exfoliation, *Carbon* 174 (2021) 227–239, <https://doi.org/10.1016/j.carbon.2020.12.050>.
- [57] W. Wei, T. Guan, C. Li, L. Shen, N. Bao, Heating Rate-Controlled Thermal Exfoliation for Foldable Graphene Sponge, *Industrial & Engineering Chemistry Research* 59 (7) (2020) 2946–2952, <https://doi.org/10.1021/acs.iecr.9b06114>.
- [58] Y. Qiu, S. Moore, R. Hurt, I. Külaots, Influence of external heating rate on the structure and porosity of thermally exfoliated graphite oxide, *Carbon* 111 (2017) 651–657, <https://doi.org/10.1016/j.carbon.2016.10.051>.
- [59] W. Gu, W. Zhang, X. Li, H. Zhu, J. Wei, Z. Li, Q. Shu, C. Wang, K. Wang, W. Shen, F. Kang, D. Wu, Graphene sheets from worm-like exfoliated graphite, *J. Mater. Chem. A* 19 (21) (2009) 3367–3369, <https://doi.org/10.1039/b904093p>.
- [60] J.S.Y. Chia, M.T.T. Tan, P. SimKhiew, J.K. Chin, H. Lee, D.C.S. Bien, A. Teh, C. W. Siong, Facile synthesis of few-layer graphene by mild solvent thermal exfoliation of highly oriented pyrolytic graphite, *Chem. Eng. J.* 231 (2013) 1–11, <https://doi.org/10.1016/j.cej.2013.06.106>.
- [61] Q. Yu, J. Lian, S. Siriponglert, H. Li, Y.P. Chen, S.-S. Pei, Graphene segregated on Ni surfaces and transferred to insulators, *Appl. Phys. Lett.* 93 (11) (2008) 113103, <https://doi.org/10.1063/1.2982585>.
- [62] A. Reina, X. Jia, J. Ho, D. Nezich, H. Son, V. Bulovic, M.S. Dresselhaus, J. Kong, Large area, few-layer graphene films on arbitrary substrates by chemical vapor deposition, *Nano Lett.* 9 (1) (2009) 30–35, <https://doi.org/10.1021/nl801827v>.
- [63] K.S. Kim, Y. Zhao, H. Jang, S.Y. Lee, J.M. Kim, K.S. Kim, J.-H. Ahn, P. Kim, J.-Y. Choi, B.H. Hong, Large-scale pattern growth of graphene films for stretchable transparent electrodes, *Nature* 457 (7230) (2009) 706–710, <https://doi.org/10.1038/nature07719>.

- [64] S. Pourbeyram, R. Bayrami, H. Dadkhah, Green synthesis and characterization of ultrafine copper oxide reduced graphene oxide (CuO/rGO) nanocomposite, *Colloids Surf. A: Physicochemical and Engineering Aspects* 529 (2017) 73–79, <https://doi.org/10.1016/j.colsurfa.2017.05.077>.
- [65] A.N. Obraztsov, E.A. Obraztsova, A.V. Tyurnina, A.A. Zolotukhin, Chemical vapor deposition of thin graphite films of nanometer thickness, *Carbon* 45 (10) (2007) 2017–2021, <https://doi.org/10.1016/j.carbon.2007.05.028>.
- [66] M. Gao, Y. Pan, L. Huang, H. Hu, L.Z. Zhang, H.M. Guo, S.X. Du, H.J. Gao, Epitaxial growth and structural property of graphene on Pt(111), *Appl. Phys. Lett.* 98 (3) (2011) 033101, <https://doi.org/10.1063/1.3543624>.
- [67] S. Bae, H. Kim, Y. Lee, X. Xu, J.-S. Park, Y. Zheng, J. Balakrishnan, T. Lei, H. Ri Kim, Y.I. Song, Y.-J. Kim, K.S. Kim, B. Özilmez, J.-H. Ahn, B.H. Hong, S. Iijima, Roll-to-roll production of 30-inch graphene films for transparent electrodes, *Nat. Nanotechnol.* 5 (8) (2010) 574–578, <https://doi.org/10.1038/nnano.2010.132>.
- [68] C. Backes, A.M. Abdellkader, C. Alonso, A. Andrieux-Ledier, R. Arenal, J. Azpeitia, N. Balakrishnan, L. Banszerus, J. Barjon, R. Bartali, Production and processing of graphene and related materials, 2D Materials 7 (2) (2020) 022001, <https://doi.org/10.1088/2053-1583/ab1e0a>.
- [69] J. Chen, Y. Li, L. Huang, C. Li, G. Shi, High-yield preparation of graphene oxide from small graphite flakes via an improved Hummers method with a simple purification process, *Carbon* 81 (2015) 826–834, <https://doi.org/10.1016/j.carbon.2014.10.033>.
- [70] X. Li, W. Cai, J. An, S. Kim, J. Nah, D. Yang, R. Piner, A. Velamakanni, I. Jung, E. Tutuc, Large-Area Synthesis of High-Quality and Uniform Graphene Films on Copper Foils, *Science* 324 (5932) (2009) 1312–1314, <https://doi.org/10.1126/science.1171245>.
- [71] A. Alnuaimi, I. Almansouri, I. Saadat, A. Nayfeh, Toward fast growth of large area high quality graphene using a cold-wall CVD reactor, *RSC Adv.* 7 (2017) 51951–51957, <https://doi.org/10.1039/C7RA10336K>.
- [72] L. Tao, J. Lee, H. Chou, M. Holt, R.S. Ruoff, D. Akinwande, Synthesis of high quality monolayer graphene at reduced temperature on hydrogen-enriched evaporated copper (111) films, *ACS Nano* 6 (3) (2012) 2319–2325, <https://doi.org/10.1021/nm205068n>.
- [73] B. Huet, X. Zhang, J.M. Redwing, D.W. Snyder, J.-P. Raskin, Multi-wafer batch synthesis of graphene on Cu films by quasi-static flow chemical vapor deposition, 2D Materials 6(4) (2019) 045032, Doi: 10.1088/2053-1583/ab33ae.
- [74] J.H. Cho, J.J. Gorman, S.R. Na, M. Cullinan, Growth of monolayer graphene on nanoscale copper-nickel alloy thin films, *Carbon* 115 (2017) 441–448, <https://doi.org/10.1016/j.carbon.2017.01.023>.
- [75] L. Jin, C. Zhao, Z. Gong, J. Pan, W. Wei, G. Wang, Y. Cui, Hydrogen-promoted graphene growth on Pt(111) via CVD methods, *Surf. Interfaces* 26 (2021) 101383, <https://doi.org/10.1016/j.surfin.2021.101383>.
- [76] C. Riedl, C. Coletti, T. Iwasaki, A. Zakharov, U. Starke, Quasi-free-standing epitaxial graphene on SiC obtained by hydrogen intercalation, *Phys. Rev. Lett.* 103 (24) (2009) 246804, <https://doi.org/10.1103/PhysRevLett.103.246804>.
- [77] S. Chaitoglou, E. Bertran, Effect of temperature on graphene grown by chemical vapor deposition, *J. Mater. Sci.* 52 (13) (2017) 8348–8356, <https://doi.org/10.1007/s10853-017-1054-1>.
- [78] M. Zhu, Z. Du, Z. Yin, W. Zhou, Z. Liu, S.H. Tsang, E.H.T. Teo, Low-Temperature In Situ Growth of Graphene on Metallic Substrates and Its Application in Anticorrosion, *ACS Appl. Mater. Interfaces* 8 (1) (2015) 502–510, <https://doi.org/10.1021/acsami.5b09453>.
- [79] M.G. Rybin, I.I. Kondrashov, A.S. Pozharov, V.C. Nguyen, N.M. Phan, E. D. Obraztsova, In Situ Control of CVD Synthesis of Graphene Film on Nickel Foil, *Phys. Status Solidi* 255 (1) (2017) 1700414, <https://doi.org/10.1002/pssb.201700414>.
- [80] S. Naghdi, K. Nešović, V. Mišković-Stanković, K.Y. Rhee, Comprehensive electrochemical study on corrosion performance of graphene coatings deposited by chemical vapour deposition at atmospheric pressure on platinum-coated molybdenum foil, *Corros. Sci.* 130 (2018) 31–44, <https://doi.org/10.1016/j.corsci.2017.10.021>.
- [81] Y.C.G. Kwan, G.M. Ng, C.H.A. Huan, Identification of functional groups and determination of carboxyl formation temperature in graphene oxide using the XPS O 1s spectrum, *Thin Solid Films* 590 (2015) 40–48, <https://doi.org/10.1016/j.tsf.2015.07.051>.
- [82] C.-S. Chen, C.-K. Hsieh, Effects of acetylene flow rate and processing temperature on graphene films grown by thermal chemical vapor deposition, *Thin Solid Films* 584 (2015) 265–269, <https://doi.org/10.1016/j.tsf.2014.12.012>.
- [83] M. Losurdo, M.M. Giangregorio, P. Capezzutto, G. Bruno, Graphene CVD growth on copper and nickel: role of hydrogen in kinetics and structure, *PCCP* 13 (46) (2011) 20836–20843, <https://doi.org/10.1039/c1cp22347j>.
- [84] Z. Li, P. Wu, C. Wang, X. Fan, J. Hou, Low-Temperature Growth of Graphene by Chemical Vapor Deposition Using Solid and Liquid Carbon Sources, *ACS Nano* 5 (4) (2011) 3385–3390, <https://doi.org/10.1021/nn200854p>.
- [85] T.J. Dransfield, K.K. Perkins, N.M. Donahue, J.G. Anderson, M.M. Sprengnether, K.L. Demerjian, Temperature and pressure dependent kinetics of the gas-phase reaction of the hydroxyl radical with nitrogen dioxide, *Geophys. Res. Lett.* 26 (6) (1999) 687–690, <https://doi.org/10.1029/1999gl900028>.
- [86] A. Guermoune, T. Chari, F. Popescu, S.S. Sabri, J. Guillemette, H.S. Skulason, T. Szkopel, M. Sajiaj, Chemical vapor deposition synthesis of graphene on copper with methanol, ethanol, and propanol precursors, *Carbon* 49 (13) (2011) 4204–4210, <https://doi.org/10.1016/j.carbon.2011.05.054>.
- [87] Y. Miyata, K. Kamon, K. Ohashi, R. Kitaura, M. Yoshimura, H. Shinohara, A simple alcohol-chemical vapor deposition synthesis of single-layer graphenes using flash cooling, *Appl. Phys. Lett.* 96 (26) (2010) 263105, <https://doi.org/10.1063/1.3458797>.
- [88] N. Soriadi, M.F. Abdullah, F.S. Md Yakin, S.A. Mohamad Badaruddin, M.I. Syono, Effect of Cu thickness and temperature on growth of graphene on 8-inch Cu/SiO<sub>2</sub>/Si wafer using cold-wall CVD reactor, *Materials Today: Proceedings* 42(5) (2021) 2948–2952, Doi: 10.1016/j.matpr.2020.12.800.
- [89] J.-B. Wang, Z. Ren, Y. Hou, X.-L. Yan, P.-Z. Liu, H. Zhang, H.-X. Zhang, J.-J. Guo, A review of graphene synthesis at low temperatures by CVD methods, *New Carbon Mater.* 35 (3) (2020) 193–208, [https://doi.org/10.1016/S1872-5805\(20\)60484-X](https://doi.org/10.1016/S1872-5805(20)60484-X).
- [90] R.R. Nair, P. Blake, A.N. Grigorenko, K.S. Novoselov, T.J. Booth, T. Stauber, N. M. Peres, A.K. Geim, Fine structure constant defines visual transparency of graphene, *Science* 320 (5881) (2008) 1308, <https://doi.org/10.1126/science.1156965>.
- [91] Tsai, Jeff, T., H., Chen, Jeng, Shiung, Chu, Kevin, K., Graphene-edge probes for scanning tunneling microscopy, *J. Light Electronoptic* 130 (2017) 976–980, Doi: 10.1016/j.jleo.2016.11.022.
- [92] H. Hiura, H. Miyazaki, K. Tsukagoshi, Determination of the number of graphene layers: discrete distribution of the secondary electron intensity stemming from individual graphene layers, *Appl. Phys Express* 3 (9) (2010) 095101, <https://doi.org/10.1143/APEX.3.095101>.
- [93] A. Shah, J.A. Schiller, I. Ramos, J. Serrano, D.K. Adams, S. Tawfick, E. Ertekin, Automated image segmentation of scanning electron microscopy images of graphene using U-Net Neural Network, *Mater. Today Commun.* 35 (2023) 106127, <https://doi.org/10.1016/j.mtcomm.2023.106127>.
- [94] Leo, Gross, Fabian, Mohn, Nikolaj, Moll, Peter, Liljeroth, Gerhard, Meyer, The chemical structure of a molecule resolved by atomic force microscopy, *Science* 325(5944) (2009) 1110–1114, Doi: 10.1126/science.1176210.
- [95] M.D. Jiménez-Sánchez, N. Nicoara, J.M. Gómez-Rodríguez, Chemical identification with non-contact atomic force microscopy of xenon atoms adsorbed on graphene on Pt(111) surfaces, *Appl. Surf. Sci.* 542 (2021) 148669, <https://doi.org/10.1016/j.apsusc.2020.148669>.
- [96] S.W. Cranford, M.J. Buehler, Packing efficiency and accessible surface area of crumpled graphene, *Phys. Rev. B* 84 (20) (2011) 205451, <https://doi.org/10.1103/PhysRevB.84.205451>.
- [97] J. Lang, Y. Li, Z. Ye, Y. Yang, F. Xu, G. Huang, J. Zhang, F. Li, Investigating the effect of substrate stiffness on the redox state of cardiac fibroblasts using scanning electrochemical microscopy, *Anal. Chem.* 93 (14) (2021) 5797–5804, <https://doi.org/10.1021/acs.analchem.0c05284>.
- [98] R. Ram, V.E. Coyle, A.M. Bond, M. Chen, S.K. Bhargava, L.A. Jones, A scanning electrochemical microscopy (SECM) study of the interfacial solution chemistry at polarised chalcopyrite (CuFeS<sub>2</sub>) and chalcocite (Cu<sub>2</sub>S), *Electrochim. Commun.* 115 (2020) 106730, <https://doi.org/10.1016/j.elecom.2020.106730>.
- [99] Y. Li, J. Lang, Z. Ye, M. Wang, F. Li, Effect of substrate stiffness on redox state of single cardiomyocyte: a scanning electrochemical microscopy study, *Anal. Chem.* 92 (7) (2020) 4771–4779, <https://doi.org/10.1021/acs.analchem.9b03178>.
- [100] H.-Y. Du, Y.-F. Huang, D. Wong, M.-F. Tseng, Y.-H. Lee, C.-H. Wang, C.-L. Lin, G. Hoffmann, K.-H. Chen, L.-C. Chen, Nanoscale redox mapping at the MoS<sub>2</sub>-liquid interface, *Nat. Commun.* 12 (1) (2021) 1321, <https://doi.org/10.1038/s41467-021-21660-z>.
- [101] X. Shi, W. Qing, T. Marhaba, W. Zhang, Atomic force microscopy-Scanning electrochemical microscopy (AFM-SECM) for nanoscale topographical and electrochemical characterization: Principles, applications and perspectives, *Electrochim. Acta* 332 (2020) 135472, <https://doi.org/10.1016/j.electacta.2019.135472>.
- [102] D. Liu, Z. Shadique, R. Lin, K. Qian, H. Li, K. Li, S. Wang, Q. Yu, M. Liu, S. Ganapathy, X. Qin, Q.H. Yang, M. Wagemaker, F. Kang, X.Q. Yang, B. Li, Review of recent development of in situ/operando characterization techniques for lithium battery research, *Adv. Mater.* 31 (28) (2019) 1806620, <https://doi.org/10.1002/adma.201806620>.
- [103] Y. Takahashi, Y. Kobayashi, Z. Wang, Y. Ito, M. Ota, H. Ida, A. Kumatanai, K. Miyazawa, T. Fujita, H. Shiku, Y.E. Korchev, Y. Miyata, T. Fukuma, M. Chen, T. Matsue, High-resolution electrochemical mapping of the hydrogen evolution reaction on transition-metal dichalcogenide nanosheets, *Angew. Chem. Int. Ed.* 59 (9) (2020) 3601–3608, <https://doi.org/10.1002/anie.201912863>.
- [104] S.C.S. Lai, A.N. Patel, K. McKelvey, P.R. Unwin, Definitive evidence for fast electron transfer at pristine basal plane graphite from high-resolution electrochemical imaging, *Angew. Chem. Int. Ed.* 51 (22) (2012) 5405–5408, <https://doi.org/10.1002/anie.201200564>.
- [105] R. Gao, M.A. Edwards, Y. Qiu, K. Barman, H.S. White, Visualization of hydrogen evolution at individual platinum nanoparticles at a buried interface, *J. Am. Chem. Soc.* 142 (19) (2020) 8890–8896, <https://doi.org/10.1021/jacs.0c02202>.
- [106] Neil, Ebejer, Aleix, G., Güell, Stanley, S. C., Lai, Kim, McKelvey, Scanning Electrochemical Cell Microscopy: A Versatile Technique for Nanoscale Electrochemistry and Functional Imaging, *Annual Review of Analytical Chemistry* 6(1) (2013) 329–351, Doi: 10.1146/annurev-anchem-062012-092650.
- [107] R. Jin, H.-Y. Lu, L. Cheng, J. Zhuang, D. Jiang, H.-Y. Chen, Highly spatial imaging of electrochemical activity on the wrinkles of graphene using all-solid scanning electrochemical cell microscopy, *Fundamental Research* 2 (2) (2022) 193–197, <https://doi.org/10.1016/j.fmre.2021.08.001>.
- [108] M.S. Seehra, A.S. Pavlovic, X-Ray diffraction, thermal expansion, electrical conductivity, and optical microscopy studies of coal-based graphites, *Carbon* 31 (4) (1993) 557–564, [https://doi.org/10.1016/0008-6223\(93\)90109-N](https://doi.org/10.1016/0008-6223(93)90109-N).
- [109] D.J. Lim, N.A. Marks, M.R. Rowles, Universal scherrer equation for graphene fragments, *Carbon* 162 (2020) 475–480, <https://doi.org/10.1016/j.carbon.2020.02.064>.

- [110] T.F. Emiru, D.W. Ayele, Controlled synthesis, characterization and reduction of graphene oxide: a convenient method for large scale production, Egyptian J. Basic Appl. Sci. 4 (1) (2017) 74–79, <https://doi.org/10.1016/j.ejbas.2016.11.002>.
- [111] A. Merlen, J. Buijnsters, C. Pardanaud, A guide to and review of the use of multiwavelength raman spectroscopy for characterizing defective aromatic carbon solids: from graphene to amorphous carbons, Coatings 7 (10) (2017) 153, <https://doi.org/10.3390/coatings7100153>.
- [112] Y. Jiang, J. Wang, L. Malfatti, D. Carboni, N. Senes, P. Innocenzi, Highly durable graphene-mediated surface enhanced Raman scattering (G-SERS) nanocomposites for molecular detection, Appl. Surf. Sci. 450 (2018) 451–460, <https://doi.org/10.1016/j.apsusc.2018.04.218>.
- [113] S.L.H. Rebelo, A. Guedes, M.E. Lipińska, A.M. Pereira, J.P. Araujo, C. Freire, Progresses on the Raman spectra analysis of covalently functionalized multiwall carbon nanotubes: unraveling disorder on graphitic materials, PCCP 18 (18) (2016) 12784–12796, <https://doi.org/10.1039/C5CP06519D>.
- [114] A.C. Ferrari, D.M. Basko, Raman spectroscopy as a versatile tool for studying the properties of graphene, Nat. Nanotechnol. 8 (4) (2013) 235–246, <https://doi.org/10.1038/nnano.2013.46>.
- [115] F. Tuinstra, Raman Spectrum of Graphite, J. Chem. Phys. 53 (3) (1970) 1126–1130, <https://doi.org/10.1063/1.1674108>.
- [116] E. Kusiak-Nejman, R. Wróbel, J. Kapica-Kozar, A. Wanag, K. Szymbańska, E. Mijowska, A. Morawski, Hybrid carbon-TiO<sub>2</sub> spheres: investigation of structure, morphology and spectroscopic studies, Appl. Surf. Sci. 469 (2019) 684–690, <https://doi.org/10.1016/j.apsusc.2018.11.093>.
- [117] E.A. Arkhipova, A.S. Ivanov, N.E. Strokova, S.A. Chernyak, A.V. Shumyatsev, K. I. Maslakov, S.V. Savilov, V.V. Lunin, Structural evolution of nitrogen-doped carbon nanotubes: From synthesis and oxidation to thermal defunctionalization, Carbon 125 (2017) 20–31, <https://doi.org/10.1016/j.carbon.2017.09.013>.
- [118] S.D. Costa, A. Righi, C. Fantini, Y. Hao, C. Magnuson, L. Colombo, R.S. Ruoff, M. A. Pimenta, Resonant Raman spectroscopy of graphene grown on copper substrates, Solid State Commun. 152 (15) (2012) 1317–1320, <https://doi.org/10.1016/j.ssc.2012.05.001>.
- [119] S.A. Chernyak, A.S. Ivanov, K.I. Maslakov, A.V. Egorov, Z. Shen, S.S. Savilov, V. V. Lunin, Oxidation, defunctionalization and catalyst life cycle of carbon nanotubes: a Raman spectroscopy view, PCCP 19 (3) (2017) 2276–2285, <https://doi.org/10.1039/C6CP04657F>.
- [120] W.W. Liu, S.P. Chai, A.R. Mohamed, U. Hashim, Synthesis and characterization of graphene and carbon nanotubes: A review on the past and recent developments, J. Ind. Eng. Chem. 20 (4) (2014) 1171–1185, <https://doi.org/10.1016/j.jiec.2013.08.028>.
- [121] C. Russo, F. Stanzione, M. Alfe, A. Ciajolo, A. Tregrossi, Spectral analysis in the UV-visible range for revealing the molecular form of combustion-generated carbonaceous species, Combust. Sci. Technol. 184 (7–8) (2012) 1219–1231, <https://doi.org/10.1080/00102202.2012.664315>.
- [122] D.K. Das, H. Bhattacharjee, S.K. Sahoo, S. Sahoo, Dependence of thermal conductivity of graphene on the coefficient of linear expansion and temperature, Mater. Today: Proc. (2023), <https://doi.org/10.1016/j.mtproc.2023.06.149>.
- [123] D.G. Papageorgiou, I.A. Kinloch, R.J. Young, Mechanical Properties of Graphene and Graphene-based Nanocomposites, Prog. Mater. Ence 90 (2017) 75–127, <https://doi.org/10.1016/j.pmatsci.2017.07.004>.
- [124] R. Rudrapati, Graphene: Fabrication Methods, Properties, and Applications in Modern Industries, (2020), Doi: 10.5772/intechopen.83309.
- [125] Y. Chandra, S. Adhikari, E.I. Saavedra Flores, L. Figiel, Advances in finite element modelling of graphene and associated nanostructures, Mater. Sci. Eng. R: Rep. 140 (2020) 100544, Doi: 10.1016/j.mser.2020.100544.
- [126] O. Aluko, S. Gowtham, G.M. Odegard, Multiscale modeling and analysis of graphene nanoplatelet/carbon fiber/epoxy hybrid composite, Compos. B Eng. 131 (2017) 82–90, <https://doi.org/10.1016/j.compositesb.2017.07.075>.
- [127] H. Ghodrati, R. Ghomashchi, Effect of graphene dispersion and interfacial bonding on the mechanical properties of metal matrix composites: An overview, FlatChem 16 (140) (2019) 100113, <https://doi.org/10.1016/j.flatc.2019.100113>.
- [128] S.A. Hosseini Kordkheili, H. Moshrefzadeh-Sani, Mechanical properties of double-layered graphene sheets, Comput. Mater. Sci. 69 (2013) 335–343, Doi: 10.1016/j.commatsci.2012.11.027.
- [129] M. Niu, L. Miao, Z. Xu, Y. Zhao, W. Hao, J. Li, C. Sui, C. Wang, Tunable tensile mechanical properties of bilayer graphene through inter-layer rotation, Diam. Relat. Mater. 130 (2022) 109522, <https://doi.org/10.1016/j.diamond.2022.109522>.
- [130] Rashi, Exploring the methods of synthesis, functionalization, and characterization of graphene and graphene oxide for supercapacitor applications, Ceram. Int. 49 (1) (2023) 40–47, Doi: 10.1016/j.ceraint.2022.10.333.
- [131] A.A. Balandin, Thermal properties of graphene and nanostructured carbon materials, Nat. Mater. 10 (8) (2011) 569–581, <https://doi.org/10.1038/nmat3064>.
- [132] R. Prasher, Graphene spreads the heat, Science 328 (5975) (2010) 185–186, <https://doi.org/10.1126/science.1188998>.
- [133] F. Liu, M. Wang, Y. Chen, J. Gao, Thermal stability of graphene in inert atmosphere at high temperature, J. Solid State Chem. 276 (2019) 100–103, <https://doi.org/10.1016/j.jssc.2019.04.008>.
- [134] X. Yang, S. Fan, Y. Li, Y. Guo, Y. Li, K. Ruan, S. Zhang, J. Zhang, J. Kong, J. Gu, Synchronously improved electromagnetic interference shielding and thermal conductivity for epoxy nanocomposites by constructing 3D copper nanowires/thermally annealed graphene aerogel framework, Compos. A Appl. Sci. Manuf. 128 (2020) 105670, <https://doi.org/10.1016/j.compositesa.2019.105670>.
- [135] A.A. Balandin, S. Ghosh, W. Bao, I. Calizo, D. Teweldebrhan, F. Miao, C.N. Lau, Superior thermal conductivity of single-layer graphene, Nano Lett. 8 (3) (2008) 902–907, <https://doi.org/10.1021/nl0731872>.
- [136] H.Y. Nan, Z.H. Ni, J. Wang, Z. Zafar, Z.X. Shi, Y.Y. Wang, The thermal stability of graphene in air investigated by Raman spectroscopy, J. Raman Spectrosc. 44 (7) (2013) 1018–1021, <https://doi.org/10.1002/jrs.4312>.
- [137] H. Lin, Q. Jian, X. Bai, D. Li, Z. Huang, W. Huang, S. Feng, Z. Cheng, Recent advances in thermal conductivity and thermal applications of graphene and its derivatives nanofluids, Appl. Therm. Eng. 218 (2023) 119176, <https://doi.org/10.1016/j.applthermaleng.2022.119176>.
- [138] K. Ruan, J. Gu, Ordered alignment of liquid crystalline graphene fluoride for significantly enhancing thermal conductivities of liquid crystalline polyimide composite films, Macromolecules 55 (10) (2022) 4134–4145, <https://doi.org/10.1021/acs.macromol.2c00491>.
- [139] L. Chen, N. Li, X. Yu, S. Zhang, C. Liu, Y. Song, Z. Li, S. Han, W. Wang, P. Yang, A general way to manipulate electrical conductivity of graphene, Chem. Eng. J. 462 (2023) 142139, <https://doi.org/10.1016/j.cej.2023.142139>.
- [140] V.A. Margulis, E.E. Muryumin, E.A. Gaiduk, Optical second-harmonic generation from two-dimensional hexagonal crystals with broken space inversion symmetry, J. Phys. Condens. Matter 25 (19) (2013) 195302, <https://doi.org/10.1088/0953-8984/25/19/195302>.
- [141] T. Kuilla, S. Bhadra, D. Yao, N.H. Kim, S. Bose, J.H. Lee, Recent advances in graphene based polymer composites, Prog. Polym. Sci. 35 (11) (2010) 1350–1375, <https://doi.org/10.1016/j.progpolymsci.2010.07.005>.
- [142] E. Tkalya, M. Ghislandi, R. Otten, M. Lotya, A. Alekseev, P. van der Schoot, J. Coleman, G. de With, C. Koning, Experimental and theoretical study of the influence of the state of dispersion of graphene on the percolation threshold of conductive graphene/polystyrene nanocomposites, ACS Appl. Mater. Interfaces 6 (17) (2014) 15113–15121, <https://doi.org/10.1021/am503238z>.
- [143] I. Medalia, Avrom, Electrical conduction in carbon black composites, Rubber Chem. Technol. 59 (3) (1986) 432–454, <https://doi.org/10.5254/1.3538209>.
- [144] D. Carponcin, E. Dantras, G. Aridon, F. Levallois, L. Cadiergues, C. Lacabanne, Evolution of dispersion of carbon nanotubes in Polyamide 11 matrix composites as determined by DC conductivity, Compos. Sci. Technol. 72 (4) (2012) 515–520, <https://doi.org/10.1016/j.compscitech.2011.12.012>.
- [145] C. Bessaguet, E. Dantras, G. Michon, M. Chevalier, L. Laffont, C. Lacabanne, Electrical behavior of a graphene/PEKK and carbon black/PEKK nanocomposites in the vicinity of the percolation threshold, J. Non Cryst. Solids 512 (2019) 1–6, <https://doi.org/10.1016/j.jnoncrysol.2019.02.017>.
- [146] P.T. Yin, S. Shah, M. Chhowalla, K.B. Lee, Design, synthesis, and characterization of graphene-nanoparticle hybrid materials for bioapplications, Chem. Rev. 115 (7) (2015) 2483–2531, <https://doi.org/10.1021/cr500537t>.
- [147] M. Tahani, B.G. Shohany, L. Motevalizadeh, Study of structural, electronic, and mechanical properties of pure and hydrogenated multilayer penta-graphene nano-plates using density functional theory, Mater. Today Commun. 28 (2021) 102608, <https://doi.org/10.1016/j.mtcomm.2021.102608>.
- [148] M.A.B. Hamid, K.T. Chan, C.H. Raymond Ooi, H. Zainuddin, N. Mohd Shah, N.N. Shahrol Nizdam, Structural stability and electronic properties of graphene/germanene heterobilayer, Results in Physics 28 (2021) 104545, Doi: 10.1016/j.rinp.2021.104545.
- [149] C.J. Raj, R. Manikandan, P. Thondaiman, P. Sivakumar, A.D. Savariraj, W.-J. Cho, B.C. Kim, H. Jung, Sonoelectrochemical exfoliation of graphene in various electrolytic environments and their structural and electrochemical properties, Carbon 184 (2021) 266–276, <https://doi.org/10.1016/j.carbon.2021.08.027>.
- [150] J. Xiang, L.T. Drzal, Thermal conductivity of exfoliated graphite nanoplatelet paper, Carbon 49 (3) (2011) 773–778, <https://doi.org/10.1016/j.carbon.2010.10.003>.
- [151] G. Shao, Y. Lu, F. Wu, C. Yang, F. Zeng, Q. Wu, Graphene oxide: the mechanisms of oxidation and exfoliation, J. Mater. Sci. 47 (10) (2012) 4400–4409, <https://doi.org/10.1007/s10853-012-6294-5>.
- [152] J. Liu, S. Chen, Y. Liu, B. Zhao, Progress in preparation, characterization, surface functional modification of graphene oxide: A review, J. Saudi Chem. Soc. 26 (6) (2022) 101560, <https://doi.org/10.1016/j.jscs.2022.101560>.
- [153] Q.L. 1, Y.G. 1, T.W. 1, W.L.C. 1, Wu, J.D.O. Phys., Astron., U.O. Kansas, Lawrence, KS, U.O. Kansas, Metal-catalyst-free and controllable growth of high-quality monolayer and AB-stacked bilayer graphene on silicon dioxide, Carbon 96 (2016) 203–211, Doi: 10.1016/j.carbon.2015.09.075.
- [154] G. Eda, C. Mattevi, H. Yamaguchi, H.K. Kim, M. Chhowalla, Insulator to semi-metal transition in graphene oxide, Physics 113 (35) (2009) 15768–15771, <https://doi.org/10.1021/jp9051402>.
- [155] X. Jiao, L. Zhang, Y. Qiu, J. Guan, Comparison of the adsorption of cationic blue onto graphene oxides prepared from natural graphites with different graphitization degrees, Colloids Surf A Physicochem Eng Asp 529 (2017) 292–301, <https://doi.org/10.1016/j.colsurfa.2017.05.094>.
- [156] Q. Yu, L. Wei, X. Yang, C. Wang, J. Chen, H. Du, W. Shen, F. Kang, Z.-H. Huang, Electrochemical synthesis of graphene oxide from graphite flakes exfoliated at room temperature, Appl. Surf. Sci. 598 (2022) 153788, <https://doi.org/10.1016/j.apsusc.2022.153788>.
- [157] L. Staudenmaier, Verfahren zur Darstellung der Graphitsäure, Ber. Dtsch. Chem. Ges. 31 (2) (1898) 1481–1487, <https://doi.org/10.1002/cber.18980310237>.
- [158] A.M. Dimiev, J.M. Tour, Mechanism of Graphene Oxide Formation, ACS Nano 8 (3) (2014) 3060–3068, <https://doi.org/10.1021/mn500606a>.
- [159] W.S.H. Jr, R.E. Offeman, Preparation of Graphitic Oxide, J. Am. Chem. Soc. 80 (6) (1958) 1339, <https://doi.org/10.1021/ja01539a017>.

- [160] J. Chen, B. Yao, C. Li, G. Shi, An improved Hummers method for eco-friendly synthesis of graphene oxide, *Carbon* 64 (2013) 225–229, <https://doi.org/10.1016/j.carbon.2013.07.055>.
- [161] E.H. Sujiono, Zurnansyah, D. Zabrian, M.Y. Dahlan, B.D. Amin, Samnur, J. Agus, Graphene oxide based coconut shell waste: synthesis by modified Hummers method and characterization, *Heliyon* 6(8) (2020) e04568, Doi: 10.1016/j.heliyon.2020.e04568.
- [162] N.I. Zaaba, K.L. Foo, U. Hashim, S.J. Tan, W.-W. Liu, C.H. Voon, Synthesis of Graphene Oxide using Modified Hummers Method: Solvent Influence, *Procedia Eng.* 184 (2017) 469–477, <https://doi.org/10.1016/j.proeng.2017.04.118>.
- [163] A. Zhou, T. Yu, X. Liang, S. Yin, H2O2-free strategy derived from Hummers method for preparing graphene oxide with high oxidation degree, *FlatChem* 38 (2023) 100487, <https://doi.org/10.1016/j.flatc.2023.100487>.
- [164] X. Chen, Z. Qu, Z. Liu, G. Ren, Mechanism of oxidization of graphite to graphene oxide by the hummers method, *ACS Omega* 7 (27) (2022) 23503–23510, <https://doi.org/10.1021/acsomega.2c01963>.
- [165] N.I. Kovtyukhova, P.J. Ollivier, B.R. Martin, T.E. Mallouk, S.A. Chizhik, E. V. Buzanava, A.D. Gorchinskiy, Layer-by-Layer Assembly of Ultrathin Composite Films from Micron-Sized Graphite Oxide Sheets and Polycations, *Chem. Mater.* 11 (3) (1999) 771–778, <https://doi.org/10.1021/cm981058u>.
- [166] M. Sohail, M. Saleem, S. Ullah, N. Saeed, A. Afzidi, M. Khan, M. Arif, Modified and improved Hummer's synthesis of graphene oxide for capacitors applications, *Mod. Electron. Mater.* 3 (3) (2017) 110–116, <https://doi.org/10.1016/j.moem.2017.07.002>.
- [167] H. Hy, M. Forster, A. Lerf, J. Klinowski, A new structural model for graphite oxide, *Chem. Phys. Lett.* 287 (1–2) (1998) 53–56, [https://doi.org/10.1016/S0009-2614\(98\)00144-4](https://doi.org/10.1016/S0009-2614(98)00144-4).
- [168] J.J. Yang, I.M. El-Nahhal, G.E. Maciel, Synthesis and solid-state NMR structural characterization of some functionalized polysiloxanes, *J. Non Cryst. Solids* 204 (2) (1996) 105–117, [https://doi.org/10.1016/S0022-3093\(96\)00412-7](https://doi.org/10.1016/S0022-3093(96)00412-7).
- [169] S. Mohammed, Graphene oxide: A mini-review on the versatility and challenges as a membrane material for solvent-based separation, *Chemical Engineering Journal Advances* 12 (2022) 100392, <https://doi.org/10.1016/j.cej.2022.100392>.
- [170] R. Yuan, J. Yuan, Y. Wu, P. Ju, L. Ji, H. Li, L. Chen, H. Zhou, J. Chen, Graphene oxide-monohydrated manganese phosphate composites: Preparation via modified Hummers method, *Colloids Surf A Physicochem Eng Asp* 547 (2018) 56–63, <https://doi.org/10.1016/j.colsurfa.2018.03.023>.
- [171] R. Trusovas, K. Ratautas, G. Račiukaitis, J. Barkauskas, I. Stankevičienė, G. Niaura, R. Mažeikienė, Reduction of graphite oxide to graphene with laser irradiation, *Carbon* 52 (2013) 574–582, <https://doi.org/10.1016/j.carbon.2012.10.017>.
- [172] D. Voiry, J. Yang, J. Kupferberg, R. Fullon, C. Lee, H.Y. Jeong, H.S. Shin, M. Chhowalla, High-quality graphene via microwave reduction of solution-exfoliated graphene oxide, *Science* 353 (6306) (2016) 1413–1416, <https://doi.org/10.1126/science.aah3398>.
- [173] J. Song, X. Wang, C.-T. Chang, Preparation and Characterization of Graphene Oxide, *J. Nanomater.* 2014 (1) (2014) 276143, <https://doi.org/10.1155/2014/276143>.
- [174] Y. Liu, Y. Zhang, L. Duan, W. Zhang, M. Su, Z. Sun, P. He, Polystyrene/graphene oxide nanocomposites synthesized via Pickering polymerization, *Prog. Org. Coat.* 99 (2016) 23–31, <https://doi.org/10.1016/j.porgcoat.2016.04.034>.
- [175] J.I. Paredes, S. Villar-Rodil, A. Martínez-Alonso, T. Jmjd, Graphene oxide dispersions in organic solvents, *Langmuir*, The ACS Journal of Surfaces and Colloids 24 (19) (2008) 10560–10564, <https://doi.org/10.1021/la801744a>.
- [176] J. Liu, X. Li, W. Jia, Z. Li, Y. Zhao, S. Ren, Demulsification of Crude Oil-in-Water Emulsions Driven by Graphene Oxide Nanosheets, *Energy Fuel* 29 (7) (2015) 4644–4653, <https://doi.org/10.1021/acs.energyfuels.5b00966>.
- [177] E. Aliyev, V. Filiz, M.M. Khan, Y.J. Lee, C. Abetz, V. Abetz, Structural Characterization of Graphene Oxide: Surface Functional Groups and Fractionated Oxidative Debris, *Nanomaterials* 9 (8) (2019) 1180, <https://doi.org/10.3390/nano9081180>.
- [178] Z. Li, L. Deng, I.A. Kinloch, R.J. Young, Raman spectroscopy of carbon materials and their composites: Graphene, nanotubes and fibres, *Prog. Mater Sci.* 135 (2023) 101089, <https://doi.org/10.1016/j.pmatsci.2023.101089>.
- [179] J.-B. Wu, M.-L. Lin, X. Cong, H.-N. Liu, P.-H. Tan, Raman spectroscopy of graphene-based materials and its applications in related devices, *Chem. Soc. Rev.* 47 (5) (2018) 1822–1873, <https://doi.org/10.1039/c6cs00915h>.
- [180] L. Newman, N. Lozano, M. Zhang, S. Iijima, M. Yudasaka, C. Bussy, K. Kostarelos, Hypochlorite degrades 2D graphene oxide sheets faster than 1D oxidised carbon nanotubes and nanohorns, *njp 2D Materials and Applications* 1(1) (2017) 39, Doi: 10.1038/s41699-017-0041-3.
- [181] A.C. Ferrari, J.C. Meyer, V. Scardaci, C. Casiraghi, M. Lazzeri, F. Mauri, S. Pisacane, D. Jiang, K.S. Novoselov, S. Roth, A.K. Geim, Raman Spectrum of Graphene and Graphene Layers, *Phys. Rev. Lett.* 97 (18) (2006) 187401, <https://doi.org/10.1103/PhysRevLett.97.187401>.
- [182] J. Park, A. Reina, R. Saito, J. Kong, G. Dresselhaus, M. Dresselhaus, G' band Raman spectra of single, double and triple layer graphene, *Carbon* 47 (5) (2009) 1303–1310, <https://doi.org/10.1016/j.carbon.2009.01.009>.
- [183] H. Renata, C.C.H. Gumz, Z.R.A.N.D. Simone, P.S. Henrique, Characterization of graphene nanosheets obtained by a modified Hummer's method, *Matería* 23 (1) (2018) e-11988, <https://doi.org/10.1590/S1517-707620170001.0324>.
- [184] A. Kaniyoor, S. Ramaprabhu, A Raman spectroscopic investigation of graphite oxide derived graphene, *AIP Adv.* 2 (3) (2012) 032183, <https://doi.org/10.1063/1.4756995>.
- [185] M. Chaudhary, R. Seugar, M. Yadav, M. Kumar, P. Kumar, Synthesis and characterization of graphene oxide, *Progress. Agric.* 19 (1) (2019) 158–160, <https://doi.org/10.5958/0976-4615.2019.00028.0>.
- [186] S.-S. Wang, D.-Y. Feng, Z.-M. Zhang, X. Liu, K.-P. Ruan, Y.-Q. Guo, J.-W. Gu, Highly Thermally Conductive Polydimethylsiloxane Composites with Controllable 3D GO@f-CNTs Networks via Self-sacrificing Template Method, *Chin. J. Polym. Sci.* 42 (7) (2024) 897–906, <https://doi.org/10.1007/s10118-024-3098-4>.
- [187] S. Wang, D. Feng, H. Guan, Y. Guo, X. Liu, C. Yan, L. Zhang, J. Gu, Highly efficient thermal conductivity of polydimethylsiloxane composites via introducing “Line-Plane”-like hetero-structured fillers, *Compos. A Appl. Sci. Manuf.* 157 (2022) 106911, <https://doi.org/10.1016/j.compositesa.2022.106911>.
- [188] D. Lin, C. Richard Liu, G.J. Cheng, Single-layer graphene oxide reinforced metal matrix composites by laser sintering: Microstructure and mechanical property enhancement, *Acta Mater.* 80 (2014) 183–193, <https://doi.org/10.1016/j.actamat.2014.07.038>.
- [189] L. Nedjar, A. Melki, Z.B.D. Sayah, M.-C. Cherfa, R.-A. Lounes, A. Manseri, J.-F. Durastanti, Z. Mekhalif, Towards an efficient pn heterojunction in ternary composite material based polypyrrole, metal oxide and surface functionalized graphene for thermoelectric properties enhancement, *Synth. Met.* 298 (2023) 117427, <https://doi.org/10.1016/j.synthmet.2023.117427>.
- [190] A. Mallik, M.S. Ali, S. Karmkar, K. Dutta, B. Gangopadhyay, M.S. Ali, T. Das, S. Panda, S. Bhattacharya, A. Chamuah, Single step synthesis of amine functionalized graphene oxide/Cu-Ni bimetallic nanocomposite and tuning its electrical properties, *Mater. Sci. Eng. B* 296 (2023) 116627, <https://doi.org/10.1016/j.mseb.2023.116627>.
- [191] A. Mulone, Z. Xia, U. Klement, Electrodeposition of FeW-graphene composites: effect of graphene oxide concentration on microstructure, hardness and corrosion properties, *FlatChem* 40 (2023) 100525, <https://doi.org/10.1016/j.flatc.2023.100525>.
- [192] J.W. Suk, R.D. Piner, J. An, R.S. Ruoff, Mechanical properties of monolayer graphene oxide, *ACS Nano* 4 (11) (2010) 6557–6564, <https://doi.org/10.1021/nn101781v>.
- [193] Y. Guo, H. Qiu, K. Ruan, Y. Zhang, J. Gu, Hierarchically multifunctional polyimide composite films with strongly enhanced thermal conductivity, *Nano-Micro Letters* 14 (1) (2021) 1–13, <https://doi.org/10.1007/s40820-021-00767-4>.
- [194] Y. Han, K. Ruan, X. He, Y. Tang, H. Guo, Y. Guo, H. Qiu, J. Gu, Highly thermally conductive aramid nanofiber composite films with synchronous visible/infrared camouflages and information encryption, *Angew. Chem.* 136 (17) (2024) e202401538.
- [195] Y. Zhang, K. Ruan, K. Zhou, J. Gu, Controlled distributed Ti3C2Tx hollow microspheres on thermally conductive polyimide composite films for excellent electromagnetic interference shielding, *Adv. Mater.* 35 (16) (2023) 2211642, <https://doi.org/10.1002/adma.202211642>.
- [196] Y. Guo, S. Wang, H. Zhang, H. Guo, M. He, K. Ruan, Z. Yu, G.S. Wang, H. Qiu, J. Gu, Consistent Thermal Conductivities of Spring-Like Structured Polydimethylsiloxane Composites under Large Deformation, *Adv. Mater.* (2024) 2404648, <https://doi.org/10.1002/adma.202404648>.
- [197] S. Yu, Y. Yang, J. Zhu, L. Ma, W. Jia, Q. Zhou, J. Wang, Wear and anticorrosive properties of graphene oxide-cellulose nanofiber composite coatings, *Mater. Chem. Phys.* 305 (2023) 128002, <https://doi.org/10.1016/j.matchemphys.2023.128002>.
- [198] S. Mallakpour, A. Abdolmaleki, S. Borandeh, Covalently functionalized graphene sheets with biocompatible natural amino acids, *Appl. Surf. Sci.* 307 (2014) 533–542, <https://doi.org/10.1016/j.apsusc.2014.04.070>.
- [199] M.J. Deka, U. Baruah, D. Chowdhury, Insight into electrical conductivity of graphene and functionalized graphene: Role of lateral dimension of graphene sheet, *Mater. Chem. Phys.* 163 (2015) 236–244, <https://doi.org/10.1016/j.matchemphys.2015.07.036>.
- [200] J. Chen, X. Zhang, X. Zheng, C. Liu, X. Cui, W. Zheng, Size distribution-controlled preparation of graphene oxide nanosheets with different C/O ratios, *Mater. Chem. Phys.* 139 (1) (2013) 8–11, <https://doi.org/10.1016/j.matchemphys.2012.12.025>.
- [201] S. Zhang, H. Wang, J. Liu, C. Bao, Measuring the specific surface area of monolayer graphene oxide in water, *Mater. Lett.* 261 (2020) 127098, <https://doi.org/10.1016/j.matchemat.2019.127098>.
- [202] S. Park, S. Ji, Y. Yoon, S.K. Kim, W. Song, S. Myung, J. Lim, H.-K. Jung, S.S. Lee, K.-S. An, Fabrication of fanlike L-shaped graphene nanostructures with enhanced thermal/electrochemical properties via laser irradiation, *Carbon* 182 (2021) 691–699, <https://doi.org/10.1016/j.carbon.2021.05.045>.
- [203] J. Chen, L. Li, Effect of oxidation degree on the thermal properties of graphene oxide, *J. Mater. Res. Technol.* 9 (6) (2020) 13740–13748, <https://doi.org/10.1016/j.jmrt.2020.09.092>.
- [204] A.P.M. Leandro, M.A. Seas, K. Vap, A.S. Tyrrell, V. Jain, H. Wahab, P.A. Johnson, Evolution of structural and electrical properties in coal-derived graphene oxide nanomaterials during high-temperature annealing, *Diam. Relat. Mater.* 112 (2021) 108244, <https://doi.org/10.1016/j.diamond.2021.108244>.
- [205] W. Gao, L.B. Alemany, L. Ci, P.M. Ajayan, New insights into the structure and reduction of graphite oxide, *Nat. Chem.* 1 (5) (2009) 403–408, <https://doi.org/10.1038/nchem.281>.
- [206] K.Z. Riahi, N. Sdri, D.J. Ennigrou, K. Horchani-Naifer, Investigations on electrical conductivity and dielectric properties of graphene oxide nanosheets synthesized from modified Hummer's method, *J. Mol. Struct.* 1216 (2020) 128304, <https://doi.org/10.1016/j.molstruc.2020.128304>.
- [207] D. Torres, S. Pérez-Rodríguez, D. Sebastián, J.L. Pinilla, M.J. Lázaro, I. Suelves, Graphene oxide nanofibers: A nanocarbon material with tuneable electrochemical

- properties, *Appl. Surf. Sci.* 509 (2020) 144774, <https://doi.org/10.1016/j.apusc.2019.144774>.
- [208] A. Amirkiai, M. Abrisham, M. Panahi-Sarmad, X. Xiao, A. Alimardani, M. Sadri, Tracing evolutions of elastomeric composites in shape memory actuators: A comprehensive review, *Mater. Today Commun.* 28 (2021) 102658, <https://doi.org/10.1016/j.mtcomm.2021.102658>.
- [209] S. Wacharawichanant, A. Sangkaphan, N. Sa-Nguanwong, V. Khamnonwat, S. Thongyai, P. Praserthdam, Effects of particle type on thermal and mechanical properties of polyoxymethylene nanocomposites, *J. Appl. Polym. Sci.* 123 (6) (2011) 3217–3224, <https://doi.org/10.1002/app.34984>.
- [210] C. Shivananda, Silk fibroin-based green colloidal silver nanoparticle synthesis and their antibacterial and anticancer properties, *Inorg. Chem. Commun.* 158 (2) (2023) 111611, <https://doi.org/10.1016/j.inoche.2023.111611>.
- [211] C. Shivananda, B. Rao, B. Lakshmeesha, G.R. Shetty, Y. Sangappa, Structural and thermal properties of silk fibroin–Silver nanoparticles composite films, *AIP Conference Proceedings*, AIP Publishing, 2018, p. 030245.
- [212] C. Shivananda, S. Asha, R. Madhukumar, S. Satish, B. Narayana, K. Byrappa, Y. Wang, Y. Sangappa, Biosynthesis of colloidal silver nanoparticles: their characterization and antibacterial activity, *Biomed. Phys. Eng. Express* 2 (3) (2016) 035004, <https://doi.org/10.1088/2057-1976/2/3/035004>.
- [213] M. Przybylak, M. Bakar, M. Mendrycka, U. Kosikowska, A. Malm, M. Worzakowska, T. Szymborski, K. Kędra-Królik, Rubber elastomeric nanocomposites with antimicrobial properties, *Mater. Sci. Eng. C* 76 (2017) 269–277, <https://doi.org/10.1016/j.msec.2017.03.080>.
- [214] K. Kushimoto, M. Moriyama, A. Shimosaka, Y. Shirakawa, J. Hidaka, S. Ishihara, J. Kano, Measurement method for dispersion states of filler particles in particulate composite materials by macroscopic permittivity, *Adv. Powder Technol.* 32 (1) (2021) 272–282, <https://doi.org/10.1016/j.japt.2020.12.003>.
- [215] J.C. Meyer, A.K. Geim, M.I. Katsnelson, K.S. Novoselov, T.J. Booth, S. Roth, The structure of suspended graphene sheets, *Nature* 446 (7131) (2007) 60–63, <https://doi.org/10.1038/nature05545>.
- [216] Z. Yang, J. Liu, R. Liao, G. Yang, X. Wu, Z. Tang, B. Guo, L. Zhang, Y. Ma, Q. Nie, F. Wang, Rational design of covalent interfaces for graphene/elastomer nanocomposites, *Compos. Sci. Technol.* 132 (2016) 68–75, <https://doi.org/10.1016/j.compscitech.2016.06.015>.
- [217] T. Takahashi, S. Tsubo, K. Inoue, R. Suzuki, H. Murata, M. Tachibana, Effect of dispersibility of carbon nanotubes on the hardness and thermal properties of polyphenylene sulphide/carbon nanotube composites obtained using solution mixing and melt blending methods, *Mater. Sci. Eng. B* 295 (2023) 116579, <https://doi.org/10.1016/j.mseb.2023.116579>.
- [218] G. Mittal, V. Dhand, K.Y. Rhee, S.-J. Park, W.R. Lee, A review on carbon nanotubes and graphene as fillers in reinforced polymer nanocomposites, *J. Ind. Eng. Chem.* 21 (2015) 11–25, <https://doi.org/10.1016/j.jiec.2014.03.022>.
- [219] G. Sui, D. Liu, Y. Liu, W. Ji, Q. Zhang, Q. Fu, The dispersion of CNT in TPU matrix with different preparation methods: solution mixing vs melt mixing, *Polymer* 182 (2019) 121838, <https://doi.org/10.1016/j.polymer.2019.121838>.
- [220] M. Hernández, M.d.M. Bernal, R. Verdejo, T.A. Ezquerro, M.A. López-Manchado, Overall performance of natural rubber/graphene nanocomposites, *Composites Science and Technology* 73 (2012) 40–46, Doi: 10.1016/j.compscitech.2012.08.012.
- [221] Y. Mao, C. Wang, L. Liu, Preparation of graphene oxide/natural rubber composites by latex co-coagulation: Relationship between microstructure and reinforcement, *Chin. J. Chem. Eng.* 28 (4) (2020) 1187–1193, <https://doi.org/10.1016/j.cjche.2020.01.015>.
- [222] S. Jiang, Z. Gui, C. Bao, K. Dai, X. Wang, K. Zhou, Y. Shi, S. Lo, Y. Hu, Preparation of functionalized graphene by simultaneous reduction and surface modification and its polymethyl methacrylate composites through latex technology and melt blending, *Chem. Eng. J.* 226 (2013) 326–335, <https://doi.org/10.1016/j.cej.2013.04.068>.
- [223] S.S. Ochigbo, A.S. Luyt, W.W. Focke, Latex derived blends of poly(vinyl acetate) and natural rubber: thermal and mechanical properties, *J. Mater. Sci.* 44 (12) (2009) 3248–3254, <https://doi.org/10.1007/s10853-009-3435-6>.
- [224] M. Zhang, Y. Li, Z. Su, G. Wei, Recent advances in the synthesis and applications of graphene–polymer nanocomposites, *Polym. Chem.* 6 (34) (2015) 6107–6124, <https://doi.org/10.1039/CSPY00777A>.
- [225] H.-N. Mao, X.-G. Wang, Use of in-situ polymerization in the preparation of graphene / polymer nanocomposites, *New Carbon Mater.* 35 (4) (2020) 336–343, [https://doi.org/10.1016/s1872-5805\(20\)60493-0](https://doi.org/10.1016/s1872-5805(20)60493-0).
- [226] H. Wang, G. Xie, M. Fang, Z. Ying, Y. Tong, Y. Zeng, Mechanical reinforcement of graphene/poly (vinyl chloride) composites prepared by combining the in-situ suspension polymerization and melt-mixing methods, *Compos. B Eng.* 113 (2017) 278–284, <https://doi.org/10.1016/j.compositesb.2017.01.053>.
- [227] J.W. Zha, H.D. Yan, W.K. Li, Z.M. Dang, Environmentally friendly polypropylene/thermoplastic elastomer composites with modified graphene oxide for HVDC application, *IEEE Trans. Dielectr. Electr. Insul.* 25 (3) (2018) 1088–1094, <https://doi.org/10.1109/TDEI.2018.007006>.
- [228] H. Kim, Y. Miura, C.W. Macosko, Graphene/Polyurethane Nanocomposites for Improved Gas Barrier and Electrical Conductivity, *Chem. Mater.* 22 (11) (2010) 3441–3450, <https://doi.org/10.1021/cm100477v>.
- [229] X. Bai, C. Wan, Y. Zhang, Y. Zhai, Reinforcement of hydrogenated carboxylated nitrile-butadiene rubber with exfoliated graphene oxide, *Carbon* 49 (5) (2011) 1608–1613, <https://doi.org/10.1016/j.carbon.2010.12.043>.
- [230] H. Lian, S. Li, K. Liu, L. Xu, K. Wang, W. Guo, Study on modified graphene/butyl rubber nanocomposites. I. Preparation and characterization, *Polymer Engineering & Science* 51(11) (2011) 2254–2260, Doi: 10.1002/pen.21997.
- [231] X. Xue, Q. Yin, H. Jia, X. Zhang, Y. Wen, Q. Ji, Z. Xu, Enhancing mechanical and thermal properties of styrene-butadiene rubber/carboxylated acrylonitrile butadiene rubber blend by the usage of graphene oxide with diverse oxidation degrees, *Appl. Surf. Sci.* 423 (2017) 584–591, <https://doi.org/10.1016/j.apusc.2017.06.200>.
- [232] J.S. Kim, J.H. Yun, I. Kim, S.E. Shim, Electrical properties of graphene/SBR nanocomposite prepared by latex heterocoagulation process at room temperature, *J. Ind. Eng. Chem.* 17 (2) (2011) 325–330, <https://doi.org/10.1016/j.jiec.2011.02.034>.
- [233] A. Mathkar, T.N. Narayanan, L.B. Alemany, P. Cox, P. Nguyen, G. Gao, P. Chang, R. Romero-Aburto, S.A. Mani, P.M. Ajayan, Synthesis of Fluorinated Graphene Oxide and its Amphiphobic Properties, Part. Part. Syst. Char. 30 (3) (2013) 266–272, <https://doi.org/10.1002/ppsc.201200091>.
- [234] T. Bharathidasan, T.N. Narayanan, S. Sathyaranayanan, S.S. Sreejakumari, Above 170° water contact angle and oleophobicity of fluorinated graphene oxide based transparent polymeric films, *Carbon* 84 (2015) 207–213, <https://doi.org/10.1016/j.carbon.2014.12.004>.
- [235] C. Bao, Y. Guo, L. Song, Y. Kan, X. Qian, Y. Hu, In situ preparation of functionalized graphene oxide/epoxy nanocomposites with effective reinforcements, *J. Mater. Chem.* 21 (35) (2011) 13290–13298, <https://doi.org/10.1039/c1jm11434d>.
- [236] H. Jeon, Y. Kim, W.-R. Yu, J.U. Lee, Exfoliated graphene/thermoplastic elastomer nanocomposites with improved wear properties for 3D printing, *Compos. B Eng.* 189 (2020) 107912, <https://doi.org/10.1016/j.compositesb.2020.107912>.
- [237] L. Zhang, Y. Li, H. Guo, H. Zhang, N. Zhang, T. Hayat, Y. Sun, Decontamination of U(VI) on graphene oxide/Al2O3 composites investigated by XRD, FT-IR and XPS techniques, *Environ. Pollut.* 248 (2019) 332–338, <https://doi.org/10.1016/j.envpol.2019.01.126>.
- [238] M. Liu, J.H. Hui, I.A. Kinloch, R.J. Young, D.G. Papageorgiou, Deformation and tearing of graphene-reinforced elastomer nanocomposites, *Compos. Commun.* 25 (2021) 100764, <https://doi.org/10.1016/j.coco.2021.100764>.
- [239] L. Yuanzheng, W. Youqi, H. Jiang, L. Buyin, Nanofiber enhanced graphene-elastomer with unique biomimetic hierarchical structure for energy storage and pressure sensing, *Mater. Des.* 203 (2021) 109612, <https://doi.org/10.1016/j.matdes.2021.109612>.
- [240] M. Das, T.R. Aswathy, S. Pal, K. Naskar, Effect of ionic liquid modified graphene oxide on mechanical and self-healing application of an ionic elastomer, *Eur. Polym. J.* 158 (2021) 110691, <https://doi.org/10.1016/j.eurpolymj.2021.110691>.
- [241] M. Aakyir, J.-A. Oh, S. Araby, Q. Zheng, M. Naeem, J. Ma, P. Adu, L. Zhang, Y.-W. Mai, Combining hydrophilic MXene nanosheets and hydrophobic carbon nanotubes for mechanically resilient and electrically conductive elastomer nanocomposites, *Compos. Sci. Technol.* 214 (2021) 108997, <https://doi.org/10.1016/j.compscitech.2021.108997>.
- [242] S.A. Najafabadi, A. Mohammadi, A.Z. Kharazi, Polyurethane nanocomposite impregnated with chitosan-modified graphene oxide as a potential antibacterial wound dressing, *Mater. Sci. Eng. C* 115 (2020) 110899, <https://doi.org/10.1016/j.msec.2020.110899>.
- [243] A. Ghozatloo, M. Sharifi-Niasar, A.M. Rashidi, Investigation of heat transfer coefficient of ethylene glycol/ graphenenanofluid in turbulent flow regime, *Int. J. Nanosci. Nanotechnol.* 10 (4) (2014) 237–244.
- [244] L.S. Severo, J.B. Rodrigues, D.A. Campanelli, V.M. Pereira, J.W. Menezes, E.W. de Menezes, C. Valsecchi, M.A.Z. Vasconcellos, L.E.G. Armas, Synthesis and Raman characterization of wood sawdust ash, and wood sawdust ash-derived graphene, *Diam. Relat. Mater.* 117 (2021) 108496, <https://doi.org/10.1016/j.diamond.2021.108496>.
- [245] P. Pareek, H. Dave, L. Ledwan, Microwave assisted modification of graphene oxide: Characterization and application for adsorptive removal of cationic dye, *Mater. Today.: Proc.* 43 (5) (2021) 3277–3285, <https://doi.org/10.1016/j.matpr.2021.01.956>.
- [246] R.S. Yadav, I. Kuritka, J. Vilcakova, D. Skoda, P. Urbánek, M. Machovsky, M. Masář, L. Kalina, J. Havlíčka, Lightweight NiFe2O4-Reduced Graphene Oxide-Elastomer Nanocomposite flexible sheet for electromagnetic interference shielding application, *Compos. B Eng.* 166 (2019) 95–111, <https://doi.org/10.1016/j.compositesb.2018.11.069>.
- [247] M. Kashif, Y.-W. Chang, Supramolecular hydrogen-bonded polyolefin elastomer/modified graphene nanocomposites with near infrared responsive shape memory and healing properties, *Eur. Polym. J.* 66 (2015) 273–281, <https://doi.org/10.1016/j.eurpolymj.2015.02.007>.
- [248] J.U. Arikpo, M.U. Onuu, Optical and electrical characterization of microwave power system chemical vapour deposited (MPS-CVD) graphene on Ni electroplated Cu foil at varying temperatures, *Vacuum* 182 (2020) 109767, <https://doi.org/10.1016/j.vacuum.2020.109767>.
- [249] L.-S. Lin, W. Bin-Tay, Y.-R. Li, Z. Aslam, A. Westwood, R. Brydson, A practical characterisation protocol for liquid-phase synthesised heterogeneous graphene, *Carbon* 167 (2020) 307–321, <https://doi.org/10.1016/j.carbon.2020.06.008>.
- [250] A. Negi, K. Bijalwan, J. Rawat, H. Sharma, C. Dwivedi, Synthesis and characterization of the nanocomposites of graphene oxide in polyethylene glycol (PEG), *Mater. Today.: Proc.* 45 (6) (2021) 4742–4745, <https://doi.org/10.1016/j.matpr.2021.01.182>.
- [251] M. Pierpaoli, M. Ficek, P. Jakóbczyk, J. Karczewski, R. Bogdanowicz, Self-assembly of vertically orientated graphene nanostructures: Multivariate characterisation by Minkowski functionals and fractal geometry, *Acta Mater.* 214 (2021) 116989, <https://doi.org/10.1016/j.actamat.2021.116989>.
- [252] C. Shivananda, R. Madhu Kumar, B. Narayana, K. Byrappa, P. Renu, Y. Wang, Y. Sangappa, Preparation and characterisation of silk fibroin–silver nanoparticles

- (SF-AgNPs) composite films, *Mater. Res. Innov.* 21 (4) (2017) 210–214, <https://doi.org/10.1080/14328917.2016.1200844>.
- [253] C. Shivananda, G.P. Kumar, M. Vivek, S. Madhu, B.L. Rao, Silver nanoparticles reinforced on silk fibroin/carboxymethylcellulose composite films for electrical applications, *Mater. Sci. Eng. B* 304 (2024) 117392, <https://doi.org/10.1016/j.mseb.2024.117392>.
- [254] S. Li, Z. Li, T.L. Burnett, T.J.A. Slater, T. Hashimoto, R.J. Young, Nanocomposites of graphene nanoplatelets in natural rubber: microstructure and mechanisms of reinforcement, *J. Mater. Sci.* 52 (16) (2017) 9558–9572, <https://doi.org/10.1007/s10853-017-1144-0>.
- [255] F.-Z. Zhang, X.-B. Liu, C.-M. Yang, G.-D. Chen, Y. Meng, H.-B. Zhou, S.-H. Zhang, Insights into robust carbon nanotubes in tribology: From nano to macro, *Mater. Today* 74 (2024) 203–234, <https://doi.org/10.1016/j.mattod.2024.03.001>.
- [256] S. Paszkiewicz, A. Szymczyk, Z. Spitalský, J. Mosnáček, K. Kwiatkowski, Z. Roslaniec, Structure and properties of nanocomposites based on PTT-block-PTMO copolymer and graphene oxide prepared by in situ polymerization, *Eur. Polym. J.* 50 (2014) 69–77, <https://doi.org/10.1016/j.eurpolymj.2013.10.031>.
- [257] J. Wu, W. Xing, G. Huang, H. Li, M. Tang, S. Wu, Y. Liu, Vulcanization kinetics of graphene/natural rubber nanocomposites, *Polymer* 54 (13) (2013) 3314–3323, <https://doi.org/10.1016/j.polymer.2013.04.044>.
- [258] Y. Luo, P. Zhao, Q. Yang, D. He, L. Kong, Z. Peng, Fabrication of conductive elastic nanocomposites via framing intact interconnected graphene networks, *Compos. Sci. Technol.* 100 (2014) 143–151, <https://doi.org/10.1016/j.compscitech.2014.05.037>.
- [259] Y. Qiu, J. Wang, D. Wu, Z. Wang, M. Zhang, Y. Yao, N. Wei, Thermoplastic polyester elastomer nanocomposites filled with graphene: Mechanical and viscoelastic properties, *Compos. Sci. Technol.* 132 (2016) 108–115, <https://doi.org/10.1016/j.compscitech.2016.07.005>.
- [260] M. Liu, I.A. Kinloch, R.J. Young, D.G. Papageorgiou, Modelling mechanical percolation in graphene-reinforced elastomer nanocomposites, *Compos. B Eng.* 178 (2019) 107506, <https://doi.org/10.1016/j.compositesb.2019.107506>.
- [261] Q. Meng, G. Guo, X. Qin, Y. Zhang, X. Wang, L. Zhang, Smart multifunctional elastomeric nanocomposite materials containing graphene nanoplatelets, *Smart Mater. Manufact.* 1 (2023) 100006, <https://doi.org/10.1016/j.smmf.2022.100006>.
- [262] X.-B. Fu, X. Tong, J.-C. Yang, G. Zhang, M.-L. Zhang, X.-J. Wang, J. Yang, In situ polymerization preparation and mechanical properties of nanocomposites based on PA10T/10I-block-PEG copolymer and graphene oxide, *Nano Materials Science* 4 (3) (2022) 276–284, <https://doi.org/10.1016/j.nanoms.2021.09.004>.
- [263] N.I.N. Haris, M.Z. Hassan, R. Ilyas, M.A. Suhot, S. Sapuan, R. Dolah, R. Mohammad, M. Asyraf, Dynamic mechanical properties of natural fiber reinforced hybrid polymer composites: A review, *J. Mater. Res. Technol.* 19 (2022) 167–182, <https://doi.org/10.1016/j.jmrt.2022.04.155>.
- [264] B. Prasad Sahoo, K. Naskar, D. Kumar Tripathy, Multiwalled carbon nanotube-filled ethylene acrylic elastomer nanocomposites: Influence of ionic liquids on the mechanical, dynamic mechanical, and dielectric properties, *Polym. Compos.* 37 (8) (2016) 2568–2580, <https://doi.org/10.1002/polc.23451>.
- [265] B. Prasad Sahoo, Fabrication of radiation crosslinked and MWCNT reinforced ethylene acrylic elastomer nanocomposites: Evaluation of mechanical, dynamic mechanical, thermal and dielectric properties, *Materials Today: Proceedings* 41 (2) (2021) 203–210, Doi: 10.1016/j.matpr.2020.08.692.
- [266] A. Kiziltas, S. Tamrakar, J. Rizzo, D. Mielewski, Characterization of graphene nanoplatelets reinforced sustainable thermoplastic elastomers, *Composites Part c: Open Access* 6 (2021) 100172, <https://doi.org/10.1016/j.jcomc.2021.100172>.
- [267] M. Carrier, A. Loppinet-Serani, D. Denux, J.-M. Lasnier, F. Ham-Pichavant, F. Cansell, C. Aymonier, Thermogravimetric analysis as a new method to determine the lignocellulosic composition of biomass, *Biomass Bioenergy* 35 (1) (2011) 298–307, <https://doi.org/10.1016/j.biombioe.2010.08.067>.
- [268] P. Song, B. Liu, C.B. Liang, K.P. Ruan, H. Qiu, Z.L. Ma, Y.Q. Guo, J.W. Gu, Lightweight, Flexible Cellulose-Derived Carbon Aerogel@Reduced Graphene Oxide/PDMS Composites with Outstanding EMI Shielding Performances and Excellent Thermal Conductivities, *NANO-MICRO LETTERS* 13 (1) (2021) 91, <https://doi.org/10.1007/s40820-021-00624-4>.
- [269] S.S. Rahman, M. Arshad, M. Zubair, M. Gharsi-Khouzani, A. Qureshi, A. Ullah, Facile fabrication of graphene oxide/poly(styrene-co-methyl methacrylate) nanocomposite with high toughness and thermal stability, *Mater. Today Commun.* 25 (2020) 101633, <https://doi.org/10.1016/j.mtcomm.2020.101633>.
- [270] P. Wang, S. Tang, F. Sheng, J. Cai, P. Fei, A. Nawaz, N. Walayat, A.B. Javaid, H. Xiong, Crystallization, thermal stability, barrier property, and aging resistance application of multi-functionalized graphene oxide/poly(lactide)/starch nanocomposites, *Int. J. Biol. Macromol.* 132 (2019) 1208–1220, <https://doi.org/10.1016/j.ijbiomac.2019.03.183>.
- [271] B.d.S.M. da Cruz, L.G.P. Tienne, F.F. Gondim, L.d.S. Candido, E.G. Chaves, M.d.F. V. Marques, F.S. da Luz, S.N. Monteiro, Graphene nanoplatelets reinforced Polyamide-11 nanocomposites thermal stability and aging for application in flexible pipelines, *J. Mater. Res. Technol.* 18 (2022) 1842–1854, <https://doi.org/10.1016/j.jmrt.2022.03.075>.
- [272] M. Akrami, I. Ghasemi, H. Azizi, M. Karrabi, M. Seyedabadi, A new approach in compatibilization of the poly (lactic acid)/thermoplastic starch (PLA/TPS) blends, *Carbohydr. Polym.* 144 (2016) 254–262, <https://doi.org/10.1016/j.carbpol.2016.02.035>.
- [273] A. Łapińska, N. Grochowska, K. Filak, P. Michałski, K.R. Szymański, P.A. Zaleski, K. Dydek, A. Daniszewska, K. Źerańska, A. Dużyńska, S. Kowalczyk, A. Plichta, Non-metallic multifunctional PVDF – Graphene nanoplatelets nanocomposites as an effective electromagnetic shield, thermal and electrical conductor, *Materials Today Advances* 18 (2023) 100365, <https://doi.org/10.1016/j.mtadv.2023.100365>.
- [274] G.-S. He, Y. Dai, P. Wang, C.-Y. Zhang, C.-M. Lin, K. Yang, J.-H. Zhang, R.-L. Zhong, S.-J. Liu, Z.-J. Yang, Achieving superior thermal conductivity in polymer bonded explosives using a preconstructed 3D graphene framework, *Energetic Materials Frontiers* 4 (3) (2023) 202–212, <https://doi.org/10.1016/j.emmf.2023.07.002>.
- [275] Y. Su, J.J. Li, G.J. Weng, Theory of thermal conductivity of graphene-polymer nanocomposites with interfacial Kapitza resistance and graphene-graphene contact resistance, *Carbon* 137 (2018) 222–233, <https://doi.org/10.1016/j.carbon.2018.05.033>.
- [276] X. Huang, C. Zhi, Y. Lin, H. Bao, G. Wu, P. Jiang, Y.-W. Mai, Thermal conductivity of graphene-based polymer nanocomposites, *Mater. Sci. Eng. R. Rep.* 142 (2020) 100577, <https://doi.org/10.1016/j.mser.2020.100577>.
- [277] A. Yu, P. Ramesh, M.E. Itkis, E. Belyarova, R.C. Haddon, Graphite nanoplatelet-epoxy composite thermal interface materials, *J. Phys. Chem. C* 111 (21) (2007) 7565–7569, <https://doi.org/10.1021/jp071761s>.
- [278] S. Gaikwad, J.S. Tate, N. Theodoropoulou, J.H. Koo, Electrical and mechanical properties of PA11 blended with nanographene platelets using industrial twin-screw extruder for selective laser sintering, *J. Compos. Mater.* 47 (23) (2012) 2973–2986, <https://doi.org/10.1177/0021998312460560>.
- [279] D.C. Marcano, D.V. Kosynkin, J.M. Berlin, A. Sinitskii, Z. Sun, A. Slesarev, L. B. Alemany, W. Lu, J.M. Tour, Improved synthesis of graphene oxide, *ACS Nano* 4 (8) (2010) 4806, <https://doi.org/10.1021/nn1006368>.
- [280] S. Khanna, S. Paneliya, P. Prajapati, R. Chaudhari, J. Vora, H. Jouhara, Investigating the thermal properties of n-hexacosane/graphene composite: A highly stable nanocomposite material for energy storage application, *Therm. Sci. Eng. Prog.* 39 (2023) 101712, <https://doi.org/10.1016/j.tsep.2023.101712>.
- [281] O. Folorunso, P. Olukanmi, S. Thokozani, Conductive polymers' electronic structure modification for multifunctional applications, *Mater. Today Commun.* 35 (2023) 106308, <https://doi.org/10.1016/j.mtcomm.2023.106308>.
- [282] C.W. Foster, M.P. Down, Y. Zhang, X. Ji, S.J. Rowley-Neale, G.C. Smith, P.J. Kelly, C.E. Banks, 3D Printed Graphene Based Energy Storage Devices, *Sci. Rep.* 7 (1) (2017) 42233, <https://doi.org/10.1038/srep42233>.
- [283] K.R. Ryan, M.P. Down, N.J. Hurst, E.M. Keefe, C.E. Banks, Additive manufacturing (3D printing) of electrically conductive polymers and polymer nanocomposites and their applications, *eScience* 2 (4) (2022) 365–381, <https://doi.org/10.1016/j.esci.2022.07.003>.
- [284] X. Lu, J. Yvonnet, F. Detrez, J. Bai, Low electrical percolation thresholds and nonlinear effects in graphene-reinforced nanocomposites: A numerical analysis, *J. Compos. Mater.* 52 (20) (2018) 2767–2775, <https://doi.org/10.1177/0021998317753888>.
- [285] M. Ali, L. Lin, D. Cartridge, High electrical conductivity waterborne dispersions of carbon black pigment, *Progress in Organic Coatings* 129 (2019) 199–208, <https://doi.org/10.1016/j.porgcoat.2018.12.010>.
- [286] Y. Wang, C. Yang, Z. Xin, Y. Luo, B. Wang, X. Feng, Z. Mao, X. Sui, Poly (lactic acid)/carbon nanotube composites with enhanced electrical conductivity via a two-step dispersion strategy, *Compos. Commun.* 30 (2022) 101087, <https://doi.org/10.1016/j.coco.2022.101087>.
- [287] A. Abbasi, A. Bose, Massive and sustained enhancement of the electrical conductivity of polystyrene using multilayer graphene at low loadings, and carbon black as a dispersion aid, *Colloids and Surfaces a: Physicochemical and Engineering Aspects* 580 (2019) 123727, <https://doi.org/10.1016/j.colsurfa.2019.123727>.
- [288] M. Mazaheri, J. Payandehpeyma, M. Khamehchi, A developed theoretical model for effective electrical conductivity and percolation behavior of polymer-graphene nanocomposites with various exfoliated filleted nanoplatelets, *Carbon* 169 (2020) 264–275, <https://doi.org/10.1016/j.carbon.2020.07.059>.
- [289] Z. Kovács, A. Pomázi, A. Toldy, The flame retardancy of polyamide 6—Prepared by in situ polymerisation of ε-caprolactam—for T-RTM applications, *Polymer Degradation and Stability* 195 (2022) 109797, <https://doi.org/10.1016/j.polymdegradstab.2021.109797>.
- [290] J. Cho, H. Lee, K.-H. Nam, H. Yeo, C.-M. Yang, D.G. Seong, D. Lee, S.Y. Kim, Enhanced electrical conductivity of polymer nanocomposite based on edge-selectively functionalized graphene nanoplatelets, *Compos. Sci. Technol.* 189 (2020) 108001, <https://doi.org/10.1016/j.compscitech.2020.108001>.
- [291] F.-L. Guan, F. An, J. Yang, X. Li, X.-H. Li, Z.-Z. Yu, Fiber-reinforced three-dimensional graphene aerogels for electrically conductive epoxy composites with enhanced mechanical properties, *Chin. J. Polym. Sci.* 35 (11) (2017) 1381–1390, <https://doi.org/10.1007/s10118-017-1972-z>.
- [292] C. Liang, H. Qiu, Y. Han, H. Gu, P. Song, L. Wang, J. Kong, D. Cao, J. Gu, Superior electromagnetic interference shielding 3D graphene nanoplatelets/reduced graphene oxide foam/epoxy nanocomposites with high thermal conductivity, *J. Mater. Chem. C* 7 (9) (2019) 2725–2733, <https://doi.org/10.1039/C8TC05955A>.
- [293] W. Tao, S. Zeng, Y. Xu, W. Nie, Y. Zhou, P. Qin, S. Wu, P. Chen, 3D Graphene-sponge skeleton reinforced polysulfide rubber nanocomposites with improved electrical and thermal conductivity, *Compos. A Appl. Sci. Manuf.* 143 (2021) 106293, <https://doi.org/10.1016/j.compositesa.2021.106293>.
- [294] S.I. Mollik, R.B. Alam, M.R. Islam, Significantly improved dielectric properties of bio-compatible starch/reduced graphene oxide nanocomposites, *Synth. Met.* 271 (2021) 116624, <https://doi.org/10.1016/j.synthmet.2020.116624>.
- [295] S. Cho, M. Kim, J.S. Lee, J. Jang, Polypropylene/polyaniline nanofiber/reduced graphene oxide nanocomposite with enhanced electrical, dielectric, and ferroelectric properties for a high energy density capacitor, *ACS Appl. Mater. Interfaces* 7 (40) (2015) 22301–22314, <https://doi.org/10.1021/acsmami.5b05467>.

- [296] Z. Chen, Y. Liu, L. Fang, P. Jiang, X. Huang, Role of reduced graphene oxide in dielectric enhancement of ferroelectric polymers composites, *Appl. Surf. Sci.* 470 (2019) 348–359, <https://doi.org/10.1016/j.apsusc.2018.11.150>.
- [297] L. Zhang, R. Xi, S.-H. Zhang, C. Wang, H.-D. Wu, L.-Y. Shi, G.-B. Pan, Enhanced dielectric properties of ferroelectric polymer with perfluoroctanoic acid doped reduced polyaniline/reduced graphene oxide fillers, *Mater. Lett.* 242 (2019) 1–4, <https://doi.org/10.1016/j.matlet.2019.01.060>.
- [298] S. Palsaniya, H.B. Nemade, A.K. Dasmahapatra, Graphene based PANI/MnO<sub>2</sub> nanocomposites with enhanced dielectric properties for high energy density materials, *Carbon* 150 (2019) 179–190, <https://doi.org/10.1016/j.carbon.2019.05.006>.
- [299] Y. Zhang, L. Seveyrat, L. Lebrun, Correlation between dielectric, mechanical properties and electromechanical performance of functionalized graphene / polyurethane nanocomposites, *Compos. Sci. Technol.* 211 (2021) 108843, <https://doi.org/10.1016/j.compscitech.2021.108843>.
- [300] A.Y. Yassin, A.M. Abdelghany, Synthesis and thermal stability, electrical conductivity and dielectric spectroscopic studies of poly (ethylene-co-vinyl alcohol)/graphene oxide nanocomposite, *Phys. B Condens. Matter* 608 (2021) 412730, <https://doi.org/10.1016/j.physb.2020.412730>.
- [301] J. Yuan, A. Luna, W. Neri, C. Zakri, T. Schilling, A. Colin, P. Poulin, Graphene liquid crystal retarded percolation for new high-k materials, *Nat. Commun.* 6 (1) (2015) 8700, <https://doi.org/10.1038/ncomms9700>.
- [302] Z. Zhang, J. Zhang, S. Li, J. Liu, M. Dong, Y. Li, N. Lu, S. Lei, J. Tang, J. Fan, Z. Guo, Effect of graphene liquid crystal on dielectric properties of polydimethylsiloxane nanocomposites, *Compos. B Eng.* 176 (2019) 107338, <https://doi.org/10.1016/j.compositesb.2019.107338>.
- [303] Y. Cui, S. Kundalwal, S. Kumar, Gas barrier performance of graphene/polymer nanocomposites, *Carbon* 98 (2016) 313–333, <https://doi.org/10.1016/j.carbon.2015.11.018>.
- [304] O.B. Seo, S. Saha, N.H. Kim, J.H. Lee, Preparation of functionalized MXene-stitched-graphene oxide/poly (ethylene-co-acrylic acid) nanocomposite with enhanced hydrogen gas barrier properties, *J. Membr. Sci.* 640 (2021) 119839, <https://doi.org/10.1016/j.memsci.2021.119839>.
- [305] L. Wang, J. Zhang, Y. Sun, T. Zhang, L. Wang, J. Wang, Y. Liang, M. Hao, Q. Fu, Green preparation and enhanced gas barrier property of rubber nanocomposite film based on graphene oxide-induced chemical crosslinking, *Polymer* 225 (2021) 123756, <https://doi.org/10.1016/j.polymer.2021.123756>.
- [306] X. Zhu, Z. Ni, L. Dong, Z. Yang, L. Cheng, X. Zhou, Y. Xing, J. Wen, M. Chen, In-situ modulation of interactions between polyaniline and graphene oxide films to develop waterborne epoxy anticorrosion coatings, *Prog. Org. Coat.* 133 (2019) 106–116, <https://doi.org/10.1016/j.porgcoat.2019.04.016>.
- [307] E. Nielsen, Lawrence, Models for the Permeability of Filled Polymer Systems, *Journal of Macromolecular Science: Part A - Chemistry* 1 (5) (1967) 929–942, <https://doi.org/10.1080/10601326708053745>.
- [308] B. Adak, M. Joshi, B. Butola, Polyurethane/functionalized-graphene nanocomposite films with enhanced weather resistance and gas barrier properties, *Compos. B Eng.* 176 (2019) 107303, <https://doi.org/10.1016/j.compositesb.2019.107303>.
- [309] N. Yousefi, M.M. Gudarzi, Q. Zheng, X. Lin, X. Shen, J. Jia, F. Sharif, J.-K. Kim, Highly aligned, ultralarge-size reduced graphene oxide/polyurethane nanocomposites: mechanical properties and moisture permeability, *Compos. A Appl. Sci. Manuf.* 49 (2013) 42–50, <https://doi.org/10.1016/j.compositesa.2013.02.005>.
- [310] F. Asai, T. Seki, Y. Takeoka, Functional polymethacrylate composite elastomer filled with multilayer graphene and silica particles, *Carbon Trends* 4 (2021) 100064, <https://doi.org/10.1016/j.cartre.2021.100064>.
- [311] M. Iliut, C. Silva, S. Herrick, M. McGlothlin, A. Vijayaraghavan, Graphene and water-based elastomers thin-film composites by dip-moulding, *Carbon* 106 (2016) 228–232, <https://doi.org/10.1016/j.carbon.2016.05.032>.
- [312] M. Liu, D.G. Papageorgiou, S. Li, K. Lin, I.A. Kinloch, R.J. Young, Micromechanics of reinforcement of a graphene-based thermoplastic elastomer nanocomposite, *Compos. A Appl. Sci. Manuf.* 110 (2018) 84–92, <https://doi.org/10.1016/j.compositesa.2018.04.014>.
- [313] Q. Meng, P. Wang, Y. Yu, J. Liu, X. Su, H.-C. Kuan, B. Wang, L. Zhang, Y. Zhang, D. Lasic, Polyaspartic polyurea/graphene nanocomposites for multifunctionality: Self-healing, mechanical resilience, electrical and thermal conductivities, and resistance to corrosion and impact, *Thin-Walled Struct.* 189 (2023) 110853, <https://doi.org/10.1016/j.tws.2023.110853>.
- [314] B. Mensah, K.C. Gupta, G. Kang, H. Lee, C. Nah, A comparative study on vulcanization behavior of acrylonitrile-butadiene rubber reinforced with graphene oxide and reduced graphene oxide as fillers, *Polym. Test.* 76 (2019) 127–137, <https://doi.org/10.1016/j.polymertesting.2019.01.026>.
- [315] M.A. Atieh, N. Nazir, F. Yusof, M. Fettouhi, C.T. Ratnam, M. Alharthi, F.A. Abu-Ilaiwi, K. Mohammed, A. Al-Amer, Radiation vulcanization of natural rubber latex loaded with carbon nanotubes, *Fullerenes, Nanotubes, Carbon Nanostruct.* 18 (1) (2010) 56–71, <https://doi.org/10.1080/15363830903291572>.
- [316] V. Phetarporn, S. Loykulnant, C. Kongkaew, A. Seubsa, P. Prapainainar, Composite properties of graphene-based materials/natural rubber vulcanized using electron beam irradiation, *Mater. Today Commun.* 19 (2019) 413–424, <https://doi.org/10.1016/j.mtcomm.2019.03.007>.
- [317] S. Araby, Q. Meng, L. Zhang, H. Kang, P. Majewski, Y. Tang, J. Ma, Electrically and thermally conductive elastomer/graphene nanocomposites by solution mixing, *Polymer* 55 (1) (2014) 201–210, <https://doi.org/10.1016/j.polymer.2013.11.032>.